Classe di Scienze

Corso di perfezionamento in
Neuroscienze

XXXV ciclo

Optobody: an intrabody-based optogenetic tool for inducible and reversible targeted protein degradation

Settore Scientifico Disciplinare **BIO/09**

Candidata

dr.(ssa) Angela Rachel Bitonti

Relatore Antonino Cattaneo

Anno accademico 2024/2025

Table of contents

Abstract

Protein homeostasis, or proteostasis, refers to the network of cellular processes that maintains the proper balance of protein concentration, localization, conformation, and interactions within the cell. Many human diseases display proteostasis alterations, hence regulating proteostasis is a crucial objective for target validation and drug discovery. While regulation of protein synthesis and folding is essential for maintaining appropriate protein levels, another critical component of proteostasis is proteolysis, the controlled degradation of proteins. Thus, removing aged, misfolded, mislocalized, or aberrant proteins is often necessary to preserve cellular function. In this context, targeted protein degradation has emerged as a groundbreaking strategy in drug discovery, enabling direct intervention at the protein level to modulate the activity of specific proteins. To date, the most common targeted protein degradation (TPD) strategy employs proteolysis targeting chimeras, which are hybrid molecules, usually of chemical synthesis, also called heterobifunctional, for their capacity of binding the target protein and connecting it to the ubiquitin-dependent degradative pathway. The bifunctional nature of such tools remains the bottleneck in the discovery processes, because the target binding moiety of the heterobifunctional degrader requires an ad hoc chemical development process for each target. To overcome the issue of the chemical nature of the target binding moiety capacity, a genetically encoded target-binding moiety would be desirable, being more general. To this aim, we harnessed the broad diversity of antibody binding repertoires and exploited the Intracellular Antibody Capture Technology (IACT) selection platform, to select antigen binders directly from the target cDNA sequence. The selected antibody domains are then equipped with a degradation signal capable of redirecting to the degradative pathway the intracellular target protein. Beyond developing a new genetically encoded heterobifunctional tool based on intracellular antibodies (the primary objective), my second goal was to create a stimulus-activated targeted degradation system. To achieve this, I fused the intrabody domain with a Light-Oxygen-Voltage (LOV) domain and incorporated an ornithine decarboxylase (ODC) degron sequence, enabling conditional engagement of the degradative pathway.

The “optobodies” developed in this work are light-activatable intrabody-based degradative tools for the reversible targeted protein degradation of intracellular targets. We tested the optobody strategy with three diverse protein targets: the misfolding protein TDP-43, the phosphorylated Tau, and the synaptic plasticity protein Arc/Arg3.1. proteins. The major part of the work aimed at assessing the validity of the optobody format in reaching the modulable

and reversible proteasomal degradation of the TDP-43 in its wild type and mislocalizing version, by using a Llama anti TDP43 nanobody VHH5. The second aim of my work was to address the LOV-based Targeted Protein Degradation strategy against a specific subset of the protein target, the phosphorylated pool of the Tau protein.
The last part of the work has been focused on the isolation of Llama VHH targeting the activity-regulated cytoskeletal-associated protein Arc, a synaptic plasticity effector, to start exploring the feasibility of applying the optobody TPD beyond the neurodegenerative-relevant protein targets.

The results obtained with these three optobodies provide proof of concept of applying the intrabody technology to create degradative tools regulated by an orthogonal signal, namely light. While the reliance on light stimulation may limit the tool's immediate translational potential, it offers a powerful research and target validation approach, to directly modulate protein function and investigate protein-level interference in a controlled manner.

Indeed, as for the TDP-43 and phospho-Tau protein the intrabody-based optogenetic tools can become tools to investigate the misfolding and the aggregation process in cellular models for ALS, FTLS and AD respectively, the anti-Arc-optobody can pave a way for investigating, with a dendritic subcellular resolution, the mechanism of the synaptic plasticity subserving behind the memory processes.

1. Introduction

1.1 Proteostasis

Protein homeostasis is the process responsible for the correct concentration, localization, conformation, and interaction of all the proteins within the cellular environment. Considering the huge variety of proteins that are constantly synthesized and available at the same time, protein homeostasis, defined as proteostasis, can be seen as a network of processes cooperating to maintain the physiological balance between proteins that are required to the cells and proteins that need to be removed (Balch et al., 2008). The proteostasis network can be divided into three major categories: proper synthesis and folding of nascent proteins, conformational status maintenance, and the degradation process. These three areas of the network require more than 2000 proteins to be assigned to each field (Hipp et al., 2019).

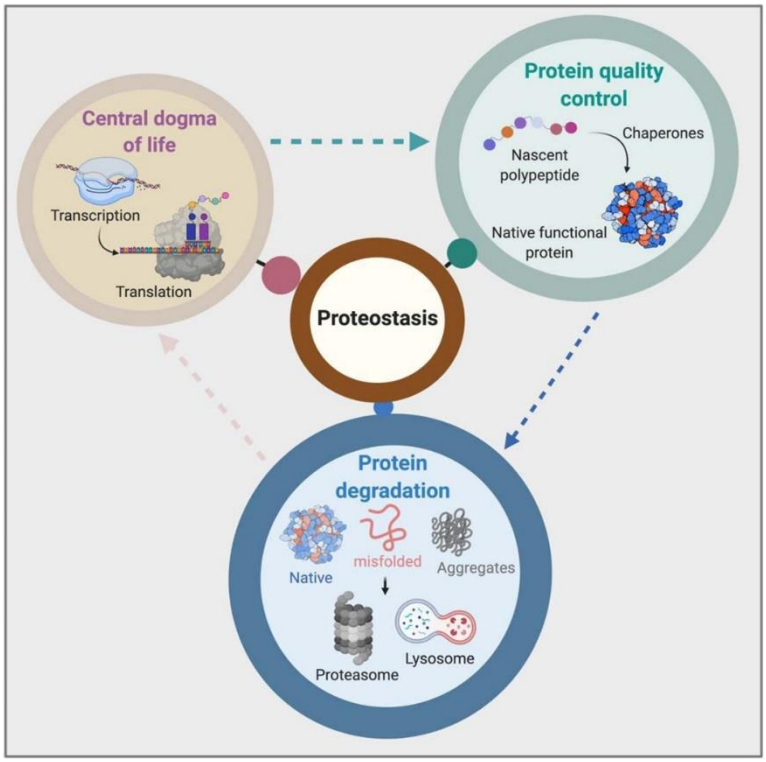

I 1 ***Protein synthesis, protein folding, and clearance are key components of the proteostasis network****, adapted from (Samarasinghe & Crews, 2021)*

The proteome of eukaryotic cells ranges from a few thousand of fungi to many tens of thousands of different proteins in human cells, and the proteome composition becomes further complex through the different cell types and tissues. Moreover, genetic mutations can alter protein stability and folding kinetics, thus resulting in metastable proteins. Thus, protein abundance control is a fundamental mechanism through which cells can maintain all the

metabolic pathways to allow the stoichiometric assembly of each macromolecular machinery, such as ribosome, respiratory chain complexes, etc (Hipp et al., 2019). The gene expression pathway mediates the formation of the entire proteome from the genetic information, and the proteome composition depends on the transcriptional and translational mechanisms. The main regulation process of protein synthesis is at the translational level, indeed, mRNA translation into proteins is the limiting step of the gene expression contribution to the protein expression levels (Gebauer & Hentze, 2004). Briefly, in Figure I2 A are shown the two general ways of translational control are the global control, that generally occurs by modification of translation-initiation factors; and, for a small class of mRNAs, by the mRNA-specific control driven by regulatory protein complexes that recognize elements of the 5' and/or the 3' untranslated regions (UTRs) of the target RNAs (Gebauer & Hentze, 2004). After the proper protein synthesis, the second branch of proteostasis control aims for the newly synthesized proteins to reach the correct folding, or, in other words, the native state. It is well known that the thermodynamic stability of the native state of a protein is reached after many intermediate folding states, indeed, the folding process can be described, through the energy landscape, as the transformation of a newly synthesized protein from the unfolded state to its native one, by organizing the intramolecular interactions to reach the most favourable energetic state (Figure I2A). The process is far from being considered linear and spontaneous for the vast majority of proteins. Although the folded state of each protein is thermodynamically favourable, and all the information for the folding is contained within the amino acid sequence, an entire class of proteins, called chaperones, assists the proper folding process and maintains the macromolecular complex assembly(Kim et al., 2013).

In summary, proteostasis in eukaryotic cells depends on the constant equilibrium of the correct concentration and folding state of the proteins. In other words, the correct concentration of the well-folded proteins strictly depends on the balance between the synthesis and the degradation process. The two main degradation pathways of eukaryotic cells are mediated by the proteasome machinery or the lysosomes (L. Zhao et al., 2022).

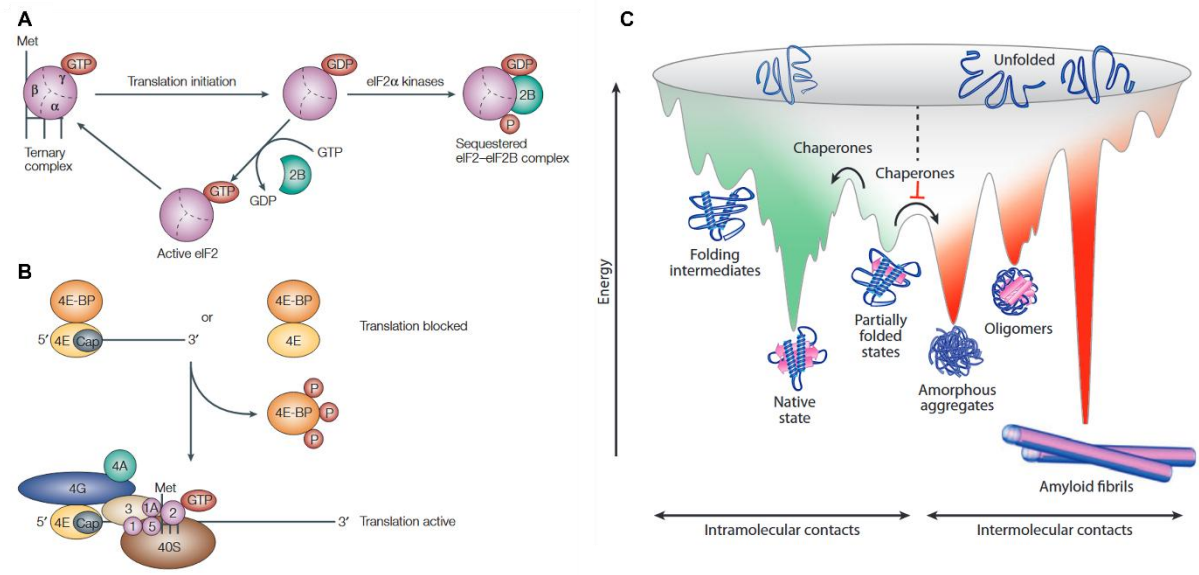

I 2 ***A) GTP Hydrolysis and Recycling of eIF2 in Translation Initiation****: The initiation of the translation process involves GTP hydrolysis and the recycling of eukaryotic initiation factor 2 (eIF2. eIF2 comprises three subunits — α, β, and γ — and is a key part of the ternary complex, the methionine-loaded initiator tRNA (L-shaped symbol). The active form is the eIF2-γ subunit bound to GTP. During translation initiation, this GTP is hydrolyzed. To regenerate active eIF2, GDP–GTP exchange must occur, a process catalyzed by eIF2B. However, phosphorylation of the eIF2α subunit slows down the dissociation rate of eIF2B, leading to sequestration of eIF2B in the cell and inhibiting the GDP–GTP exchange reaction.* ***B) Role of eIF4E-Binding Proteins (4E-BPs)****: 4E-BPs bind to eIF4E, preventing it from interacting with eIF4G, thus inhibiting translation. When 4E-BPs are phosphorylated, they release from eIF4E, enabling eIF4E to interact with eIF4G. This interaction facilitates the initiation of translation; A and B adapted from (Gebauer & Hentze, 2004).* ***C) Competing processes of protein folding and aggregation****. Proteins fold by exploring various conformations within a folding energy landscape. Energetically favourable intramolecular interactions (highlighted in green) are stabilized as the protein moves along a downhill path toward its native state. However, energetically favourable but nonnative conformations can lead to kinetically trapped states occupying low-energy regions such as partially folded or misfolded states. Chaperones help these trapped states overcome free energy barriers and prevent intermolecular interactions (shown in red) that could lead to aggregation, including amorphous aggregates, β-sheet-rich oligomers, and amyloid fibrils. This process ultimately promotes proper folding into the native state, adapted from(Kim et al., 2013).*

Proteasomal-mediated protein degradation is applied to misfolded or short-lived proteins. Lysosomes, on the other hand, are responsible for the degradation of properly folded protein, long-lived proteins, insoluble aggregates, macromolecular compounds, extracellular proteins, nucleic acids, lipids, damaged organelles, and parasites, such as bacteria and viruses (Paudel et al., 2023).

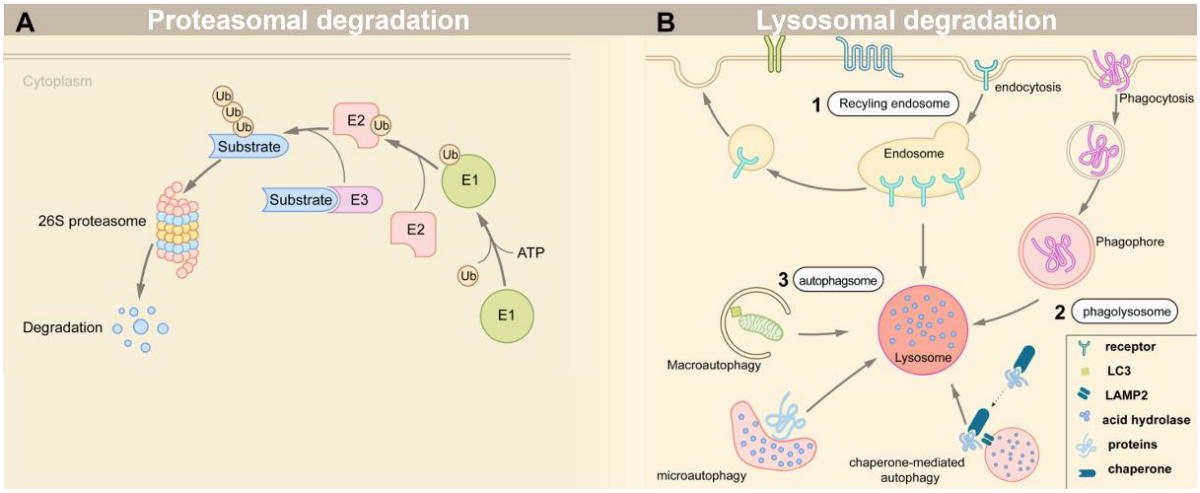

I 3 ***A)*** *proteasomal and* ***B)*** *lysosomal mediated degradation representation, adapted from (L. Zhao et al., 2022)*

1.1.1 Proteasome-dependent protein degradation (Pdpd)

1.1.1a Proteasome activation

The proteasome machinery is a multimeric protease complex that allows for the proteolysis of target proteins within the cellular environment, and it can be described in its two main parts. The core is composed of the 20S core particle, with four heptameric rings which form a cylindrical shape; these rings are stacked on top of each other. The two central rings consist of seven related β-subunits that are arranged to create an internal cavity; three of these subunits in each ring contain a proteolytic site that faces the internal cavity. This cylindrical cavity is added by a pore that narrows down the cavity's entrance, making it inaccessible to properly folded protein (Inobe & Matouschek, 2014). The other subunits are the two regulatory particles, among the four existing regulatory particles, 19S is the best characterized. The complex between 20S and one or two of these 19S is the 26S proteasome and is the most common form of the proteasome in cells. The two 19S, which represent the cap of the machinery, are located at the two ends of the 20S. Each 19S cap is composed of nineteen subunits, six of which are ATPase (Rpt1-6) and represent the motor of the entire machinery, while the remaining are non-ATPase subunits. Those six subunits form a long channel and end in a ring structure that docks into the 20S core particle and triggers the core opening (Inobe and Matouschek 2014). The role of the proteasome in the degradation process is to catalyze the hydrolysis of the polypeptide chain into short peptides between two and ten amino acids long. The digestion of the substrate lasts a few seconds and then the cytosolic peptidase can act on those peptides, releasing amino acids. In mammalian cells the small peptides coming from the proteolysis become the precursor to be presented to the MHC class-I. Since hydrolysis is an irreversible process, it is clear that

the access to the proteasome machinery of each ubiquitinated substrate must be tightly controlled (Collins & Goldberg, 2017)

1.1.1b Ubiquitin-proteasome system (UPS)

Most of the cellular proteins are degraded through the ubiquitin-proteasome system (UPS). The UPS acts by binding a ubiquitin-protein monomer to the intracellular protein target; three groups of enzymes are required for this process. E1, the ubiquitin-activating enzyme, catalyzes the covalent bond between the ubiquitin monomer and the ATP molecule, and the transfer of activated ubiquitin to E2, the ubiquitin-conjugating enzyme. The last step involves E3 ubiquitin ligases, which are responsible for the binding of the ubiquitin molecule to a lysine residue of the protein target. The ubiquitination process may require the binding of many monomers to the substrate as a polyubiquitin chain. On this chain, every monomer can be bound to Lys 48 or Lys 63 of the ubiquitin protein (Cowan & Ciulli, 2022). The three families of E3 ligases, RING, HECT, and RING-between-RING (RBR), differ in their mechanisms for transferring ubiquitin protein from the E2 enzyme to the substrate and in their architectures. The E3 ubiquitin ligases family in humans comprises three major families: the RING -E3 with more than 600 members, the HECT with 28 members, and the RING between RBR that accounts for 14 members. After the ubiquitination process, the proper proteolysis starts when the proteasome machinery is recruited to recognize the ubiquitinated protein and triggers the degradation process (T. R. Cotton & Lechtenberg, 2020)

1.1.1c Ubiquitin-independent protein degradation (UbInPD)

Only a few eukaryotic proteins undergo ubiquitin-independent proteasomal degradation, with the first and best-characterized enzyme that undergoes UbInPD being the ornithine decarboxylase ODC1 (Murakami et al., 1992). ODC1 is a pyridoxal phosphate (PLP)-dependent amino acid decarboxylase enzyme that catalyzes the first step in the polyamine biosynthesis, converting L-ornithine into putrescine the precursor to spermine and spermidine. The ODC1 active enzyme is a homodimer, and its activity is regulated through the interaction with the regulatory protein antizyme1 (AZ1) and ODC antizyme inhibitor 1 (AzIN). High intracellular polyamine levels induce AZ1 expression, which binds to ODC1, disrupting the homodimer and exposing intrinsically disordered regions, including the C-terminal PEST sequence. This structural alteration allows direct recognition by the 26S proteasome, leading to degradation without ubiquitination (Wu et al., 2015). On the other hand,AzIN competes with ODC1 for AZ1 binding, having a higher affinity and thus preventing ODC1 degradation by

displacing it from the ODC/AZ1 complex (Pegg, 2006). In summary, in the presence of high levels of polyamine, AZ1 newly expressed enzyme, recognizes the C-tail of ODC1 and forms an inactive heterodimer; the ODC/AZ complex exposes a proteasome-targeting signal in the C-terminal region of ODC1, thus triggering the degradation process26S (Wu et al., 2015).

1.1.2 Lysosome-mediated protein degradation

Lysosomal-mediated protein degradation is the other degradative pathway, and can be resumed as subcellular machinery working on degradation and recycling. Lysosomes are organelles enclosed by a membrane that contain hundreds of integral and peripheral membrane proteins. The ion channels and the vacuolar-ATPases (V-ATPases) maintain the acidic lysosomal lumen. The internal pH, which ranges from 4.5 to 5.5, allows for the activation of intralysosomal hydrolase enzymes involved in the digestion of macromolecules, proteins, nucleic acids, lipids, and carbohydrates. Since lysosomes are active organelles of the intracellular environment, their generation is a complex mechanism that starts from the synthesis of every lysosomal protein; but, since their degradation activity depletes the lysosomal pool, on the other hand, their re-generation represents a critical mechanism to maintain the lysosomal homeostasis (Yang & Wang, 2021). The three main routes providing substrates to the lysosomes are autophagy, endocytosis, and phagocytosis.

1.1.2a Autophagy

Autophagy encompasses three main degradation pathways: macroautophagy, microautophagy, and chaperone-mediated autophagy. Microautophagy starts with membrane invagination of the lysosome compartment to take up the cellular material. The chaperone-mediated autophagy depends on the interaction between HSPA8/HSC70 with the protein target and the LAMP2A receptor of the lysosome. The so-called macroautophagy, also known as proper autophagy, involves the formation of an autophagosome surrounding the material that must be removed from the cells. The membrane fusion between the autophagosome and the lysosome then allows for the delivery of the trapped material to the last destination for the degradation process (Paudel et al., 2023).

1.1.2b Endocytosis

The endosomal-lysosomal pathway starts with the clathrin-dependent internalization of the proteins with an endosome formation from the plasma membrane. After their formation, the endosomes can fuse with other pre-existing endosomes in the peripheral cytoplasm. These early

endosomes mainly act as a sorting station: at this stage the cargo protein can either be recycled back to the cell surface or being escorted to the lysosomes. The maturation of early endosomes requires four steps; the increase of the number of intraluminal vesicles, forming the multivesicular bodies; the increase in luminal acidification and the increase of hydrolases concentration; the movement from the cell periphery towards the microtubule organizing center (MTOC); and the switching of Rab proteins, from Rab5 to Rab7 (Hu et al., 2015). Ubiquitinated cargo is targeted for degradation via the ESCRT complex, which mediates sorting and invagination, while also recycling ubiquitin (Raiborg & Stenmark, 2009).

1.1.2c Phagocytosis

Phagocytosis enables the uptake of various cargoes via specific receptors. After engulfment, cargo enters an early phagosome, which matures and fuses with lysosomes to form phagolysosomes (PLs). The PL fusion involves a wide array of fusion-related proteins, including approximately 30 SNAREs (soluble N-ethylmaleimide-sensitive factor attachment protein receptors), around 20 Rab GTPases, six multi-subunit tethering complexes, and four tethering proteins from the Sec1/Munc18 (SM) family. While the full mechanism of PL fusion remains incompletely understood, phagocytosis and autophagy are interconnected processes. These pathways work together during PL formation, with components of the autophagy machinery either enhancing phagosome maturation or contributing to microbial killing and cellular homeostasis (Nguyen & Yates, 2021).

1.2 Targeted protein degradation

One of the emerging approaches in the drug discovery process is the modulation of the overall levels and activity of disease-causing protein targets and their related activity; this can be achieved by identifying small molecules or antibodies with affinity for the target protein and bridging the binding moieties with the degradation machinery of the cell. The concept of targeted protein degradation with genetically encoded intrabodies was first proposed in 1997 (Biocca & Cattaneo, 1997) : “Targeting to a degradative compartment would be one effector function that could be conferred to intracellularly expressed antibodies to create “suicide antibodies”. In this scheme, an antibody targeted to a degradative compartment could be engineered to cause the concomitant transport and degradation of the bound antigen. The transit time towards the degradative compartment should be long enough to allow the interaction between the antibody and the corresponding antigen”. Following this early suggestion, genetically encoded targeted protein degradation was first experimentally demonstrated with a

target-binding peptide fused to an F-box protein (Zhou et al., 2000) and subsequently generalized to the intrabody application field in the pivotal study by Melchionna and Cattaneo (2007).

The first era of chemical targeted protein degradation (TPD) formally began with the patent application from Proteinix (Kenten & Roberts, 2001) that proposed " novel compounds comprising a ubiquitination recognition element and a protein binding element" .
Subsequently, the pivotal proteolysis-targeting chimera (PROTAC) paper by Sakamoto *et al.* in 2001 was the first demonstration of the concept that protein targets could be intentionally dragged to a ubiquitin ligase to induce their degradation using chemical tools. TDP has become a breakthrough in the drug discovery field. Two approaches have been pursued initially targeting protein versus mRNA interference. The engineered ubiquitin-proteolytic apparatus operates at the post-translational level, providing a new tool for reverse genetics to dissect complex protein functions with higher resolution than knockout or knockdown approaches, which function at the level of DNA or RNA. Among the possible methods for protein knockdown, targeted protein degradation (TPD) is a therapeutic strategy that involves depleting or reducing a disease-causing protein to maintain proteostasis, rather than identifying a specific binding site on the target to achieve competitive or non-competitive inhibitors. Although in the pre translational phase of a protein, the selected methods to alter the gene or the transcript encoding a protein are represented by the CRISPR/Cas9 system and the RNA interference, those strategies can knock down the target protein during the translational phase but result to be ineffective with already expressed or over-expressed and sometimes unfolded proteins (Luh et al., 2020). In the past two decades, the TPD approach has significantly advanced, moving beyond its initial focus on well-known and cancer-related targets (L. Zhao et al., 2022). Moreover, the rise of genomics and proteomics has allowed for the identification of numerous clinically relevant targets in human disorders that can become targets for the TPD approach; on the other hand, an entire category of disease-relevant proteins has been identified as unfeasible for the rational drug discovery process. "Undruggable" is the correct definition, and it refers to proteins whose functional interfaces are flat and lack defined binding sites for ligands and interactors, transforming the rational drug design into a major challenge (Xie et al., 2023). Even though these undruggable targets can be alternatively considered as "not yet druggable" due to the limitations in the understanding of their binding surfaces and or their functions, it is possible to identify 5 categories to collect all those proteins. Briefly, those categories are represented by the small-GTPases due to the lack of targetable binding pocket;

the phosphatases, due to the structural similarity between the tyrosine phosphatases (PTPs) and the serine/threonine phosphatases (PSTPs), the specificity for the drug design that hinders the drug discovery process. Another class of undruggable is represented by the transcription factors (TFs) and belonging to the class is related to the huge heterogeneity and the lack of binding sites. Epigenetic targets, in other words, are proteins and enzymes involved in epigenetic processes such as DNA methylation, Histone modifications, and chromatin remodelling. Another major class of undruggable includes all the proteins whose protein-protein interactions are difficult to identify, and a subclass of that is represented by the intrinsically disordered proteins, in which the lack of a defined structure makes the rational design of chemical binders an unfeasible strategy (Xie et al., 2023). In this view, TPD can offer a route to drug discovery focused on the so-called undruggable or "not yet to be drugged" or "difficult to be drugged" targets.

1.2.1 PROTAC

Targeted protein degradation became a powerful strategy, together with the understanding of the ubiquitin-proteasome system. As previously described, the selectivity of UPS machinery resides in the activity of E3 ligases. One of the best-characterized E3 families is the Skp1-Cullin-F box (SCF) complex. The target specificity is mediated by the F box protein, which is composed of a Skp1 binding domain and a WD40 domain a leucine-rich motif that mediates the protein-protein interaction with the substrate. The identification of the modularity of the SCF complex in its substrate-binding domain allowed for the engineering of F box protein to targeted proteolysis of candidates that are not physiological substrates (Zhou et al., 2000). The first example of targeted protein degradation was obtained with Rb protein, and the proof of concept was conducted in yeast cells. Briefly, in the work of Zhou *et al*., once identified a physiological binder of Rb protein, represented by the E7 protein of human papillomavirus type 16, the F box was fused with the 35 residues at the N-terminal of E7, containing the Rb binding motif. The resulting F box chimera was demonstrated to be able to target Rb protein to proteolysis, even though it is not a physiological substrate of the SCF complex. The engineering of a member of the SCF complex allows for targeted degradation only in transgenic organisms, thus representing a limitation of the strategy. In this view, an alternative strategy can be to act on the target protein rather than on the degradation machinery.

In the past twenty years, the major class of molecules that allow for TPD has been defined as heterobifunctional, composed of a moiety involved in the binding of the protein of interest (POI) and a moiety for UPS activation through the binding of E3 ligases. These

heterobifunctional chimeras can simultaneously bind the POI and the E3 ligases, thus leading to the ubiquitination of the POI and its proteasome-mediated degradation. In contrast, the chimera is recycled to target another substrate (Békés et al., 2022). The first proteolysis targeting chimera (PROTAC) was proposed in 2001 when the Skp1-Cullin-F box class of E3 ubiquitin ligases was investigated in their mechanism of targeted protein degradation. Briefly, Skp1-Cullin-F box (SCF) complexes in mammalian cells interact through the F-box β-TRCP with Ikβα, a negative regulator of NFkβ, leading to ubiquitination and subsequent degradation of Ikβα. The key element for Ikβα degradation is the 10-aa phospho peptide within Ikβα, DRHDSGLDSM. Upon diverse inflammatory signals, this motif undergoes phosphorylation on both its serine residues, from Ikβ Kinase (IKK) then, the phosphorylation of the Ikβα triggers the formation of the complex with $SCF^{\beta TRCP}$. The idea behind the first PROTAC was to fuse the Ikβα phosphopeptide (IPP) to a target protein, the ovaciclin, a potent inhibitor of methionine aminopeptidase-2 (MetAP-2). The protac-1 was able to tether MetAP-2 to $SCF^{\beta TRCP}$ complex and escort MetAP-2 to degradation (Sakamoto et al., 2001) .The discovery of protac-1 represents a milestone for targeted protein degradation as a therapeutic strategy; in 2019 the first two PROTACs, targeting androgenic receptor and oestrogenic receptors, the ARV-110 (NCT03888612) and ARV-471 (NCT04072952), respectively, were introduced in clinical trials (Békés et al., 2022).

1.2.2 LYTAC

A variant of the PROTAC mechanism was proposed when the heterobifunctional chimera targeting the lysosomal degradation pathway (LYTAC) was created(Banik et al., 2020). The LYTAC mechanism of action works through the binding of both cell-surface lysosome-targeting receptors (LTRs) and extracellular proteins and then it induces internalization and lysosomal degradation of the target. The LTR used in the first LYTAC proposed is the cation-independent mannose-6-phosphate receptor (CI-M6PR, also called IGF2R), which transports proteins bearing N-glycans capped with mannose-6-phosphate to lysosomes. The first LYTAC proposed is composed of a glycopolypeptide ligand for CI-M6PR conjugated to an antibody to traffic secreted and membrane-associated proteins to lysosomes (Banik et al., 2020).

1.2.2.a GlueTAC

Another lysosome-based strategy, the GlueTAC, for the degradation of cell-surface proteins, has been developed using the nanobody format. In the GlueTAC technology, on one side, the nanobody became able to bind covalently to its antigen for the presence of unnatural amino

acids in its sequence; on the other side, the so-called Gluebody is conjugated to a cell-penetrating peptide, and lysosome-sorting sequence (CPP-LSS). The resulting chimera promotes the uptake and subsequent degradation of programmed death-ligand 1 (PD-L1). (H. Zhang et al., 2021).

1.2.3 Molecular glues

Similar to PROTAC technology, the molecular glue degraders are bridging molecules that induce the interaction between a ubiquitin ligase and a POI. Although molecular glues and Protac are based on UPS activation, the two mechanisms are quite different. Molecular glues are more frequently involved in the binding only of E3 ligases, rarely of the POI, and then can stabilize or induce the interaction between E3 and POI (L. Zhao et al., 2022). The first molecular glue identified, thalidomide, belongs to the class of immunomodulatory imide drugs (IMiDs). IMiDs are responsible for the formation of a ternary complex with E3 ligase cereblon (CRBN) and POI, leading to the ubiquitination and subsequent degradation of proteins that are not normally targeted to CRBN (Oleinikovas et al., 2024). Structural studies on three different physiological substrates of CRBN, CK1α, G1 to S phase transition protein 1 (GSPT1), and Zinf-finger (ZF) demonstrate that these three candidates share a degron motif described as an eight-amino acid stretch containing an invariant glycine at position six. In the case of CRBN-MGD this stretch is called the G-loop, showing both the features of an alpha-turn, for the two hydrogen bonds between the amino acid in the first and fifth position, and a beta-hairpin because it connects two beta-strands. The presence of a G-loop is necessary for the binding of the target to CRBN, but it is not sufficient for target degradation; on the other hand, in the presence of MGDs, the binding affinity between the substrate and CRBN increases from 4 to 30-fold (Oleinikovas et al., 2024).

1.2.4 AUTAC

When the proteasomal and lysosomal pathways are not the designed pathways for a specific degradation substrate, autophagy may represent the route. The autophagy-targeting chimera (AUTAC) arises from the best-characterized autophagy mechanism against bacteria, the xenophagy process. Group A Streptococci (GAS) in the cytoplasm are initially tagged with ubiquitin and subsequently enclosed within autophagosome-like structures, known as GAS-containing vacuoles (GcAVs), before being degraded in lysosomes. The ubiquitination process of the bacterial GAS is triggered by the presence of 8-nitroguanosine3’-5’-cyclic monophosphate (8-nitro-cGMP) and then is followed by K63-linked polyubiquitination and

culminates in the clearance of the bacteria (Ito et al., 2013). The AUTAC is the substrate specific S-guanylation to trigger the autophagy pathway. The substrate-specific S-guanylation is reached through HaloTag (HT) technology. Briefly, the Halo-Tag-POI forms a covalent bond with cGMP Halo-Tag-ligands containing a haloalkane unit; the complex is then responsible for K-63 polyubiquitination and degradation of the target cargoes. Even though AUTAC, similar to PROTAC, introduces a degradation targeting chimera for intracellular targets, the powerful advantage of the AUTAC technology is the applicability to non-proteinous biomolecules and subcellular organelles, such as mitochondria (Takahashi et al., 2019).

1.2.5 ATTEC

Beyond the identification of molecular tag that triggers the autophagy process, as the case of AUTAC; another technology that aims to induce the same degradation pathway is the autophagosome-tethering compound (ATTEC) that directly tethers the target protein to the autophagosome protein microtubule-associated protein 1A/1B light chain 3 (LC3) for degradation (Z. Li et al., 2019) (Z. Li et al., 2020).

1.2.6 AUTOTAC

The direct interaction with the LC3 protein on the autophagic membrane is the key point of an alternative strategy, the AUTOphagy-TArgeting Chimera (AUTOTAC), without involving ubiquitination of the target. AUTOTAC technology arises from the understanding of the N-degron pathway; briefly, the N-terminal Arg of arginylated substrates is bound by N-recognins to induce substrate ubiquitination and proteasomal degradation via the N-end rule pathway of the ubiquitin (Ub)-proteasome system (UPS)(Bartel et al., 1990). In mammals, Nt-Arg is recognized by UBR boxes of N-recognins; upon binding to Nt-Arg, these N-recognins promote substrate ubiquitination and proteasomal degradation of short-lived regulators via the UPS. However, when the UPS is compromised, the Nt-Arg of the same substrates is recognized by the ZZ domain of p62, facilitating p62 self-polymerization, autophagosome biogenesis, and lysosomal degradation of autophagic protein cargoes (Yoo et al., 2018). Thus, the AUTOTAC is composed of target-binding ligands (TBLs) linked to p62-ZZ-binding moieties via a repeating polyethylene glycol (PEG) moiety (Ji et al., 2022).

1.2.7 CMA-based degrader

Chaperon-mediated autophagy (CMA) is a variant of the pathway, specific for protein cargoes, in which the heat-shock protein 70 (HSP70) recognizes a specific motif in the substrate protein

sequence and then, the HSP70-substrate complex binds the lysosome-associated membrane protein type 2a (L2AAs a result of this interaction, LAMP-2A (L2A) undergoes multimerization to form a translocation complex, which facilitates the uptake of substrate proteins into the lysosome for degradation (Bourdenx et al., 2021). The cargo selectivity of CMA is a key feature of the pathway and is mediated by a pentapeptide KFERQ, which is necessary to bind HSP70 and sufficient to target proteins for lysosomal degradation. While the chaperone protein HSP70 also participates in essential cellular processes like protein folding by binding to hydrophobic regions of target proteins, its specific interaction with the KFERQ-like motif is exclusively associated with directing proteins for selective degradation (Kaushik & Cuervo, 2018). Thus, CMA-based degraders are peptides consisting of three domains: a cell membrane penetrating domain (CMPD), a protein binding domain, and the CMA targeting motif(Fan et al., 2014).

1.2.8 Bispecific aptamer chimera

A common feature of all the TPD tools is the bispecific activity of the degradation targeting molecule, that is very often represented by chimeric proteins. On the other hand, bifunctional oligonucleotides are designed to simultaneously bind a cell surface receptor involved in lysosomal trafficking and a target protein located on the cell membrane, thereby facilitating the delivery of the bound complex to the lysosome (Miao et al., 2021).

1.2.9 Degradation tags

When the heterobifunctional molecule is not a chimeric peptide, as in the case of PROTAC, the alternative is to have a chemical compound that can be both a ligand of the POI and a degradation signal. Degradation tags (dTAGs) have been inspired by the thalidomide mechanism in recruiting cereblon E3 ligase (Oleinikovas et al., 2024). The bridging mechanism of recognizing a binding site on the POI and recruiting CRBN is the core of dTAGs that can mediate targeted POI degradation (Nabet et al., 2018; Winter et al., 2015).

1.2.10 Specific and non-genetic inhibitors of apoptosis protein-dependent erosive agents

The cellular inhibitors of apoptosis are a class of proteins that all contain the baculoviral IAP repeat (BIR) domain, which mediates cell proliferation by inhibiting the caspase activity that triggers the apoptosis process. The IAP1 family not only contains three BIR domains but also a carboxyterminal RING domain that confers the E3 ubiquitin ligase activity upon binding between the BIR3 domain and methyl bestatin (MeBS, 2) (Fulda & Vucic, 2012). Inspired by

the bestatin-induced targeted protein degradation, the specific and non-genetic inhibitors of apoptosis protein-dependent erosive agents (SNIPERs) is a hybrid molecule consisting of MeBS coupled to a ligand for the target protein that induces c-IAP1 mediated ubiquitination and proteasomal degradation of the POI(Itoh et al., 2010).

1.2.11 AbTAC

Taking together PROTAC and LYTAC technologies, acting on intracellular and extracellular target proteins respectively, aims to escort its target to the degradation pathway. Conversely, those mechanisms may not be ideal when the target is a membrane protein. For transmembrane proteins, the proposed solution is represented by AbTAC, an application of PROTAC in which the degradation mechanism is referred to transmembrane proteins and is mediated by an E3 ligase transmembrane as well. The bifunctional molecule of the AbTAC strategy is a bispecific IgG that can bind simultaneously to two proteins, the single-pass transmembrane E3 ligase RFN43 and the degradation target. The bispecific IgG of this technology (Ridgway et al., 1996), is first a classical antibody selected through phage display against the RFN43, and then it is engineered to target also the POI (A. D. Cotton et al., 2021).

1.2.12 Trim- away

During adaptive immunity, proteasome-mediated degradation of the antibody-antigen complex is mediated by polyubiquitination of an Fc binding protein with an E3 ubiquitin ligase domain, the tripartite motif-containing 21 (TRIM21). The TRIM family is so called because of the presence of the N-terminal RBCC domains: a RING finger encoding the E3 ligase activity, a B-box domain, and a coiled-coil domain mediating the oligomerization. On the other side, the C-terminal part, the PRYSPRY, is fundamental for the target recognition. TRIM 21 with the sub-nM affinity for IgG is the highest-affinity antibody receptor in the human body (James et al., 2007). Acting during adaptive immunity response, it has been reported that, upon viral infection, IFNα activates the transcription of antiviral genes among which TRIM21 endogenous levels became strongly increased. Then, although many targeted protein degradation tools aim to tag the target protein with degradation signals, TRIM21 acts differently: coherently with its high affinity for ubiquitin protein, the RING E3 ligase undergoes polyubiquitination, upon antibody recognition, without transferring the ubiquitin monomers to the substrate. Thus, the autoubiquitination of TRIM21 triggers proteasomal recruitment for substrate degradation (Mallery et al., 2010). The trim-away technology is a rapid degradation tool for endogenous proteins that requires three steps: the introduction of

endogenous TRIM21, the introduction of an antibody against the POI, and the TRIM21-mediated ubiquitination before reaching the degradation (Clift et al., 2017).

The increasing interest in targeted protein degradation research can be attributed to the key advantages offered by degrader-based strategies. First, the degraders are interactors that do not require a specific binding pocket on the POI, since the perfect allosteric or competitive inhibitor generally requires a time-consuming strategy, and this can extend the feasibility of TPD to the undruggable proteins. Second, allowing for the removal of the entire POI rather than keeping it inactive, the effect of the reduction of the POI can be more pronounced and durable. On the other hand, being a bridging molecule between the POI and the E3 ligase, in the case of PROTAC requires finding the best match between the target protein and one of more than 600 different E3 ligases coded by the human genome, while most efforts in the recent 20 years have been focused on CRBN and von Hippel-Lindau (VHL). Lastly, one of the key features of the discovery process of a degrader requires the optimal experimental design to test the efficacy of the degradation activity, which requires the formation of a ternary complex to trigger the proteasomal or lysosomal activation. The ideal interaction among the POI, the degrader, and the E3 ligase resides in the balance between the concentration of these three. At high concentrations of the degrader, due to the "hook effect" the degrader can saturate the binding site on either the POI or the E3 ligase, inhibiting the formation of the ternary complex and, as a consequence, the degradation activity (Kostic & Jones, 2020).

1.3 Antibodies and antibody formats

All the previous emerging technologies reside in the necessary condition of matching two different activities on the same chimera or bifunctional protein: the recognition of the target protein, and the trigger of the degradation process. Antibodies are highly selective binders that can be potentially developed on a limitless range of protein targets; thus, an overview of their structure is necessary to introduce the tool developed in this work. Antibodies are globular glycoproteins produced and then secreted by B-cells and can recognize and to bind their antigen partner with high specificity. An antibody molecule shows a symmetrical structure composed of two heavy chains (50-70 kDa) and two light chains (23 kDa). Each antibody chain is made up of both variable (V) and constant (C) domains. The chains are linked by interchain disulfide bonds. The light chain has one constant (CL) and one variable (VL) chain, while the heavy chain presents one variable domain (VH) and at least three constant regions (CH1, CH2; CH3). The antigen-binding site of an antibody is formed by the variable regions of both the heavy

(VH) and light (VL) chains. The smallest fragment capable of retaining antigen-binding activity consists solely of these two variable domains and is called the Fv region. The Fragment antigen binding format is a monovalent region of an antibody only composed of one constant and one variable region of both the heavy and light chain. It can be obtained by proteolytic cleavage followed by a mild reduction (Abbas, et al., 2011).

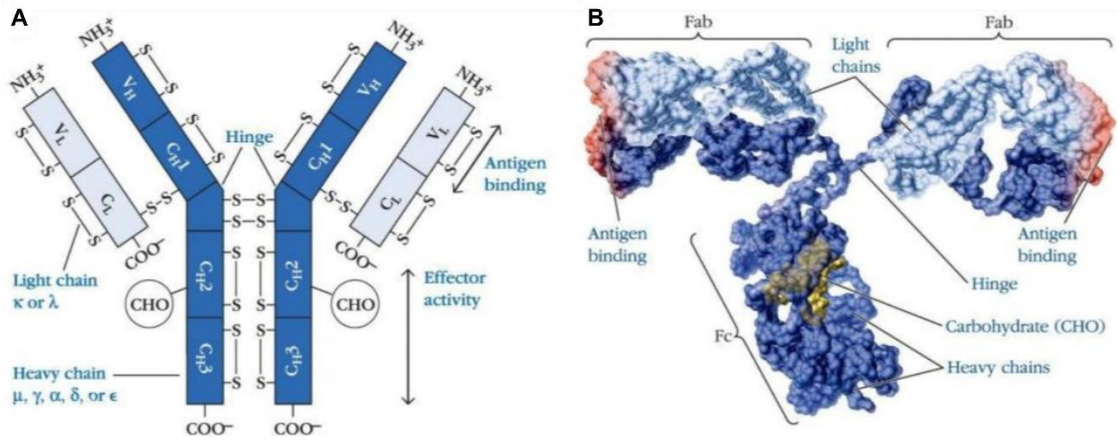

I 4 ***A) Structure of an immunoglobulin and B) 3D representation****. A) The classical "Y" shape comprises two heavy and two light domains connected by an unstructured hinge. Both the light and the heavy domains contain a variable region, VL and VH respectively. (B) Each antibody has at least two Antigen Binding regions (Fab) and an Effector domain (Fc). CDRs=Complementarity Determining Regions (Punt et al. 2019)*

The variability among different antibodies is mainly confined to the three short stretches in the V region of both the heavy and the light chains. These three diverse stretches are also known as the hypervariable region and, each of them is about 10 amino acids long. The so-called antigen-binding surface of an antibody resides in these six variable regions, three from the heavy and three from the light chain. These regions make up the region that turns out to be complementary to the antigen-binding moiety, thus, the variable regions constitute the three complementarity-determining regions (CDRs) of the antibody. Among the three CDRs, the CDR3 of both the V_H and V_L segment, is the most variable, and crystallographic analyses of the antigen-antibody complex show that most of the interaction reside in the hypervariable region, and that CDR3 contains the most extensive contact region (Abbas, et al., 2011). Beyond the antibody format, many different sub-formats have been created to maintain only the variable regions. DNA recombinant technology allowed for the creation of Fv format in 1989 when, the V_H and V_L region were separately expressed in E. coli cytoplasm, then separately transported into the oxidating environment of the periplasm that allowed for the S-S bond formation and assembly of the light and heavy chain (Plückthun & Skerra, 1989). To avoid the dissociation of the two fragments, the Fv format of Plückthun and Skerra was then improved genetically,

adding a linker between V_H and V_L sequence, thus creating a single chain antigen binding protein (SCA), nowadays known as single chain Fragment variable (scFv) (Bird et al., 1988).

Another "naturally occurring" antibody format has been discovered in camelids, representing a considerable fraction of the antibody repertoire. This format is a homodimer of heavy variable chain also defined heavy chain antibody (HCAb) shown in Figure I5 B (Hamers-Casterman et al., 1993). The H-chain within HCAbs only contains three globular domains since CH1 is missing from the Fc, consequently, the antigen-binding fragment is reduced to a single variable domain. The variable domain of HCAb is referred to as VHH but its organization is similar to the variable domain of a classical immunoglobulin. From the sequence alignment between VH and VHHs, the first difference is in the CDR1 and CDR3, which are longer in VHHs compared to VH (Muyldermans et al., 2009).

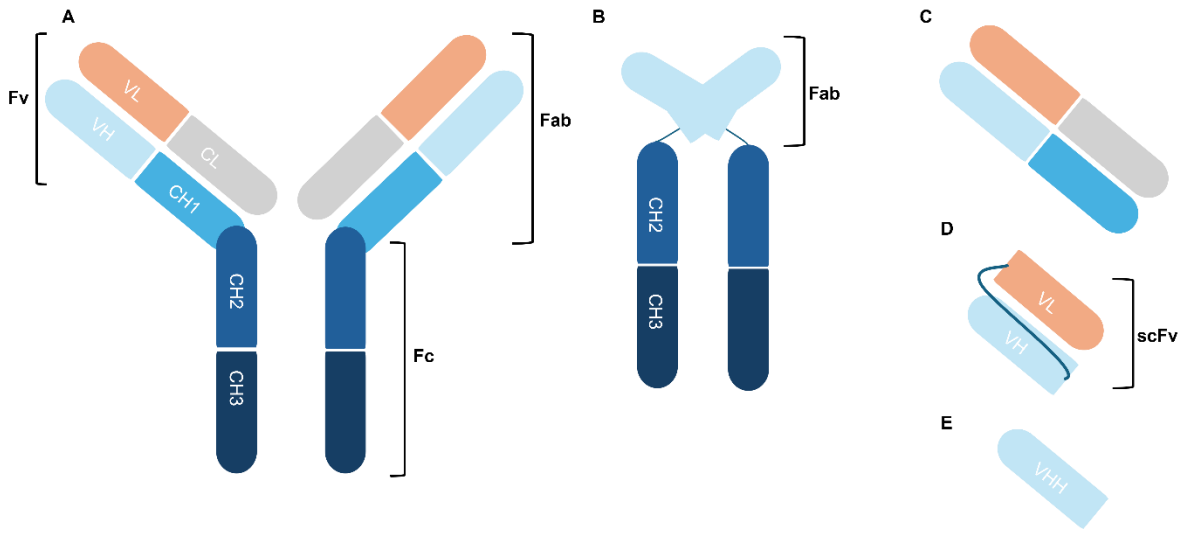

I 5 ***Antibody formats.*** ***A)*** *Complete immunoglobulin with the two constant fragments and the two antigen binding fragments.* ***B)*** *Heavy-chain antibodies are composed of the two Fc regions connected to only the heavy variable domain (VH).* ***C)*** *Fab are a single antigen binding region of the full-length antibody* ***D)*** *scFvs are composed of light and an heavy variable chain connected by a linker sequence* ***E)*** *VHH are a single heavy variable chain; adapted from (Muyldermans et al., 2009)*

1.3.1. Antibody selection platforms

The source for antibodies in the scFv or VHH format can be either the naïve, "biased" from animal immunization, or a synthetically designed repertoire of DNA libraries. For this project antibodies from *llama glaba* heavy chain antibody (VHH) naïve library (Gilodi et al., 2022) in the Single Pot Library of INTrabodies (SPLINT) format have been used (Visintin et al., 2002a; Visintin, Quondam, et al., 2004). These libraries are the input source for the display technology of antibody selection procedures. The most popular selection platform is Phage Display (McCafferty et al., 1990); briefly, the antibody fragments are displayed on filamentous phage

M13 by fusing them to pIII or pVIII coat proteins, this is done by cloning the antibody chains libraries into the phagemid vector that allows for the packaging and then the helper phage allows for the release. Phage particles exposing the antibody fragments are incubated with target proteins, which can be immobilized to the surface of a microtiter plate or an affinity column. The phages able to bind the target are then eluted and used to infect bacteria to enrich them in the phage pool. This step is repeated several times, in a process defined as "panning", and culminates in isolating the best antibody candidate (Barbas et al., 1991). Researchers often think of the antibody as a protein probe, since the efficient selection method culminates in the identification of the best antigen-binding candidate; on the other hand, during the various screening processes, antibodies from the libraries are protein-coding genes whose target-binding activity confers a phenotype, which in turn allows for the identification. Indeed, antibody fragments can be used as genes to be ectopically expressed in living cells to interact with intracellular antigens. The first example of an antibody gene was an IgM ectopically expressed and secreted by transfectants of non-lymphoid cells (Cattaneo & Neuberger, 1987). These stay-in-cell antibodies, also referred to as intrabodies, to interfere with and or interact with the intracellular antigen need to deviate from the classical secretory pathway, indeed, they are equipped with targeting sequences that redirect them to intracellular compartments. By deviating from the secretory pathway, the intracellular antibody is also excluded from the ER compartment, where immunoglobulins generally reach proper folding. Thus, the ectopic expression of an intracellular antigen-binding protein requires two conditions to be fulfilled: to be used as a protein-coding gene and to be correctly folded in the intracellular compartment (Biocca et al., 1990). In other words, the potential of intrabodies, used as genes to interact and/or interfere with cytosolic antigens, strictly depends on stability and solubility. Thus, the potential of an antibody fragment library that can code for intrabodies against any intracellular target needs to be exploited with intracellular selection methods.

1.3.2 Intracellular antibodies capture technology

The intracellular antibody capture yeast two-hybrid base technology (IACT) is an application of the two-hybrid system for the in vivo selection of functional intrabodies against various antigens using yeast cells. This technology allows isolating functional intrabodies from a gene library, and the selected intrabodies can tolerate the absence of disulfide bonds and efficiently recognize the intracellular target (Visintin et al., 2002b). Briefly, in the IACT, the L40 yeast strain is histidine-auxotrophic and cannot grow without histidine due to the absence of the HIS3 gene. L40 yeast is co-transformed with two vectors: the "prey", which carries an intrabody

clone from the antibody domain library fused to the VP16 activation domain, and the “bait”, which codes for the LexA DNA-binding domain fused to the antigen to be screened. The LexA portion binds the related operon flanking the HIS3 and LACZ genes. A positive interaction between the bait and prey triggers the expression of His3 and LacZ enzymes, allowing yeast cells to form colonies on histidine-deficient media. Cells without an antigen-intrabody interaction will not grow on the same medium. Colonies that grow on His-deficient media are tested for beta-galactosidase activity using X-Gal to confirm the interaction and avoid false positives. Colonies that are both "Double Positives" (good growth and blue color) are selected for further binding confirmation and epitope mapping. Intrabodies are then typically validated in mammalian cells and through in vitro binding assays to confirm their affinity and specificity for the target (Visintin et al., 1999, 2002).

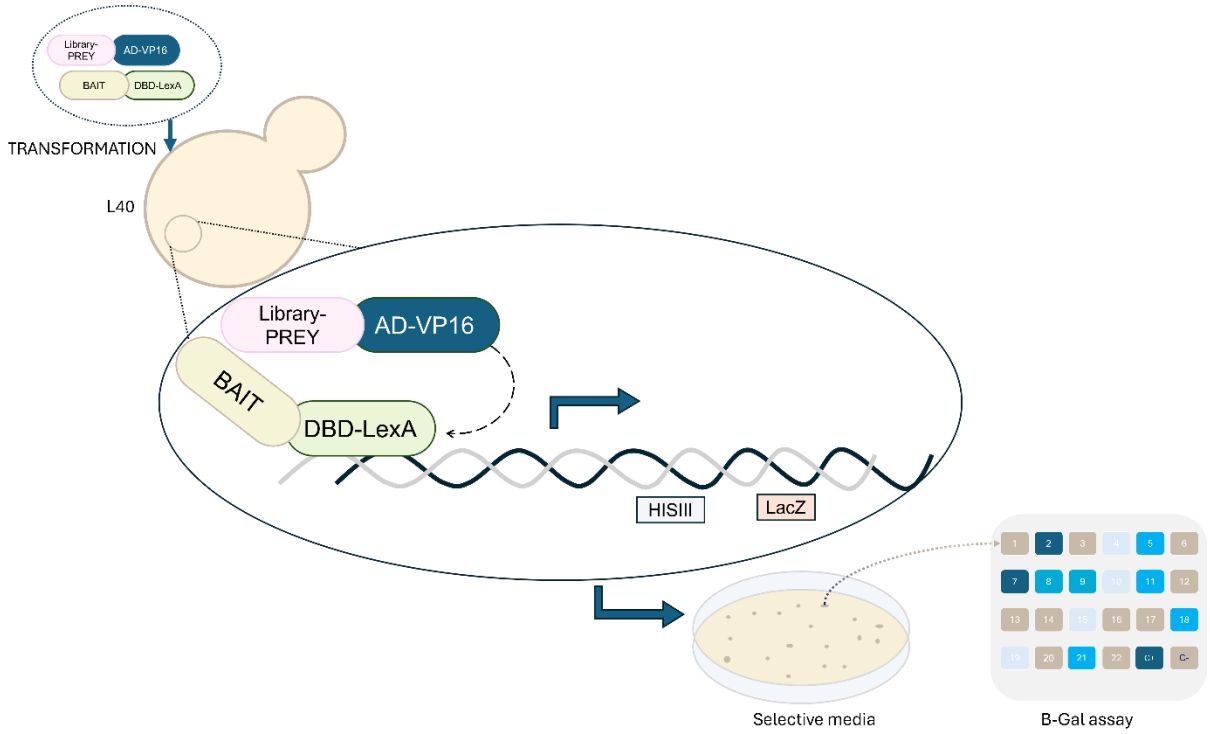

I 6 ***IACT schematic representation.*** *A library of intrabodies fused with the VP16 protein is screened against a bait (target protein) fused with the LexA protein in the L40 yeast strain. If the intrabody binds to the bait, it reconstitutes the DNA binding domain (LexA) with its activation domain (VP16). This leads to the transcription of the His3 and LacZ genes, enabling yeast cells to grow on selective media that lacks Histidine. Positive clones are identified through the β-gal assay. Double-positive clones are then subjected to secondary screening for confirmation of true positivity. Adapted from (Visintin et al., 1999)*

Although the IACT represents a valuable strategy to isolate intrabodies against a very large number of different protein antigens, an implementation of the technology arrived when it was combined with Tethered Catalysis, creating the Post Translational Intracellular Silencing Antibodies (PISA) Technology (Chirichella et al., 2017). Briefly, tethered catalysis is another

yeast two-hybrid system application in which the protein interaction requires a post-translational modification (PTM) of the bait protein (Guo et al., 2004). This constitutive modification of the protein to be screened for interactions is achieved by fusing it to its cognate modifying enzyme, allowing in vivo catalysis due to their physical linkage. PISA technology leverages this approach by combining the yeast two-hybrid-based intrabody selection system with enzymatic modification of the antigen, typically phosphorylation or acetylation, to enable the isolation of intrabodies specific for PTM-bearing target proteins.

1.4. Intrabody-based degradation tools

An intrabody-based tool designed to trigger and modulate target protein degradation in a stimulation-dependent manner can be better understood through the lens of the various modules involved in achieving this complex function. The key feature of these tools is their heterobifunctionality, in other words, their ability to bind the target protein and activate the degradation pathway. If the binding capacity of an intrabody-based tool is undoubtedly the major advantage of such a tool, all the variants I will briefly illustrate can differ depending on the degradation system activated and the stimulus selected to modulate them.

1.4.1 Proteasome-directed intrabodies

An intrabody with its antigen binding capacity but retargeted to the degradation pathway is, in other words, a new version of the intracellular antibody with a shorter half-life. Once validated that the lifespan of a protein could be affected by modifying its amino acid sequence, by adding specific regions (X. Li et al., 1998), the next step was the creation of a degradation-pathway directed intrabody. The scFv-13R4 anti-β-galactosidase enzyme represents the first example of a proteasome-targeting intrabody. The intrabody was modified with the addition of selected degron, which was the proline (P) glutamic acid (E) serine (S) and threonine (T) rich regions typical of the short-lived proteins (Sibler et al., 2005). Then, in December 2011 David C. Butler and Anne Messer developed a bifunctional intrabody against a protein involved in neurodegeneration, the huntingtin protein (htt). Huntington's disease, caused by the CAG expansion on htt1 exon, results in misfolding and formation of nuclear and cytoplasmic inclusions of huntingtin protein. The transgenic mice model for HD's (HDR6/1) underwent a reduction in size and number of aggregates upon intrastriatal delivery of the adeno-associated virus vector (AAV2/1) coding for the intrabody scFv-C4 anti-N-terminal of htt. However, this protective effect against nuclear and cytosolic inclusions was observed to diminish over time after the injection. Thus, to enhance the phenotypic effect, an evolution of the scFv-C4 was

proposed: the addition of the PEST rich sequence to the intrabody. The resulting proteasome-directed intrabody was the scFv-C4 fused to the PEST in the C-terminal domain of the mouse Ornithine decarboxylase enzyme (Butler & Messer, 2011).

When the intrabody-based approach was combined with the most widely studied strategy in the targeted protein degradation field, the PROTACs, a new concept known as bio-PROTACs was introduced. This approach fuses an intrabody to the Fc domain of IgG, creating a chimeric protein that can bind the antigen and is recognized by the tripartite motif-containing protein 21 (TRIM21) (please see section 1.2.12). The degradation mechanism resides in the interaction between TRIM21 and the RING E3 ligase and allows for targeted protein degradation of the intrabody-Fc complex bound to its antigen. The first bio-PROTAC was developed against Human antigen R (HuR), a ubiquitously expressed RNA-binding protein that functions as a key post-transcriptional regulator of gene expression (Fletcher et al., 2023).

1.4.2 Light-switchable proteasome targeting-degron domain

The first bio-PROTAC and the intrabody C4 anti-Htt described in the previous section both exemplify bifunctional intrabodies that bind their target antigen and facilitate its degradation via the proteasome. This is achieved either through the ubiquitination pathway activated by the bio-PROTAC (section 1.1.1a), or via the most extensively studied degron for this pathway, in the case of the C-terminal region of mODC1 (section 1.1.1c). A further implementation of the mODC1 degron was then reached by Renicke and collaborators with the addition of a stimulus-dependent modulation domain to obtain an inducible and reversible photosensitive degron (psd) domain activated by blue light (Renicke et al., 2013).

The psd module resulted from the fusion between a Light Oxygen Voltage (LOV) domain from CRY2 phototropin protein and the mODC1. LOV domains were first identified during the study of plant phototropism, that is, the ability to grow in the direction of blue light exposure. The phototropins were the first light-responsive proteins to be studied in plant growth in the direction of light stimulation. Thus, the three elements: light stimulus, photosensitive proteins, and effector functions, were the required conditions for the emergence of the optogenetic field. The combination of optical and genetic methods was first applied in neuroscience to modulate with light specific neuronal functions with genetically encoded photosensitive proteins (Deisseroth, 2011).

Phototropism depends on a signaling pathway in which a key role is played by the protein encoded by the nonphototropic hypocotyl 1 (NPH1) gene. In the N-terminal portion of the NPH1 protein of Arabidopsis thaliana, beyond the serine-threonine kinase domain, two sequences with 43% identity and 61% similarity were found, namely Light Oxygen Voltage domains 1 and 2 (Huala et al., 1997). Later, LOV domains were located in the Per Arnt Sim (PAS) subfamily, which is present in all three kingdoms of life: Bacteria, Archaea, and Eukarya. The PAS acronym includes three different motifs and is composed of the names of the proteins in which each motif has been first identified. Specifically, these include the Drosophila period clock protein (PER), the vertebrate aryl hydrocarbon receptor translocator (ARNT), and the Drosophila single-minded protein (SIM) (Möglich et al., 2009). LOV domain proteins are distributed across all range of taxa, and LOV domains are mainly located at or near the N-terminus of the protein. These LOV proteins can be divided into five different categories based on their function: phototropins, proteins regulating circadian rhythms, LOV histidine kinases, LOV Sulphate Transporter AntiSigma-factor antagonist proteins (LOVSTAS), and LOV phosphodiesterases (Crosson et al., 2003). The LOV domain functions as a flavin-binding site; the FMN, on the other hand, acts as a sensor for environmental stimuli such as light or oxygen (hence LOV)(Huala et al., 1997). The secondary structure of the LOV domain consists of five anti-parallel β-sheets and two α-helices, which tightly enclose the FMN cofactor. When exposed to blue light, LOV domains enter a reversible photocycle characterized by the formation of a thiol adduct between the C4a position of the FMN's isoalloxazine ring and a conserved cysteine residue in the protein. Once it reaches the light-activated state, it decays back to the dark state within tens to thousands of seconds, depending on the biophysical origin of the LOV domain (Christie et al., 2012). The significant innovation arising from the light modulation of a degradation sequence, coupled with the reversibility of the tool, can mark a breakthrough in the development of a modulable and reversible TPD process. Moreover, it opens a new frontier for the use of optogenetics for protein knockdown studies with time and spatial control.

1.4.3 Intrabody-mediated targeted degradation and its modulation

Functionalizing intrabodies with the addition of a degron domain offers a promising strategy for retargeting their intracellular activity. Thanks to their high antigen-binding specificity, intrabody-degron chimeras can be used to study protein function at the protein level or to degrade disease-relevant, undruggable proteins. However, while this approach holds great

potential, developing a universally applicable in vitro cellular system for achieving targeted protein degradation and studying loss-of-function or phenotypic rescue remains a challenge.

1.4.3a Autophagy-targeting intrabody

One way of escorting a protein to degradation is the lysosomal pathway, which preferably refers to extracellular substrates or transmembrane proteins, as previously described. Nevertheless, lysosomal degradation can be applied to an intracellular target protein if the intrabody is modified with an autophagy activation domain or sequence. He and collaborators in 2023 created an autophagy-targeting module fused to a nanobody fragment that is composed of the intrabody sequence equipped with LC3 interacting region (LIR) of the C-terminal of ATG4B protein (DSEDEDFEILSL), since LC3 protein is a key marker in autophagy and localizes to preautophagosomal structures (PAS) during autophagosome formation. The first version of the autophagy-targeting nanobody chimera ATNC allowed for the targeted degradation of anti-GFP nanobody, and then the autophagy-targeting module was transferred to other Nbs against human epididymis protein 4 (HE4), to apply the autophagy-dependent degradation on a disease-relevant protein. The evolution of this system towards the modulation of the activity was reached by combining the chemically induced proximity (CIP) to the ATNC. Briefly, the ATNC was split into two chimeras, the nanobody portion fused to the abscisic acid (ABA) insensitive complementary surface (ABI_{cs}) and the LIR region fused to the pyrabactin resistance-like complementarity surface (PYL_{cs}). The ABI_{cs} and the PYL_{cs} cannot interact in the absence of ABA. However, upon the addition of ABA, the PYL_{cs} undergoes a conformational change that creates a binding surface that leads to an increase in the affinity to ABI_{cs}. Thus, in a CIP-controlled fashion, the target antigen-bound nanobody then interacts with LIR, resulting in the recruitment of the antigen for degradation (He et al., 2023).

1.4.3b Ligand-modulated proteasome-targeting intrabody

An evolution of the PEST-sequence equipped intrabody is then proposed with the idea of conjugating the intrabody domain directly to a ubiquitinable protein rather than a chimeric ubiquitination enzyme. The proof of principle of this paradigm was proposed in 2007 with the creation of the “suicide” intrabody, whose targeted degradation was also made inducible by a ligand-dependent activation of the degradation signal. The idea of this alternative defined silencing intrabody resides in the fusion with the ubiquitin-proteasome pathway substrate IkBα protein (Melchionna & Cattaneo, 2007). The IkBα protein belongs to the IkB class of inhibitors of NF-kB inducible transcription factor family. IkB family includes IkBα, IkBβ, and IkBε, and

the inhibition of NF-kB is mediated by binding it in the cell cytoplasm, preventing it from migrating into the nucleus. The IkBs contain two serine repeats at the N-terminal domain (DSGXXS); upon stimulation, these residues can undergo phosphorylation, which triggers their ubiquitination and the recruitment of the 26S proteasome(Zinatizadeh et al., 2021). The discovery of phosphorylation-dependent degradation of IkBs led in turn to the identification of the kinases responsible for it. The IK kinases (IKK) family includes IKKα, IKKβ kinases and NEMO, a regulatory enzyme. The so-called canonical activation of NF-kB strictly depends on NEMO, while the non-canonical activation is activated by a restricted group of stimuli, among which the activation of TNFα receptor (TNFR) by its extracellular ligand(Hinz & Scheidereit, 2014). The use of IkBα as a degron fused to the intrabody sequence and TNFα as inducer allowed the creation of a ligand-inducible proteasome targeting intrabody, and the first application of this paradigm was represented by the scFv#2 anti-Tau protein (Melchionna & Cattaneo, 2007).

1.5 TPD mediated by intracellular antibody application and perspectives

To the moment of writing this thesis targeted protein degradation has been applied on targets relevant for autoimmune disorders (Cao et al., 2020), cardiovascular diseases (Kargbo, 2019), infectious disease (De Wispelaere et al., 2019) and neurodegenerative diseases (W. Wang et al., 2021). In the neurodegenerative field there are many examples of intracellular antibodies applied as degradative tools to either reach a phenotypic rescue with the removal of the neurodegeneration-related target, in the case of Tau protein (Gallardo et al., 2019), and to further interfere with pathological processes such as misfolding and aggregation of α-synuclein (Chatterjee et al., 2018) and Huntingtin protein (Butler & Messer, 2011).

Collectively, these technologies aim to evolve into a new form of immunotherapy, where the "immune" aspect focuses on harnessing the antibody domain to directly target neurodegenerative-related molecules, rather than solely triggering an immune response against the neurodegeneration process.

Regardless of the potential use as a therapeutic strategy, targeted protein degradation (TPD) can even go beyond the therapeutic strategy; it can be a powerful research tool for understanding physiological processes. By selectively degrading a protein of interest (POI), researchers can directly interfere with its function, gaining insights into the biological processes

it regulates. This approach enables a deeper understanding of how disrupting a specific protein affects corresponding physiological pathways.

The greater potential for TDP that cannot be addressed with gene-based or mRNA-based interference approaches is related to the possibility of targeting post-translationally modified POI or conformational subsets of a POI. This is particularly relevant for neurodegeneration.

Neurodegenerative disorders can arise from genetic mutations that lead to loss-of-function, but the majority of cases are sporadic. In other words, the disease-causing protein is a wild type, physiological protein whose proteostasis the balance of its synthesis, folding, and degradation fails, resulting in misfolding and accumulation within neuronal cells.

When applied to neurodegeneration, which is often protein-specific, TPD can offer a critical means of studying mechanisms such as protein misfolding and aggregation. While therapeutic strategies using intracellular antibodies aim to target disease-related proteins, understanding the mechanisms behind these pathological changes is equally important. By promoting the degradation of misfolded proteins, TPD can advance our understanding of neurodegenerative diseases and pave the way for future therapeutic approaches.

1.6 Targets for intrabody-mediated protein degradation used in this work

1.6.1 VHH5-anti TDP-43

One intrabody used in this work, the VHH5, selected in our laboratory, targets the TDP-43 protein (Gilodi et al., 2022). The trans-activation response DNA-binding protein of 43 kDa (TDP-43) is widely expressed and highly conserved across mammals and invertebrates. TDP-43 consists of an N-terminal domain (NTD; residues 1–103), two RNA recognition motifs (RRM1 and RRM2; residues 104–200 and 191–262), and a C-terminal domain (CTD; residues 274–413). The two RRMs have been shown to bind UG/TG rich DNA/RNA regions having a role in transcriptional repression, pre-mRNA alternative splicing, and translational regulation (Jo et al., 2020). Although TDP-43 is primarily localized in the nucleus under normal conditions, its physiological function involves shuttling between the nucleus and cytoplasm.

However, in pathological states, mislocalization and cytoplasmic accumulation of TDP-43 become key features of several neurodegenerative diseases, including Amyotrophic Lateral Sclerosis (ALS) and Frontotemporal Lobar Dementia (FTLD). TDP-43 aggregation and neuropathology have been identified in a range of neurodegenerative disorders, collectively

referred to as TDP-43 proteinopathies, indicating that TDP-43 plays a central role in the pathogenesis of neurodegenerative diseases (Cohen et al., 2011). While certain mutations in the nuclear localization sequence (NLS) within the NTD lead to the cytoplasmic mislocalization and aggregation of TDP-43, the majority of TDP-43 proteinopathies are sporadic rather than genetically driven (Jo et al., 2020).

1.6.2 ScFv-p231-p235 anti-phosphorylated Tau

The microtubule-associated protein tau gene, MAPT, composed of 16 exons on chromosome 17q21, codes for the human tau protein, which plays an important role in microtubule assembly and stabilization. In the adult human brain, six different tau isoforms are expressed, mainly in the neuronal cells, but low levels of tau proteins are also present in the glia. The longest tau isoform comprises two near-amino-terminal inserts (N) and four carboxy-terminal repeat domains (R). Misfolding, mislocalization, and aggregation of Tau isoforms are the hallmarks of a group of neurodegenerative diseases called tauopathies (Y. Wang & Mandelkow, 2016). The tauopathies can be classified as primary, if the tau contribution is the main driving cause of the disease, as in the case of progressive supranuclear palsy (PSP), corticobasal degeneration (CBD), and Pick's disease (PiD). The secondary tauopathies are mainly represented by Alzheimer's Disease (AD) and are caused by amyloid-β (Aβ) plaques, but tau proteinopathy remains a key feature. Moreover, tauopathies can be classified based on the composition of the phosphorylated tau protein in insoluble aggregates, which varies depending on the tau isoforms present, with the 3R and 4R resulting in the most represented isoforms in frontal and grey matter (Lantero-Rodriguez et al., 2024).

Thus, the phosphorylated form of tau must be selected as the target if the aim is to specifically interfere with tau-related pathological processes. To this end, the intracellular antibody used in the second part of this thesis is an scFv designed to target the phosphorylated tau protein (Shih et al., 2012).

1.6.3 Activity-regulated cytoskeleton-associated protein

To fully leverage the potential of targeted protein degradation, not only for pathological targets but also for physiological ones, the activity-regulated cytoskeleton-associated protein (Arc) is a key candidate, particularly when considering neuronal-specific activity. Arc mRNA is transcribed in response to synaptic activity and subsequently transported to the activated spines for local translation. Although the structure of full-length arc has not been resolved yet, a

detailed description of its regions can be provided by dividing the sequence into N- and C-terminal domains. The monomeric full-length Arc adopts a compact conformation (Figure I7), in which the oppositely charged N-terminal domain (NTD) and CTD are juxtaposed, bridged by a flexible linker. The NTD includes two coiled coils and carries a positive charge that is likely responsible for the association of Arc with phospholipid membranes, RNA, or microfilaments. The different functions of the protein are likely related to its various forms and environments, including free monomeric Arc, Arc associated with membranes, endosomes, actin filaments, or nuclear bodies, as well as virus-like Arc capsids (Hallin et al., 2018). The C-terminal domain is composed of two lobes, the N-lobe and the C-lobe, which share structural similarity (W. Zhang et al., 2015).

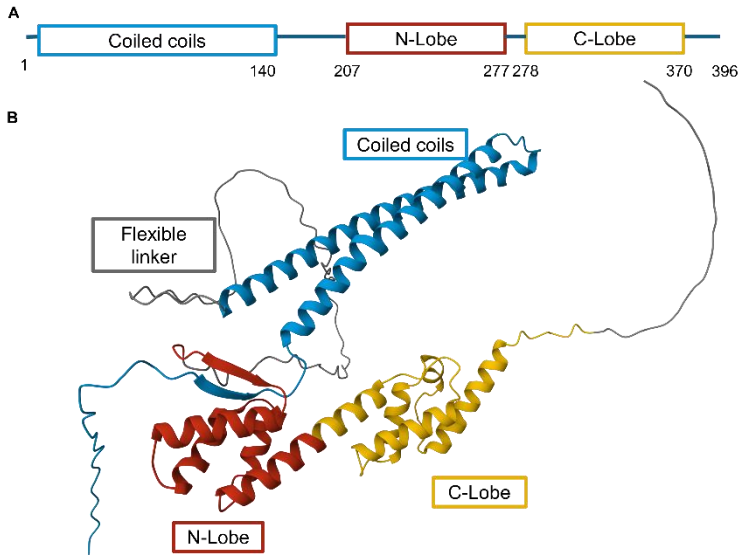

I7 ***Representation of human Arc protein****. **A)** Arc sequence, **B)** Alpha fold 3 prediction of the Arc protein. NTD aa 1-140 (blue), the CTD is composed of N-Lobe (red) and C-Lobe (yellow). Image adapted from (Hallin et al., 2018), representation from the Alfa fold server.*

The molecular mechanisms governing learning and memory processes are heavily dependent on Arc protein function. Although a detailed discussion of memory processes and the brain regions involved is beyond the scope of this work, a brief overview is warranted. Synaptic plasticity is defined as the activity-dependent modulation of both the efficiency and strength of synaptic transmission. In other words, the relationship between stimulation and synaptic plasticity is closely tied to the intensity and frequency of the stimuli. Long-term potentiation (LTP) is the long-lasting increase in the synaptic strength identified as a consequence of a high-frequency stimulation (HFS) protocol applied to the hippocampus (Bliss & Lømo, 1973). LTP has been categorized into two phases: early LTP, which relies on existing proteins, and late

LTP, which depends on *de novo* protein synthesis (Reymann & Frey, 2007). The immediate early genes (IEGs) code for the pool of proteins that are synthesized after LTP induction in stimulated neurons and play a crucial role in LTP maintenance. The activity-dependent IEG Arc is transcribed upon stimulation and then transported to the stimulated dendrites to be locally translated, modulating synaptic structure and strength (Korb & Finkbeiner, 2011). Once translated locally in the dendritic cleft, Arc is known to downregulate synaptic AMPA-type glutamate receptors by promoting their endocytosis. However, the precise binding partners and regulatory mechanisms connecting Arc to AMPA receptor trafficking remain unclear (W. Zhang et al., 2015).

One approach to study the role of Arc in synaptic plasticity involves using antisense oligodeoxynucleotides (ASODNs) to knock down Arc protein. This method has been shown to disrupt the maintenance of LTP (Messaoudi et al., 2007). Therefore, given that the translated Arc protein plays a crucial role in memory consolidation, interfering directly with its function at the protein level could be achieved using intracellular antibodies, offering a potential alternative strategy to oligonucleotide-based approaches.

2. Aim

This work aims to address targeted protein degradation by equipping intabody target binders with a degradation signal. We propose intracellular antibodies as the selected antigen binders to be modified with a degron able to trigger the ubiquitin-independent proteasome-mediated degradation, thereby facilitating the targeted degradation of proteins involved in both pathological and physiological neuronal processes. To fully exploit the antigen-binding potential of an intrabody-based degradative tool, this work seeks to develop a modulable system that can be activated upon stimulation. Ideally, this system would allow for target recognition and subsequently escort the antigen-intrabody complex to the proteasome machinery for degradation. While the inducibility of the process is a critical aspect of the design of the tool, its reversibility remains equally important. The reversibility of the system ensures recyclability, allowing for the retargeting of the intrabody once the light activation has occurred.

To achieve this, I applied the intracellular antibody capture technology (IACT) developed in our lab to explore targeted protein degradation of TDP-43, using VHH5. I then applied the technology to a phospho-specific intracellular antibody targeting the phosphorylated form of Tau protein. In the last part, the aim was to apply the optobody format to a newly isolated intrabody targeting the Arc protein.

Aim 1: Develop an intrabody-based light-activable tool to degrade TDP-43

1. The photosensitive degradation domain was applied to the intrabody sequence to obtain the retargeting of the intrabody to the degradation pathway
2. The L40 yeast strain was chosen to set the conditions for the proof of concept of targeted protein degradation mediated by intracellular antibodies.
3. Light-induced degradation of TDP-43 was tested in higher cellular systems, the mammalian HEK293T cells
4. Finally, the last part aimed to correlate the targeted protein degradation of mislocalizing TDP-43 with variation of the TDP-43-dependent global translation pattern

Aim 2: Targeted protein degradation of post-translationally modified proteins involved in neurodegeneration, such as the case of phosphorylated Tau protein.

1. Validation of tau protein degradation in yeast cells.
2. Assessment of the phosphorylation status of tau protein affected by degradation.

Aim 3. Targeted protein degradation of physiological targets, the activity-regulated cytoskeleton-associated protein (Arc)

1. Selection of Llama VHH anti-Arc protein using intracellular antibody capture technology
2. Epitope mapping of the selected candidate
3. Validation of the in vitro interaction of the candidate VHH in mammalian cells
4. Targeted protein degradation in mammalian cells

Aim 3.1

5. Targeted protein degradation of endogenous Arc protein in mouse ESCs transduced for the expression of intrabody-based anti-Arc tool.

3. Materials and methods

Part I

3.1.1 Plasmids

pMicBD1 (Visintin, Meli, et al., 2004)

pLinker220 (Visintin, Meli, et al., 2004)

pP2A-mCherry-N1 (Addgene #84329)

pCI-neo (Genebank #U47120.2)

scFv-express (Persic et al., 1997)

pDS142 -AtLOV2-K121M N128Y G138A-cODC1 Dr. Christof Taxis (Universität Marburg) (Usherenko et al., 2014)

Table 1 Schematization of the constructs and the vectors.

** Modified version of the p-P2a-mCherry-N1 lacking the mCherry protein*

Promoter	Construct	Vector	Expression system
ADH1	LexA-Bait	pMicBD1-2	L40
ADH1	Prey-VP16	pLinker220	L40
ADH1	Optobody	pLinker220	L40
CMV	MYC-Target	p-P2a-mcherry	Mammalian cells
CMV	MYC-Target-p2a-HA-Optobody	*p-P2a-m-cherry	Mammalian cells

3.1.2 Constructs

- YFP-HA-AtLOV2 (- K121M N128Y G138A) -cODC1
- LexA-TDP43
- HA-VHH5
- HA-VHH5-AtLov2(K121M N128Y G138A) -cODC1
- HA-VHH5-Ikβ
- MYC-TDP43
- MYC-TDP43-NLS1 mut (K86S-R87S-K88S)
- MYC-TDP43-P2A-HA-VHH5-AtLov2-cODC1
- MYC-TDP43-P2A-HA-VHHantiGFP-AtLov2-ΔODC1
- MYC-TDP43-P2A-HA-VHH5-AtLov2-ΔcODC1
- MYC-TDP43-P2A-HA-VHH5-AtLov2-Δjα-cODC1
- MYC-TDP43-NLS1 mut (K86S-R87S-K88S) -P2A-HA-VHH5-AtLov2-ODC1
- HA-VHH5-Ikβ
- MYC-TDP43-P2A-HA-VHH5-Ikβ

3.1.3 PCR protocols

All the cloning was performed through DNA assembly protocol. The fragments were amplified by PCR reaction with Q5 polymerase (NEB #M0491) and all the PCR products were then

assembled using NEBuilder® HiFi DNA Assembly Master Mix (NEB #E2621).
The PCR reactions have been prepared as shown in the following table.

Table 2: PCR reaction mix

REAGENT	FINAL CONCENTRATION
dNTPs	200µM
Q5 buffer	1X
Q5 polymerase	0,02 U/µL
Forward primer	0,5 µM
Reverse primer	0,5 µM
Template	1 ng/µL
H_2O	to 25 µL

The thermocycling conditions for the reaction are the following:

Table 3: PCR thermal profile

STEP	TEMPERATURE	TIME	N° of cycles
Initial denaturation	98°C	30''	1
Denaturation	98°	5-10''	25-35
Annealing	50-72°C	10-30''	
Extension	72°C	20-30''/kb	
Final extension	72°C	2'	1
Hold	4° C	∞	1

The length of PCR fragments has been checked through agarose gels. The purified bands (QIAGEN Gel Extraction Kit/ ID: 28704) have been used for the DNA assembly reaction.

3.1.4 Gibson assembly

The PCR product mixture to obtain the DNA assembly reaction was calculated considering the ratio between the fragments; in most cases, the ratio used has been 1:2 for three fragments of the Gibson assembly and 1:3 for two fragments of the Gibson assembly reaction. The total amount of DNA (0.02 -0,5 pmol) is then diluted 1:2 in 2X Gibson assembly Master Mix. The DNA assembly reactions were performed for 1h at 50°C.

3.1.5 *E.coli* competent cell transformation

Assembled DNA was transformed into DH5α competent cells using the heat shock protocol. 5 µL of assembled DNA was incubated with DH5α competent cells for 30'' on ice. Then, heat shock is performed for 90'' at 42°C. Then, LB broth is added to the cells, and the cells are

incubated for 1h at 37°C. Cells were then plated onto selective plates. Plates were then incubated at 37 °C overnight.

3.1.6 Colony PCR

The day after, the colonies were used as a template for colony PCR screening; the same colonies were re-streaked onto a new plate and left in the incubator at 37°C.
The primers for the colony PCRs anneal to the ends of the fragment inserted into the vector. The PCR reaction was added to the CFU dissolved in 10 µL in H_2O: 200 µM dNTPs, 1X GoTaq buffer, 0,25 µL GoTaq polymerase (Promega #M3001), 0,4 µM Forward primer, 0,4 µM Reverse primer, H_2O to a final volume of 10 µL.

Table 4: Colony-PCR thermal profile

STEP	TEMPERATURE	TIME	N° of cycles
Initial denaturation	95°C	30''	1
Denaturation	95°	10''	20-30
Annealing	50-72°C	30''	
Extension	72°C	1'/kb	
Final extension	72°C	5'	1
Hold	4° C	∞	1

On the following day, the positive colonies were picked from the re-streaked plate and inoculated into LB medium, supplemented with the right antibiotic, at 37°C overnight. Minipreps of the inoculated samples were carried out with the appropriate kit (Promega A1223), according to the manufacturer's instructions. The extracted plasmid was then quantified, and the cloned region was confirmed by sequencing. Glycerol stocks of the positive confirmed bacteria colonies (1 mL of overnight culture of the colony and 500 µL of 100% glycerol) were then stored at 80°C.

3.1.7 Yeast transformation

Table 5: Media for yeast transformation

COMPONENT	CODE	YNB	YPD
Yeast nitrogen base	SIGMA # Y-125	1,2 g/L	-
yeast extract	BD # 211931	-	10 g/L
bacto peptone	BD # 211840	-	20g/L
2% D-glucose	SIGMA # G-7021	-	20g/L
bacto-agar	BD # 214010	20g/L*	20g/L*

*bacto-agar is added to obtain solid plates.

All media are autoclave sterilized for 15' at 121°C

1L of YNB media was supplemented as shown in Table 6.

Table 6: Selective media for L40

	CODE	**-W**	**-L**	**-WH**	**-WL**	**-WHL**
YNB	SIGMA # Y-125	800 mL	800 mL	800 mL	800 mL	800 mL
Salts	*	150 mL	150 mL	150 mL	150 mL	150 mL
AA. mix	**	10 mL	10 mL	10 mL	10 mL	10 mL
W (5g/L)	SIGMA #T0254	-	10 mL	-	-	-
H(10g/L)	SIGMA #H5659	10 mL	10 mL	-	10 mL	-
L (10g/L)	SIGMA #L8000	10 mL	-	10 mL	-	-
H_2O	-	20 mL	20 mL	20 mL	20 mL	20 mL

*SALTS:

5.4g NaOH (SIGMA #567530), 10g succinic acid (SIGMA # S-7501), 5g ammonium sulfate (SIGMA # 09980), 22g D-glucose (SIGMA # G-7021). H_2O is added to 100 ml to dissolve the components one by one; then H_2O is to the final volume of 150 mL.

**Amino acid mix:

5.8 g NaOH,1g Adenine hemisulfate salts (SIGMA#A-9126), 1g L-Arginine HCl (SIGMA #A-5131), 1g L-Cysteine (SIGMA # C-6852),1g L-Threonine (SIGMA # T-8625),0.5 g L-Aspartic acid (SIGMA # A-4534), 0.5 g L-Isoleucine (SIGMA # I-2752), 0.5 g L-Methionine (SIGMA # M-9625), 0.5 g L-Phenylalanine (SIGMA # P-2126), 0.5 g L-Proline (SIGMA # P-038), 0.5 g L-Tyrosine (SIGMA # T-3754), 0.5 g L-Serine (SIGMA # S-4500). Dissolved in 80 mL H_2O.

Yeast Transformation reagent stocks

Table 7: Yeast transformation reagent stocks

REAGENT		STOCKS CONCENTRATION	CODE
Polyethylene glycol		50%	SIGMA # 95904
Lithium acetate dehydrate		1M pH 7.5	SIGMA # L-6883
10XT.E.	TrisHCl	100 mM pH7.5	SIGMA #93362
	EDTA	120 mM	SIGMA #03620
DMSO		100%	SIGMA #D8418
Salmon testis DNA		2 mg/mL	Roche # 1467140

LiOAc transformation protocol can generate more than 10^6 transformants. It can be used to create stable yeast lines and for the initial transformation of the bait plasmid. The following protocol is a modification of Visintin *et al,* 2004. A single colony of L40 yeast strain is inoculated in YPD media and kept shaking at 220 r.p.m at 30°. The day after, the OD600 of the overnight culture is measured, and the culture is diluted to an OD600 of 0,3 is inoculated in the appropriate volume of YPD medium. When the culture reaches an OD600 of 0.6, the culture is ready to be transformed. The pelleted culture (1000 G 5' RT) is first resuspended in sterile water and then, after a second centrifugation (1000 G 5' RT) is resuspended in 1XLiOAc-1XTE, 100µL for each transformation. In LiOAc-TE, the cells are stable for 1h up to 24h at 4°C. Each transformation reaction requires the DNA-STD mixture (100 ng of denatured salmon sperm DNA denatured at 100°C for 10 min and 200 ng of bait plasmid). 100µL of cells in LiOAc-TE can be mixed with 50µL of DNA STD mixture, and the mix is vortexed for 30'' before the addition of 600 µL of freshly made TE-PEG-LiOAc. The transformation reaction is then incubated at 30°C, shaking at 220 r.p.m. After the incubation, 70µL of DMSO is added and gently mixed to the reaction, and then the reaction undergoes heat shock with a step at 42°C for 15' and then 0° 2'. At the end of the heat shock, the transformation reaction mixture is removed by centrifugation (3000 G 5') and the pellet is resuspended in 1X TE (100 µL for each transformation) before plating onto selective media. In three days at 30°C, colonies will appear and will be ready to be checked for expression. These plates are stable for a week if stored at 4°C and sealed with parafilm. From the transformation plate, single clones are picked and re-streaked onto a new plate, called the master plate, to be tested for the expression of the protein. Once the expression of the target protein from the transformed yeast strain is confirmed, the selected clone from the master plate is used to prepare a glycerol stock of the culture.

3.1.8 Protein extract from yeast cell culture

Lysis buffer: 1X Tris-HCl-EDTA, 1X Protease inhibitor (Sigma-Aldrich #11836170001), 0,3mg/ 10 mL yeast culture pellet, Acid-washed glass beads (SIGMA #G8772).

Yeast cells were grown on selective media up to OD 0.6, shaking at 225 rpm, 30°. Cells were then ready to be centrifuged at 3000 G 5' RT. The pellet is resuspended in 1X TE with Protease inhibitor and kept on ice. To break the cells, 0.3 mg of glass beads are added to each 100µL of resuspended pellet, then, 10 cycles of vortex for 10 sec and ice for 10 sec are performed. After the last cycle, the sample is moved into a new tube, and Triton-x100 is added to a final concentration of 2%. The sample is then vortexed and centrifuged at 1400 G for 10 min at 4°C. The supernatant is then ready for SDS-PAGE.

3.1.9 Mammalian cell culture and transfection

HEK293T (ATCC) are grown in DMEM complete medium: 87% DMEM (Euroclone #ECM0060), 10% FBS (Euroclone #ECS0172L), 1% Penicillin,1% Streptomycin, 1%L-glutamine, at 37°C, 5% CO_2.

HEK293 T cells were transfected using Effectene Transfection Reagent (Quiagen ID: 301425). Cells at 80% of confluence were plated the day before the transfection. The amount of DNA used in each transfection must respect the ratio 1µg DNA:8 µL Enhancer, and the DNA effectene ratio used in all the transfections has been 1:25. 24h after the transfection, cells were split into 3.5mm cell culture dishes. 48 hours after the transfection, each plate has been treated with blue light, and one of them is kept in a dark condition.

3.1.10 Soluble fraction protein extraction method

After blue light stimulation protocols, cells were collected and resuspended in PBS1X and centrifuged at 1200 G for 5 mins RT. The pellet was then resuspended in RIPA buffer (150mM NaCl,50 mM Tris HCl pH 7, 1% NP-40 ,0,5% Na-deoxycholate, 0,1% SDS, 1mM EDTA) with PI 1X in PBS (Roche #11873580001). The resuspended pellet was pipetted repeatedly every 10 minutes for 1 hour on ice to break the cells. Then, the samples were sonicated for 3 sec on ice. After sonication, samples are centrifuged at 14000 G for 20 min at 4°C. The supernatant represents the soluble part, which is ready to be quantified with the Bradford assay (Biorad #5000006).

3.1.11 Insoluble fraction protein extraction method

The pellet resulting from the centrifugation described above is ready to be washed in RIPA buffer to undergo the treatment in Urea buffer (7M Urea in PBS 1X, 1% SDS) on a thermomixer at RT 800-900 rpm for at least 2h to overnight. The day after, the sample is directly boiled in Laemmli buffer or quantified through the BCA assay (Thermo-Fisher # 23225).

3.1.12 Immunoprecipitation

The soluble protein extract was used to check for the binding between the intrabody and the target in co-immunoprecipitation experiments. Anti-HA agarose beads (Thermo Scientific # 26181) were incubated with blocking solution BSA 0,4 mg/mL in PBS (Sigma-Aldrich #A9418) for 1h RT. The following step is the dilution of 500-1000 µg of protein extract in 250 µL of TBS-T, this solution is then added to the blocked anti-HA agarose beads ON 4°C. The unbound fraction is removed the day after, and after three washes in TBS-Tween 0,05%, the immunoprecipitated fraction is eluted with Laemli buffer 2X and β-mercaptoethanol. Input unbound and immunoprecipitated fractions are then loaded onto an SDS page for western blotting analysis.

3.1.13 Evaluation of cell viability and metabolic activity

MTT assay (Promega #G4001) has been used to measure the cell viability of mammalian cell culture after blue light stimulation. 10000 cells/well have been plated into a 96-well plate 24h before the light stimulation protocol. At the end of the protocol, the cells were incubated with dye solution for 4h at 37°C CO_2 5% CO_2, and then the stop solution was added for 1h at RT. The assay is then ready to be recorded on a 96-well plate reader at 570nm.

3.1.14 Illumination protocol and device

The illumination protocols on yeast and mammalian cells have been performed using LED lamps with 465nm blue light. Thanks to the collaboration with Dr. Raffaele Mazziotti, we have built the LED device shown in Figure M1. The system can be characterized as an electrical circuit governed by an Arduino, which controls the operation of an LED matrix. The program, executed through the Arduino Integrated Development Environment (IDE), determines the illumination pattern, duration, and intensity of the LEDs.

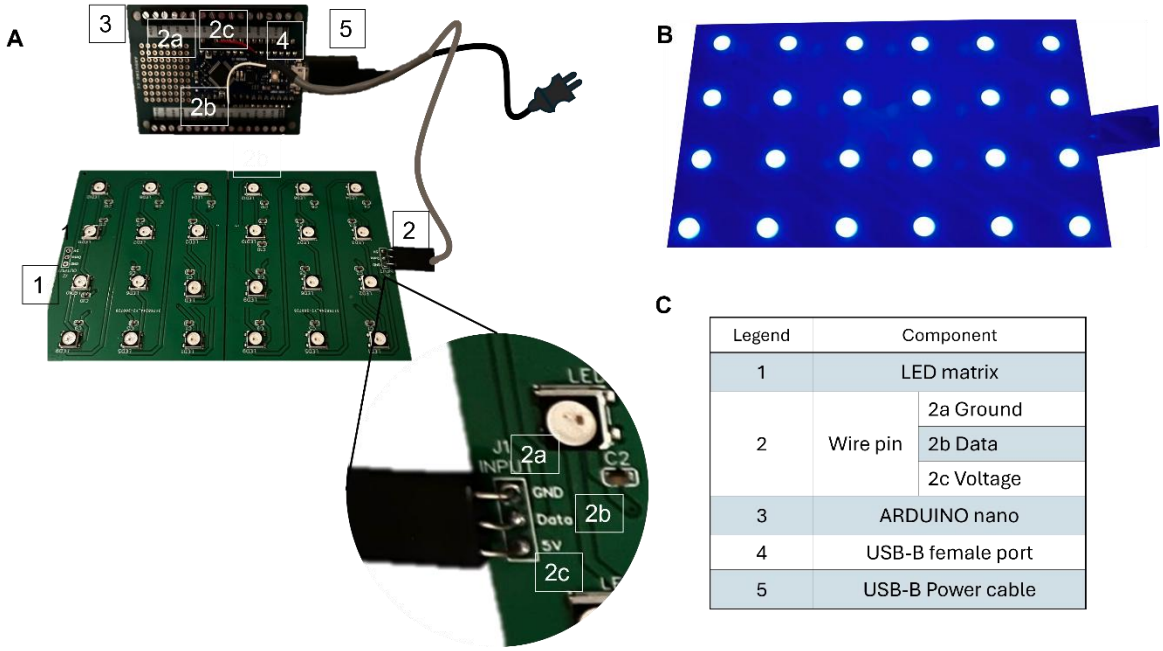

Legend	Component	
1	LED matrix	
2	Wire pin	2a Ground
		2b Data
		2c Voltage
3	ARDUINO nano	
4	USB-B female port	
5	USB-B Power cable	

M 1 ***Blue-light illumination device. A)*** *Arduino device and the LED matrix* ***B)*** *Blue LED* ***C)*** *Table of the components in A.*

3.1.15 Western blotting

Materials:

Antibodies:

Table 8: List of antibodies used in wester blotting analysis

ANTIBODY	CODE	CONCENTRATION
Rabbit anti-LexA	Merk #06-719	1:1000
HRP-anti-HA	Roche #12013819001	1:1000
Mouse anti-PGK	Invitrogen #459250	1:5000
HRP-anti-MYC	Cell Signalling #2040	1:1000
Rabbit anti-TDP43	Abcam #109535	1:1000
Mouse anti-Vinculin	Merk #V9131	1:500
Mouse anti-Rack1	BD Bioscience #610178	1:2000
Mouse anti-puromycin	Merk #MABE343	1:10000
HRP-anti-Rabbit	Santa Cruz #sc-2357	1:2000
HRP-anti-Mouse	Santa Cruz #sc-516102	1:2000

The degradation experiments performed in yeast cells required 30µg of protein extract, quantified with Bradford assay (Biorad #5000006), and boiled at 95°C for 5’ in laemli buffer and then run onto a 12% TGX Stain-free gel (Biorad #1610183, #1610185) for western blotting analysis.

For protein degradation analysis in mammalian cells, 10 µg of the soluble fraction of HEK293T cells transfected with the optobody and its target were prepared in laemli buffer and denatured for 5 min at 95°C. For insoluble and total extracts, the protein quantification has been done with a BCA assay (Thermo-Fisher # 23225). Once standardized, the number of cells in each plate for the degradation experiments was determined, the insoluble and total fractions were loaded onto the SDS-page by resuspending the pellet into 30µL of laemli buffer 2X and boiled at 95°C for 10', and 10µL of the sample was used for analysis. Protein extracts were loaded onto 10 or 12% TGX Stain-free gel (Biorad #1610183, #1610185). In both cases, the running buffer was composed of 25 mM Trizma Base, 190 mM Glycine, 0.1% SDS.

After the run, proteins on the gel were transferred to Amersham Protran 0.45 NC nitrocellulose membrane (GE Healthcare Life Science) using the trans blot semy-dry (BIORAD), using the transfer buffer (25 mM Tris-HCl, 192 mM Glycine,10% Methanol). The post-transfer membrane was then blocked with the blocking solution prepared with 5% milk (Millipore #70166) in T-TBS (1X TBS, 0.01% Tween 20), at least 45' RT, gently shaking. The primary antibody or the HRP-conjugated antibody was then prepared in blocking solution 2.5% in T-TBS and incubated ON 4°, gently shaking.

After overnight incubation, any excess antibody was removed by washing the membrane three times with washing buffer (1X TBS, 0.01% Tween 20) for 10 minutes each at room temperature. For membranes incubated with HRP-conjugated antibodies, signal acquisition followed immediately. For membranes incubated with primary antibodies, a secondary incubation with HRP-conjugated secondary antibodies was required before the signal acquisition. The chemiluminescence signal was produced with Clarity Western ECL Substrate (Biorad #1705061). When the signal resulted in being very low the reagent used was the Clarity™ Western ECL Substrate (Biorad #1705060S).

6.1.16 Densitometric analysis of western blotting

Western blotting acquisition and quantification has been done using ImageLab software from BIORAD. The densitometric analysis of the bands has been performed by measuring the row intensity density of the bands, normalized on the total lane protein of the stain-free gel technology.

3.1.17 Statistical analysis

Statistical analysis has been performed using GraphPad Prism 8. The degradation experiments have been inferred using One-way ANOVA and the Bonferroni multiple comparisons test to compare light-induced degradation at different light exposure times, in at least 4 independent experiments. The degradation experiments in the presence of proteasome inhibitors and or protein synthesis inhibitors have been inferred with Two-way ANOVA in at least 8 independent experiments. The comparisons between the dark condition and the light have been inferred using the unpaired t-test. All indicated p values ns>0,05; *<0.05; ** <0,01 ***>0,001¸****<0,0001

3.1.18 Immunofluorescence

Immunofluorescence experiments have been performed on HEK293T cells 48 hours after the transfection and or after the blue light stimulation experiments.

Cells plated onto 8-well chamber slides were fixed with cold methanol for 4', then the methanol was washed 3 times with PBS1X, and each well was incubated with blocking solution with Triton X 100-0,3%. After at least 30' of blocking, each well is incubated with the primary antibody in blocking solution with Triton X-100 0,1% overnight. The day after, the primary antibody is removed from each well and washed 3 times for 5' with PBS 1X. Then the secondary antibody conjugated with the appropriate fluorophore is incubated in a blocking solution for at least 1h at room temperature. The secondary antibody is then washed 3 times with PBS1X for 10'. To visualize the nuclei, DAPI [4′,6-diamidino-2-phenylindole 1:10000 in PBS 1X (Sigma-Aldrich #MBD0015)] staining is performed for 10' at RT in PBS1X. The coverslips are then mounted, and each well is ready to be acquired. Imaging was performed using a Leica Stellaris 5 or Zeiss LSM 900 confocal microscope

Table 9: List of antibodies used in immunofluorescence analysis

ANTIBODY	CODE	CONCENTRATION
anti-Ha-Rat	Merk 11867423001	1:1000
Anti-Myc- Mouse	Cell Signaling #2276	1:1000
Rabbit anti-TDP43	Abcam #109535	1:1000
Rabbit-Alexa-488	Invitrogen A-11008	1:1000
Rat-Alexa-546	Invitrogen A-11081	1:1000
Mouse-Alexa-488	Invitrogen A-11001	1:1000

3.1.19 Quantification of YFP fluorescence in HEK293T living cells

Cells transfected with YFP-AtLov2(3m); hereafter called opto-YFP, have been treated with blue light. To evaluate the reduction of fluorescence due to YFP light-induced degradation, 24h after transfection of HEK293T with opto-YFP, the fluorescence emitted by the cells was acquired with a Nikon Ts2R Eclipse microscope, 20x objective, 60msec exposure time, 17.1x gain, at time 0 and after 4h of light stimulation. The fluorescence of the images acquired before and after the light exposure and then has been quantified with Fiji software. ROIs corresponding to single cells have been drawn on the image in 8-bit format, corresponding to t =0 and t = 4 h; ROIs with a mean pixel intensity >200 have been excluded from the analysis to avoid saturated signals. Random ROIs have been drawn to measure the background fluorescence signal, again from acquisition at t=0 and t=4h. The mean of the background's RawInt Density has been subtracted from all the ROIs of positive fluorescent cells.

3.1.20 Evaluation of transfection efficiency

The co-transfection efficiency has been calculated by detecting both the protein targets coded in the plasmids through immunofluorescence. To evaluate how many cells expressed TDP-43 and optoanti-TDP-43, 48h post-transfection, HEK293T cells were fixed on coverslips, and the protein target was detected with primary antibody anti-TDP-43 and anti-HA, and secondary antibody Alexa-fluor-488 and 547 conjugated, respectively, while the nuclei were stained with DAPI. A total of 10 acquisitions were taken in random fields, for the three channels, for each field, the DAPI, the TDP-43, and the HA-optoantiTDP-43 positive cells were counted. The number of co-transfected cells was evaluated by merging the signals of the three channels. Since TDP-43 is ubiquitously expressed, to be able to detect the signal coming from the transfected form of the protein, the acquisition parameters were set on the untransfected HEK293T cells, where the signal was considered background.

3.1.21 Nuclear vs cytosolic localization of immunostaining

The different localization between nucleus and cytoplasm of TDP-43 WT and TDP-43 NLS1 mutant has been evaluated at the single cell level through immunofluorescence analysis on HK293T cells transfected with MYC-TDP43-P2A-HA-VHH5-AtLov2-cODC1 and MYC-TDP43-NLS1 mut-P2A-HA-VHH5-AtLov2-cODC1. For each cell imaged, two ROIs have been created: ROI (N), the one merging with the DAPI staining to localize the nuclear green fluorescent signal, and one corresponding to the cell body, ROI(T). The fluorescent area of the

cytoplasm ROI(C) has been measured by subtracting the ROI (N) from the ROI (T). The fluorescent areas from the ROI (N) and the ROI (C), respectively, are defined as local fluorescent areas. The localization of the signal has been reported as the ratio between the $\frac{local\ fluorescent\ area}{total\ fluorescent\ area}$. The total number of cells analysed results from three independent experiments. Statistical analysis has been performed with two-way ANOVA.

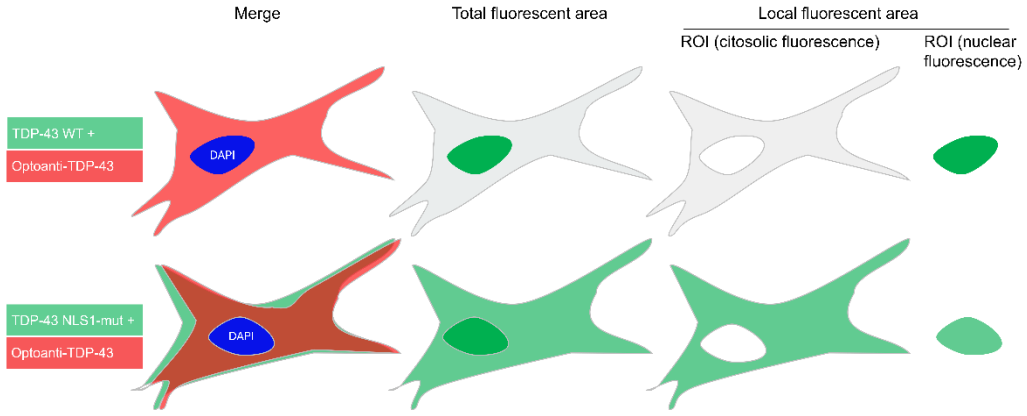

*M **1 Illustration of the quantification pipeline for TDP-43 WT and mutant localization of fluorescence**. Red represents HA staining for optobody expression, green represents TDP-43 staining, and blue represents DAPI staining for nuclear identification*

3.1.22 Proteasome inhibitor chase experiments

HEK293T cells in P60 mm wells have been transfected with the TDP-43-p2a-VHH5-AtLov2(3m)-cOCD1 following the protocol of Effectene transfection reagent. 24h after transfection, cells were split into 4 conditions onto a P35 mm plate. 48h after transfection, cells were treated with blue light for 6h or kept in dark conditions; in the last 2h of the experiment, 5µM MG-132 was added to the media. At the end of the light stimulation protocol cells have been collected and lysed; 15µg of protein extract has been used for SDS-PAGE.

3.1.23 Cycloheximide chase on global translation

The global translation variation on Hek293T cells was assessed using surface sensing of translation SuNSET technique (Piecyk et al., 2024; Schmidt et al., 2009). Briefly, the protein translation process can be monitored through western blotting analysis by evaluating the total protein synthesis level by detecting puromycin incorporation into nascent polypeptides. Puromycine (PMY) is an aminonucleoside antibiotic produced by Streptomyces alboniger, which is a structural analog of aminoacyl tRNAs; by treating cells with small amounts of PMY for at least 10 minutes, all the proteins that are being synthesized from the translation machinery will be labelled. To first assess the technique, non-transfected HEK293 T cells were plated into

4 different wells of a 12-well plate, and two of them were then treated with cycloheximide 100μM to inhibit protein translation, and two with DMSO for 2h. After the treatment, PMY was added at 5μM for 15 minutes in one well with CHX and one with DMSO. Thus, from all 4 samples, cells were then lysed in SDS2% and then sonicated for 3'' at amplitude 5. 10 μg of the total extract was loaded for the SDS-PAGE, and western blotting was performed with anti-puromycine antibody to detect all the labeled proteins. Western blotting quantification was performed with ImageLab (BIORAD) software, and the evaluation of all the proteins labeled with PMY was done by measuring all picks on each lane. The quantification of the PMY bands was referred to as the total lane protein. Densitometric values of the four samples were normalized to the DMSO-PMY sample. Statistical analysis: two-way ANOVA on six independent experiments.

3.1.24 Protein knocking down

The RACK1 repression has been performed by transfecting the RACK1 siRNA sc-36354 (Santa Cruz Biotechnology) into HEK293T using Lipofectamine 2000 (Invitrogen) transfection reagent. 180 pMol of RACK1 siRNA have been transfected using 1μL of Lipofectamine. 72 h post transfection, cells have been transfected with MYC-TDP43-NLS1 mut-P2A-HA-VHH5-AtLov2-ODC1 for the following blue light exposure experiment. RACK1 knockdown has been evaluated through western blotting analysis by normalizing the band of the siRNA-transfected lane to the band obtained from non-transfected cells.

Part II

3.2.1 Constructs

- LexA-TAU-2N4R-WT
- LexA-TAU-2N4R-(T231A-S235A)
- LexA-(R157G- K159E) -TAU-2N4R-WT
- LexA-(R157G- K159E)-TAU-2N4R-(T231A-S235A)
- scFv-T231-S235-HA-AtLov2-cODC1

The TAU-2N4R sequence (Addgene #177653), was cloned into pMicBD1 and pMicBD2 (please see section 3.1.1 for references) vector obtaining the constructs LexA-TAU-2N4R-WT, used for yeast two-hybrid screening, and LexA-(R157G- K159E) -TAU-2N4R-WT, used for light degradation experiments. The scFv-T231-S235 provided by Shih *et al.* 2012, was cloned in the pLinker220 vector, fused to the VP16 activation domain for yeast two-hybrid interaction assay, or with AtLov2-cODC1 for degradation experiments. The cloning procedures are described in sections 3.1.3-6. Each construct was then transformed into the L40 yeast strain as described in section 3.1.7.

3.2.2 Transactivation curve and in vivo interaction assay

L40 *Saccharomyces cerevisiae* expressing LexA-Tau-2N4R WT and mutant strains were plated onto SD-WH plates with a growing concentration of 3-amino-triazole (3AT) to check for autoactivation of the HIS3 gene without interaction with an intrabody.

After determining the concentration of 3-AT necessary to inhibit trans-activation, the L40 clones expressing LexA-Tau-2N4R baits were transformed with a plasmid containing the intrabody sequence. This transformation was performed to assess the interaction, which would result in growth on selective media lacking histidine. For the yeast transformation protocol, the yeast cell lysis protocol to protein extraction, and light-induced degradation experiments, refer to the previous session in Materials and Methods Part I, sections 3.1.7 and 3.1.8. For western blotting analysis, 30µg of protein extract was loaded on SDS-PAGE (section 3.1.15).

3.2.3 Protein dephosphorylation

Protein extract (see section 3.1.8) has been treated with Lambda Protein Phosphatase LPP (NEB P0753S) following the manufacturer's instructions to remove all phosphorylation residues for 30' at 30°C.

3.2.4 Phosphorylated protein SDS-PAGE analysis

The phosphorylation state of protein samples can affect the electrophoretic run onto acrylamide gel; thus, using Phos-tag SDS-PAGE it has been checked for the phosphorylation state of the protein sample has been checked (Kinoshita & Kinoshita-Kikuta, 2011). Yeast cells expressing the LexA-Tau2N4R WT and T231A-S235A were lysed in PBS 1X, protease inhibitor (Sigma-Aldrich #11836170001), and phosphatase inhibitor (Sigma-Aldrich #4906845001) using glass beads as described above. The same protein samples were loaded onto a stain-free gel to check for the correct molecular weight. Phos-tag acrylamide gel was prepared using 5 mM phos-tag (NARD #304-93521) and 5 mM $MnCl_2$. After the run, the gel was washed three times with transfer buffer (described in Materials and methods 6.15) with 10 mM EDTA before sandwich assembly for the semi-dry transfer.

Part III

3.3.1 IACT screening

Constructs (see Table 1):

- LexA-Arc-1-140
- LexA-Arc-1-76
- LexA-Arc-31-108
- LexA-Arc-77-140
- LexA-AQPN8
- MYC-mARC-P2A-HA-VHH213-AtLov2-cODC1

The Arc sequence, provided by Professor Clive Bramham, was cloned into the pMicBD1 vector. For the bait characterization, a transactivation curve was prepared as described in Materials and Methods, part II, section 3.2.2

*Table 10: Growth media for IACT selection. * 5g/L for solid plates*

COMPONENT	**CODE**	**YNB**	**YPD**	**YPAD**	**YPA**
Yeast nitrogen base	SIGMA # Y-125	1,2 g/L	-	-	-
yeast extract	BD # 211931	-	10 g/L	10g/L	10g/L
bacto peptone	BD # 211840	-	20g/L	20g/L	20g/L
2% D-glucose	SIGMA # G-7021	-	20g/L	20g/L	-
Adenine hemisulfate	SIGMA #A9126	-	-	0,1 g/L	0,1 g/L
Bacto-agar	BD # 214010	*	*	*	*

L40 *Saccharomyces cerevisiae* yeast strain expressing LexA-mArc1-140 was transformed with Llama VHH library (Gilodi et al., 2022). The screening procedure consists of a Maxi-Scale LiAc transformation of the mArc1-140-baiy with the Llama VHH library (naïve, 10^6).

Day 1. Some colonies of the L40 yeast strain expressing LexA-mArc-1-140 bait were grown overnight at 30 °C, 225 rpm in 50 ml of -W selective medium, to obtain the culture in a mid-log phase the next day.

Day 2. In the morning, the temperature was lowered to 25°C, and in the late afternoon, the culture was diluted to OD_{600} = 0.2 into 150 ml of -W selective media, and incubated overnight, 220 rpm at 30 °C.

Day 3. The culture was diluted to OD_{600} = 0.3 into 1 L of YPAD and incubated 3 h, 220 rpm at 30 °C. Once reached OD_{600}=0,6-0,7 cells were centrifuged at 3000 rpm at room temperature (22-25 °C) for 5 min. The pellet was washed several times in a total amount of 500 ml of 1xTE. After the washing steps, the pellet was resuspended into 15 ml of 1xLiAc/1xTE. In the meantime, a mix of 10 mg of salmon testis DNA (STD) (previously denatured at 95° 5') and

250 µg VHH llama DNA library cloned in the pLinker220 prey plasmid were prepared. The mixture, library+STD, was then added to the resuspended cells. Then, the cells were transferred in a flask with 140 ml of 50% PEG/1xTE/1xLiAC and incubated 30 min, 150 rpm at 30 °C. After the incubation, 17,6 ml of sterile DMSO was added and the cells were heat shocked at 42 °C for 15 min under gentle mixing and then were put in ice for 5 mins. After the heat shock, the cells were washed three times with a total amount of 1 L of YPA (previously cooled on ice). Then the cells were centrifuged at 4500 rpm at room temperature (22-25 °C) for 5 min, and recovered in 1 L of YPAD (previously heated at 30 °C) for 1 h at 30 °C. After the recovery, 1 ml of cells was centrifuged and resuspended in 1 ml of -WL medium to make the serial dilutions $10^{-3}, 10^{-4}, 10^{-5}, 10^{-6}, 10^{-7}$ and 10^{-8} to evaluate the transformation efficiency. After the dilutions, the cells were plated on -WL Petri dishes and incubated at 30 °C. The culture was then processed as follows. The cells were harvested at room temperature (22-25 °C), 4500 rpm for 5 min, and washed three times in a total amount of 450 ml of -WHL. The pellet was then resuspended in 5 ml of -WHL and plated on twenty -WHL+ 2mM 3AT Petri dishes (250 µL per plate). Plates were incubated at 30 °C for 4-5 days. After that time, the colonies were restreaked into -WL and -WHL plates for the further steps.

3.3.2 β-gal assay

The second selection marker of the interaction between the antigen-bait and the intrabody-prey was the expression of lacZ, which allows for the application of the β-galactosidase assay for the screening of the blue colonies positive for the interaction. In the IACT screening, a liquid -galactosidase (-gal) assay, adapted from (Möckli & Auerbach, 2004) was performed in a 96-well plate. A small amount of the biomass from single colonies (99 clones) was resuspended and incubated in 50 µl of lysis buffer made of 20 mM Tris HCL pH 7.5 containing 333 U/ml lyticase, and incubated at 37 °C, 150 rpm for 2 h. Then, 50 µl of Z buffer, a solution made of 60 mM Na_2HPO_4 , 40 mM $NaH_2\,PO_4$, 10 mM KCl, 1 mM $MgSO_4$, pH 7.0, X-gal at 20 mg/ml (170 µl), and βmercaptoethanol (30 µl), was added to each well and incubated at 37 °C for 2 h.

3.3.3 Colony PCR and Fingerprint

Colony PCR and fingerprint analysis were performed only on double-positive colonies (His+/LacZ+). The clones were lysed using 10 µl of buffer 20 mM Tris HCl pH 7.5, 300 U/ml Lyticase, and incubated for 45 min at 37 °C, followed by Lyticase inactivation at 95 °C for 5 min. Then, the VHH of each clone was amplified by PCR. The primers were pL220 Fw (5'-

AAG CTT ATT TAG GTG ACA CTA TAG-3') and pL220 Rev (5'- CTT CTT CTT GGG TGC CAT G-3'). The PCR master mix reaction was prepared as previously described in Table 2. The PCR reaction was performed as shown in Table 3. PCRs were analysed using 1.3% agarose gel, followed by EtBr (10 mg/ml stock, DIL 1:16000) staining. Images were acquired using Chemidoc XRS (Bio-Rad). The clones producing the band of a molecular weight corresponding to the VHH were then digested with the frequent cutter PSTI enzyme to obtain the fingerprinting of the clones. The digestion was then run onto an 8% acrylamide gel in TBS, and images were acquired using Chemidoc XRS (Biorad). From the pattern of the bands, the identical clones were excluded.

3.3.4 Secondary screening

A pool of selected candidates of VHHs positive for the interaction with LexA-Arc bait was then further tested for the interaction in yeast two-hybrid with an unrelated bait to exclude potential LexA DBD binders.

3.3.5 In Vivo Epitope Mapping

The selected true binder of mArc protein was then further characterized by testing the interaction with a specific region of the original bait protein. The mArc sequence was split and subcloned into the pMicBD1 vector. The fragments were: N-coil (1-76), the C-coil (77-140); and the inter-coil (31-180). All these new baits were co-transformed with the selected intrabody into the L40 yeast strain to evaluate the growth in -WHL media.

Immunoprecipitation

Once the true interactor was selected, and the putative epitope was characterized, the VHH sequence was subcloned into the mammalian expression vector to test for the in vitro interaction. The immunoprecipitation assay has been performed in HEK293T cells, as described in section 3.1.12; the only protocol modification was made during the washing steps before eluting the glass beads. The three washes were made using T-TBS buffer supplemented with decreasing concentrations of NaCl, 50, 100, and 150 mM, while the last three were made in T-TBS.

3.3.5 Light-induced degradation in HEK293T cells

The intrabody anti-Arc and the intrabody anti-GFP (Fridy et al., 2014) were equipped with psd domain, the resulting optobody format was then cloned into the modified p-P2a-mcherry vector

(see Table 1). The proof of principle experiments of the targeted protein degradation for both mArc and GFP proteins was set in HEK293T cells transfected as described in section 3.1.9.

Vectors:

- p-CMV-MYC-ArcFL-P2A-HA-VHH213anti-Arc-AtLov2-cODC1 (derived from Addgene #84329)
- p-CMV-MYC-EGFP-P2A-HA-VHHanti-EGFP-AtLov2-cODC1 (derived from Addgene #84329)
- pAAV-hsyn-rtTa-tdTomato (generated in our laboratory, Bio@SNS unpublished)
- pWpXLD-TRE-HA-VHH213anti-Arc-AtLov2-cODC1 (Addgene #12258)

The optobody VHH-anti GFP (Fridy et al., 2014), was selected as an unrelated intrabody in the following part.

3.3.6 MiBi mESCs culture

The entorhinal cortex neurons derive from mouse embryonic stem cells (mESCs) differentiated into dual MAPK/ERK and BMP signalling pathway inhibited cells (MiBi) as described in (Tonelli et al., 2025)

3.3.7 Real-Time qPCR on MiBi cell culture

RNA extracted from in vitro samples of MiBi culture at DIV 25, 35 and 50, was retrotrascribed using the Reverse Transcriptase Core Kit 300 (Eurogentec, RT-RTCK-03). Approximately 200 ng of RNA was reverse transcribed into cDNA for RT-qPCR analysis. SensiFAST SYBR mix (12µl, BioLine, BIO-98020) and cDNA (8µl) were combined in 4titude PCR quality tubes and quantified using Qiagen 72-Well Rotorgene. Briefly, amplification take-off values were assessed using the built-in relative quantification analysis function of the Rotor-Gene 6000, and relative expression was calculated with normalization to the housekeeping gene Actb using the 2^-ΔCt method.

Table 11 Primers for RealTime qPCR

Gene symbol	Forward (5'-3')	Reverse (3'-5')
Actb	AATCGTGCGTGACATCAAAG	AAGGAAGGCTGGAAAAGAGC
Arc	TTGGCCTCACCCTCTACACT	GATGTCCCCTGGGTTTTGGT

3.3.6 Lentivirus generation and cell culture transduction

Lentiviral vectors were obtained by transfection of HEK293 T cells with Lipofectamine 2000 (Invitrogen, 11668019) using the manufacturer's protocol to adjust the DNA mixture. The DNA mixture consisted of the lentiviral vector with coding for TRE-HA-VHH213-AtLov2-cODC1,

or prtTA-td-TOMATO, together with the psPAX2 packaging (Addgene #12260), the pCMV-VSV-G envelope (Addgene #8454), and the pCMV-Rev (NL4.3) (Addgene #115776) expressing plasmids, with 4:3:1:1 ratio. The transfection mixture was incubated overnight, and the next morning the viral particles were collected 24 and 48 hours later, pooled and used immediately, or kept frozen at -80°C. The best cell transduction rate has been reached by diluting the 1:1 lentiviral vector with the culture medium, along with 8µg/mL Polybrene (Sigma-Aldrich, TR-1003). Cells were typically transduced O/N after passaging to increase lentiviral access to the cell surface. The lentiviral vectors used in this work consisted of the pWPXLd lentiviral backbone (Addgene #12258) containing either the anti- EGFP or the anti-Arc optobody

3.3.8 Doxycycline induction and light degradation experiments

For the degradation of endogenous Arc in cortical neurons, MiBi cells were plated at DIV 14 and directly transduced for lentiviral expression of the optobody 213. To do so, the cells were both transduced with the lentivirus for the rtTA cassette under the CMV promoter, and the optobody213 or optobody anti-GFP, under the tetracycline-responsive element promoter (TRE). At DIV 34 and cells were induced with 1µg/mL doxycycline ON (see Figure M2).

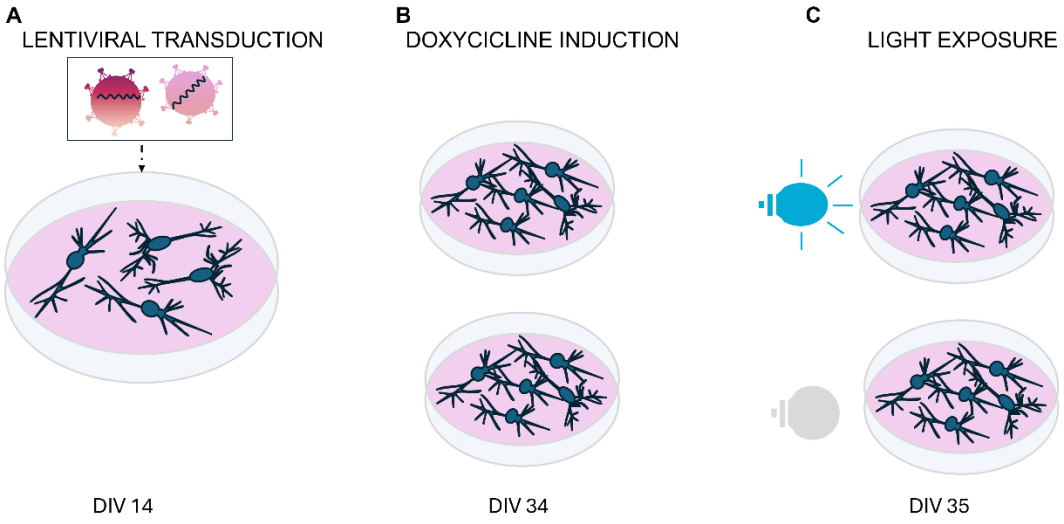

M 1 ***Experimental design for light-induced degradation of endogenous Arc in MiBi cortical neurons. A)****MiBi cells were plated at DIV14 and transduced with lentiviruses for the expression of TRE-optobody213 and the CMV-rtTA.* ***B)*** *MiBi cells were kept in culture up to DIV33 and then split into two different coverslips.* ***C)*** *At DIV 35, cells were either treated with light or kept in dark conditions. At the end of the experiment, cells were fixed for immunostaining.*

3.3.9 Immunofluorescence (IF) on iPSCs-derived cortical neurons (MiBi)

Immunofluorescence experiments on MiBi cortical neurons have been performed immediately after the blue light stimulation experiments.

For IF imaging, cells were fixed in 4% paraformaldehyde for 10 minutes at room temperature (RT), then permeabilized and blocked in a solution containing 10% normal goat serum (NGS) and 0.25% Triton-X100 in PBS at RT for 1 hour. Primary antibodies were incubated O/N in PBS and 10% NGS at 4°C. Secondary antibodies were applied under the same conditions for approximately 1.5 hours at RT. After PBS washes and nuclear staining with DAPI, cells were mounted with Aqua/Poly-Mount (Polysciences, 18606-100) and stored at 4°C before imaging. Imaging was performed using a Leica Stellaris 5 or Zeiss LSM 900 confocal microscope.

Table 12 List of antibodies used for immunofluorescence analysis

ANTIBODY	CODE	CONCENTRATION
antiArc-Guinea Pig	SYSY 156 005	1:1000
anti-Ha-Rat	Merk 11867423001	1:1000
anti-mcherry-chicken	Abcam 205402	1:1000
Guinea Pig-Alexa-488	Invitrogen A-11073	1:1000
Rat-Alexa-647	Invitrogen A-21247	1:1000
Chicken-Alexa-546	Invitrogen A-11040	1:1000

3.3.10 Immunofluorescence analysis

Images were captured at 63x magnification with a zoom factor of 3. For each acquisition, a tile of 10 fields was captured simultaneously, with focus was manually adjusted on the channel corresponding to the tdTomato staining, which was detected using an anti-mCherry antibody. Each acquisition consisted of a z-stack with a step size of 2.01 µm, with a total of 7 steps per z-stack.

Image analysis was performed using Fiji software. The z-stack images for each field were merged by summing pixel intensities across the individual z-steps. To quantify the degradation of endogenous Arc protein in cortical neurons transduced for the inducible expression of optobody213, only cells positive for Arc, tdTomato, and the HA tag were included in the analysis. For each image, at least 3-7 regions of interest (ROIs) were selected based on the tdTomato staining, ensuring consistent ROI placement across images. The mean area for each ROI was calculated, ranging from 0,11 to 0,8 µM. An additional ROI corresponding to the background signal was selected for background subtraction.

Fluorescence intensities for the Arc, tdTomato, and HA-tag channels were measured within each ROI, and background fluorescence was subtracted from the corresponding values. The mean fluorescence intensity for each channel was calculated for every ROI, and the overall

fluorescence intensity for each channel in the image was determined as the mean of the values across all ROIs. A total of 10 images per sample were acquired, and analysis was performed across three independent biological replicates. The data in Figures R 38 -39 represent the mean fluorescence intensity for each channel across the 10 fields from each biological replicate.

4. Results

4.1 Part I

4.1.1 Opto-YFP light-induced degradation

My first aim was to assess the feasibility of equipping an intrabody with a light-inducible degron. To first assess the efficacy of the photosensitive degradation domain (psd) I created the HA-tagged opto-YFP by fusing the *Arabidopsis thaliana* LOV2 domain of phototrophin1 protein, with the C-terminal domain of ornithine decarboxylase enzyme described in Renicke *et al.* 2013; the resulting YFP- AtLov2(3m) -cOCD1 construct was used to transform yeast cells and to transfect mammalian cell culture. The construct, hereafter called opto-YFP, was cloned in the pLinker-220 vector containing the LEU gene, that is used for the IACT procedure (Visintin et al., 2002) , thus, L40 *Saccharomyces cerevisiae* yeast strain was transformed with the plasmid and the positive clones were selected in SD- lacking leucine plates; the expression of the opto-YFP protein was confirmed by western blotting (data not shown), and the selected clone was used for light-induced degradation experiments. In Renicke *et al.* (2013), it was shown that the degradation of RFP protein was reached within 4 hours of blue light exposure; this information allowed us to have a range of time to investigate the activity of our opto-YFP. We decided to check for protein degradation by monitoring the protein level after 2, 4, and 6 hours of continuous blue light stimulation (Figure R1 A-B). The validation of opto-YFP as a photosensitive degradation tool in the L40 yeast strain was the first proof of principle before moving into the mammalian cellular model. To achieve this, we cloned opto-YFP into the scFV-express vector to express the construct under the CMV promoter in the human embryonic kidney (HEK293T) cell line. Mammalian cell expression allowed us to check for degradation through western blotting analysis on cell lysate and monitor the reduction of cell fluorescence due to degradation of YFP protein (Figure R1 C- D- E).

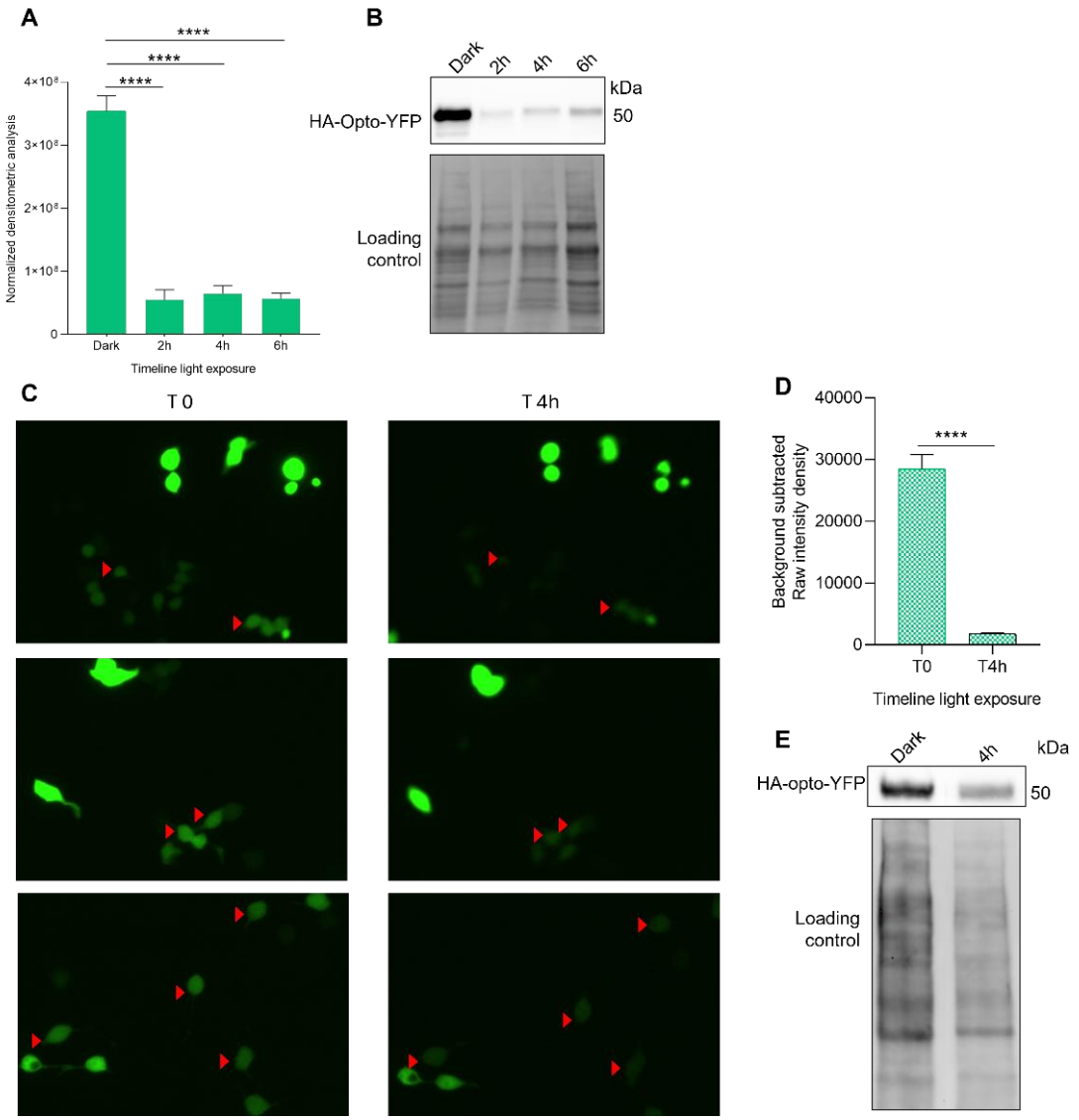

R1 ***Photosensitive degradation domain in the YFP-AtLOV2(3m)-cOCD1 format in L40 Saccharomyces cerevisiae yeast strain and Hek293T mammalian cells****. **A)** quantification of the western blotting bands of n=4 independent degradation experiments and **B)** representative western blotting of the degradation experiments shown in **A. C** representative images of Hek293T cells expressing opto-YFP at time 0 of blue light exposure and after 4h of illumination, and **D** quantification of the mean fluorescence of the single cells, in the single ROIs and **E** western blotting of the cells shown in **C** compared to the dark condition. Statistical analysis A) Bonferroni-corrected one-way Anova, D) unpaired t-test; Error bar = mean with S.E.M.; p-value ns non-significant >0,05; *< 0,05; **<0,01; ***<0,001; ****< 0,00001*

4.1.2 Optobody anti-TDP-43

The second step towards the creation of the optobody was the fusion of the intrabody sequence with the psd light-dependent degron module previously validated in its light-inducible degradation activity. For TDP-43 targeted protein degradation, we applied the psd module to the VHH5 anti-TDP43 intrabody previously isolated in our laboratory through IACT from the Llama VHHs library, and validated in vivo and in vitro for the in cell interaction with its antigen (Gilodi et al., 2022). The design for the construct was grounded in the idea to keep the N-terminal portion of the intrabody free, not to interfere with the binding capacity of the CDR3.

In this view, the final construct, shown in Figure R2, defined optobody, contains the intrabody at the N-terminal portion and the AtLov2 fused to the degron at the very C-terminal end. This orientation was selected to favour both the antigen binding and the C-tail exposure.

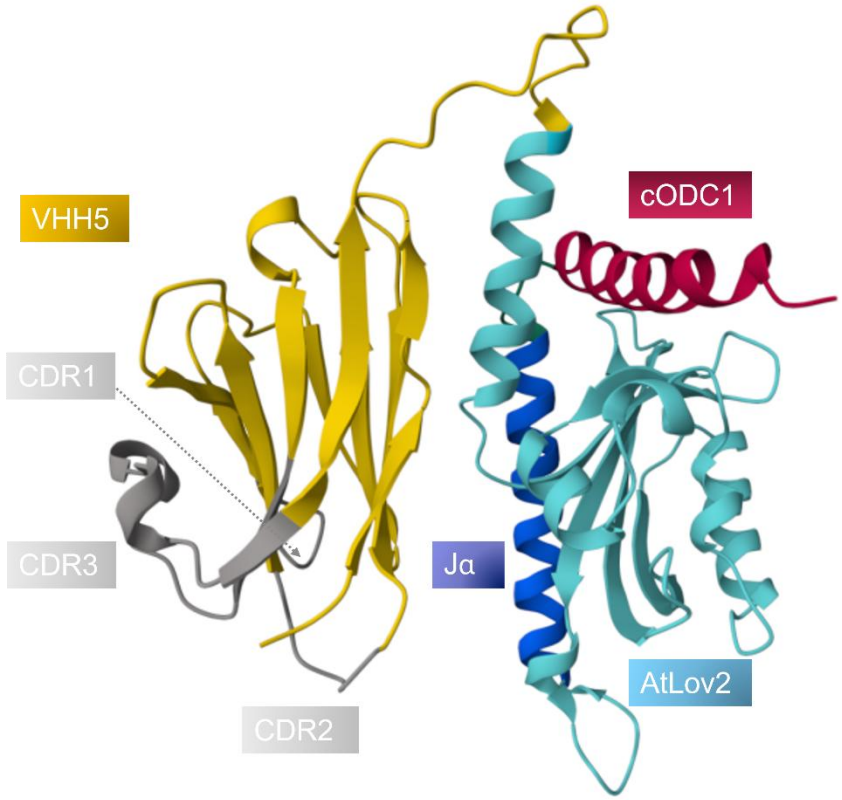

R 1 ***Representation of the optobody VHH5-antiTDP-43 fused with cODC1 degron****. The* ***VHH5*** *is represented in yellow while the* ***CDR1*** *(EGSGNKY),* ***CDR2*** *(SWSGTR) and* ***CDR3*** *(CAASVSVPPFLELTAAHFGSW) are highlighted in grey. The Lov domain is represented in blue while the* ***Jα chain*** *(ETAVKEAEDLVKKTAVNIDEAV) is highlighted in light blue. The* ***ODC1*** *degron (MSCAQESITSLYKKAGSENLYFQ) is shown in red. Representation from the Alpha fold 3 server.*

4.1.3 Light-induced and reversible targeted protein degradation mediated by optoanti-TDP-43

After the cloning of the optobody VHH5 in the pLinker 220 plasmid for yeast expression, its sequence was verified with Sanger sequencing. Then I checked whether the transfer of the psd domain to the intrabody protein was effective to ensure the degradation behaviour of the construct. Then the second question to be addressed was whether the light-dependent degradation of the optobody could have the same reduction trend shown by the optoYFP. Since the aim was to follow the degradation process in a time window coherent with the time window of a canonical growth curve, I evaluated the degradation after 4 and 6 hours of continuous blue light stimulation. The first proof of principle of the optobody activity was obtained in L40 yeast

cells expressing the optobody alone. As shown in Figure R3 A-B, in 4 hours of stimulation, the level of the HA-tagged anti-TDP-43 optobody was halved, while in 6 hours, the signal results being dramatically low. The validation of the degradation activity of the optobody allowed me to move towards the targeted protein degradation in the same cellular model. Since 4 and 6 hours resulted to be the time window for a significant degradation of the optobody to occur, I tested whether the same light exposure time was sufficient to obtain the TDP-43 degradation. To do so, I transformed the L40 yeast strain with both the pMicBD1 plasmid containing the LexA-TDP-43 sequence and the pLinker 220 containing the optobody-antiTDP-43. To maintain the experimental design in a time range far from the saturation point of the growth curve, I exposed the L40 strain expressing LexA-TDP-43 protein, hereafter referred to as TDP-43, and its optobody to 4 and 6 hours of light stimulation. As expected, in the double transformed cells, the degradation trend for the optobody remains the same shown in Figure R3A, where the anti-TDP-43 optobody is expressed alone. On the TDP-43 target side, protein levels show a significant reduction after 4 and 6 hours of stimulation, although the degradation patterns between the time points remain similar (Figure R3E). This proved the light dependent degradation of TDP-43 in the L40 yeast model.

Once proved the efficacy of the L40 cellular model to achieve optobody-mediated TDP-43 degradation, I checked cell viability, to verify whether the proteasomal activation could in some way affect the growth curve compared to a control L40 yeast strain expressing both the TDP-43 protein and VHH5 anti-TDP-43 without the psd domain, thus lacking the activation of the degradation pathway by the blue light exposure (Figure R3 C). This experiment allowed to conclude that the proteasomal activation by the light activation of the degron has no effect whatsoever on cell viability and cell growth.

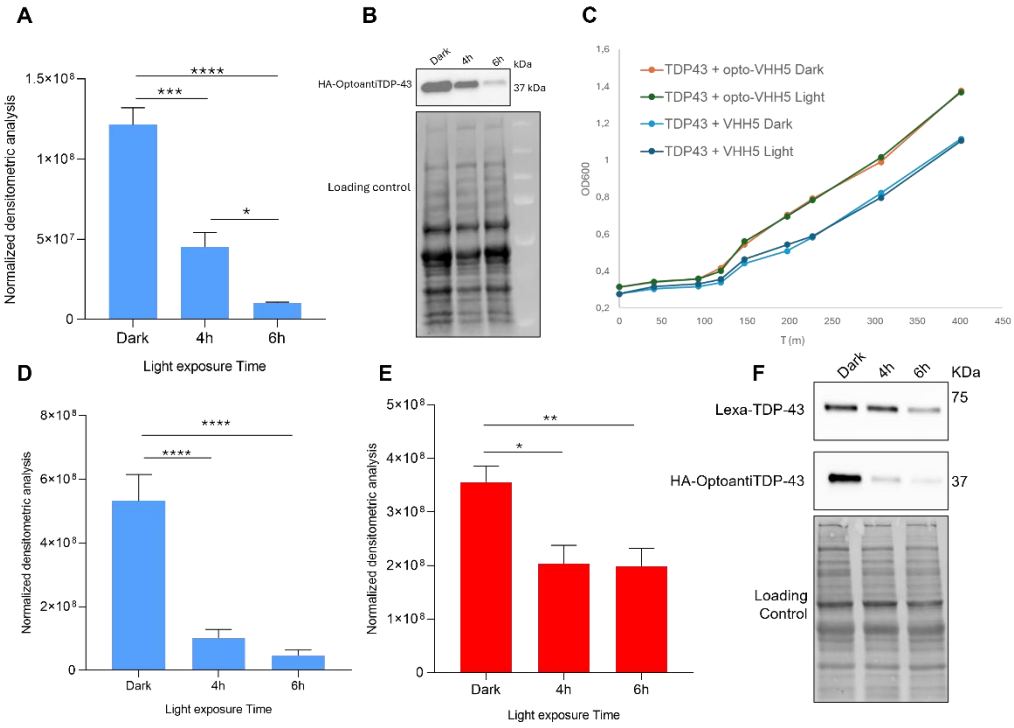

*R 2**Light-induced and reversible target protein degradation in L40 yeast strain mediated by optoanti-TDP-43**. **A)** Light-dependent degradation of the optobody5 in L40 yeast strain, and **B)** representative western blotting of the quantification of the n=4 independent experiments shown in A. **C)** Growth curve of a degradation experiment in L40 expressing both optobody 5 and TDP-43 proteins in dark and light conditions, compared with the cotransformed L40 strain expressing TDP-43 and intrabody 5 without the psd domain. **D)** and **E)** quantification of the n=6 degradation experiments in L40 coexpressing optobody 5 and TDP-43, and **F)** representative western blotting. F) Growth curve of the experiments in D and E. Statistical analysis A) Bonferroni-corrected one-way Anova; Error bar = mean with S.E.M.; p- value ns>0,05; *< 0,05; **<0,01; ***<0,001; ****< 0,00001.*

Having successfully demonstrated the targeted protein degradation mediated by our optogenetic intrabody, after 4h of light exposure (Figure R3E), the second aim was to assess the reversibility of the targeted degradation tool. To this aim, I checked whether a recovery period condition, performed after 4h of light stimulation, was sufficient to rescue the protein level of both the optobody and the target. The recovery pattern of the protein level is different for the optobody and for TDP-43, as shown in Figure R4 A -B. Indeed, while the optobody level rises after two hours of recovery in the dark, for the TDP-43 I observed a small increase in the protein level, which was not, however, significant (Figure R4B). This might be due to a lower synthesis rate for TDP43, with respect to the synthesis rate of the optobody. Thus, a longer recovery period might be required to reveal a recovery of TDP43 levels following a 4 hours degradation time.

Lastly, since the starting culture of L40 coexpressing the optobody and its target is the same up to the moment of the split in dark versus light condition, and that after the 4h time point a an aliquot of the culture either was collected for the analysis or splitted into a new flask to undergo

the recovery phase, I compared the growth curve of the strain by monitoring the OD_{600} the three growth conditions: dark, light and recovery. The curve is quite similar among the three conditions (Figure R4D).

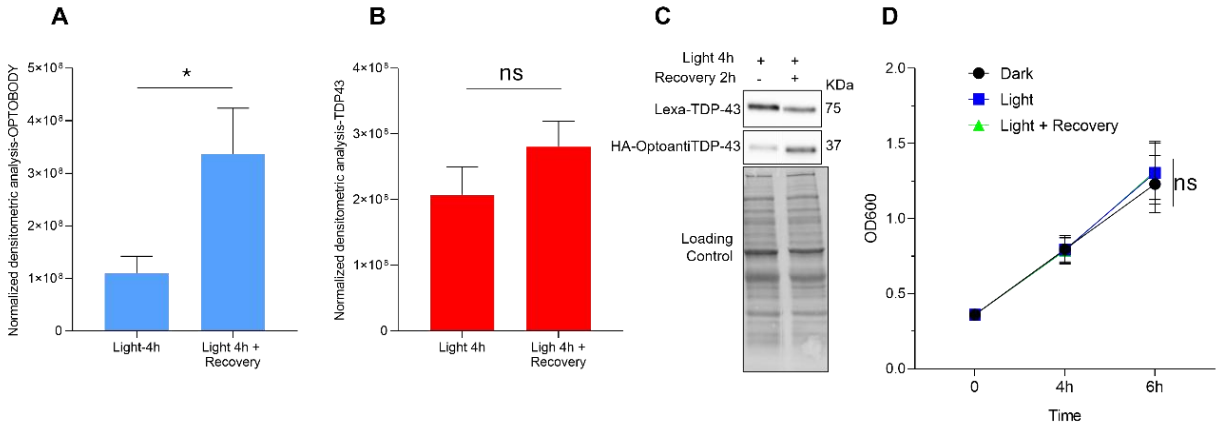

R 3 ***Reversibility of the optobody mediated degradation.*** ***A)*** *and* ***B)*** *comparisons between the protein level after 4h of light exposure without and with 2h of recovery in dark conditions for both the optobody (A) and TDP-43 (B) of n=5 independent experiments.* ***C)*** *Representative western blotting.* ***D)*** *Growth curve in light-exposed conditions with and without recovery compared to the dark condition. Statistical analysis A) and B) unpaired t-test; Error bar = mean with S.E.M.; p-value ns>0,05; *< 0,05; **<0,01; ***<0,001; ****< 0,00001.*

4.1.4 anti TDP-43 VHH5 interacts with TDP-43 in Hek293T mammalian cells

The strong evidence in yeast cells allowed the extension of the optobody application beyond the yeast cellular model used for the intrabody selection, and for the in vivo interaction, and the newly explored optobody retargeting to the degradation pathway. Before moving into a more complex cellular model, I first checked that the interaction between the intrabody could maintain its expression and folding level in mammalian cells, thus preserving its antigen binding capacity. Thus, I co-transfected HEK293T cells with MYC-tagged TDP-43 and HA-tagged-VHH5 to verify the in-cell interaction of the two proteins, after obtaining a protein extract in which to investigate the interaction by immunoprecipitating the intrabody and detecting the antigen with MYC-tag immunoblotting (Figure R5). The result of the co-IP demonstrates that the anti TDP-43 VHH5 intrabody interacts effectively with the TDP-43 target inside the cell.

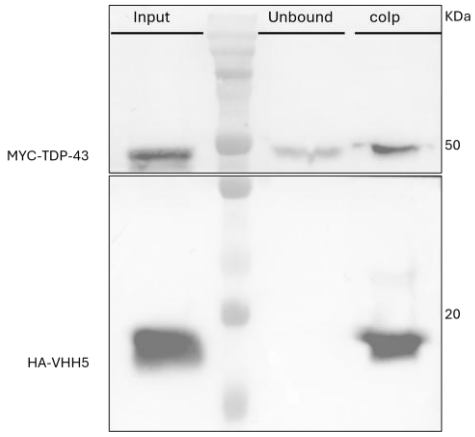

R5 ***Co-immunoprecipitation of TDP-43 in HEK293T cells expressing VHH5.*** *Protein extract from HEK293T cells co-transfected with MYC-TDP-43 and HA-OptoantiTDP-4, for immunoprecipitation of HA-tagged intrabody. Blotting of the Input extract (before immunoprecipitation), Unbound sample (collected before elution), Co-immunoprecipitated sample detected with anti-MYC antibody, and immunoprecipitated sample detected with anti-HA antibody.*

4.1.5 Targeted protein degradation mediated by opto-anti-TDP-43 in mammalian cells

Light-induced degradation of the anti-TDP-43 optobody and TDP-43 in HEK293T mammalian cell line in co-transfection conditions

Modifications to the experimental design were necessary to enable accurate comparison of protein levels across different light exposure conditions, in the adherent mammalian HEK293T cell line, as collecting aliquots during the experiment risked compromising culture viability. The initial approach involved replicating the light-dependent targeted protein degradation in cells co-transfected with MYC-tagged TDP-43, cloned into the pP2a-mCherry vector, and HA-tagged optobody, cloned into the pCiNEO backbone. To avoid potential bias in protein expression, the experimental setup was modified so that 24 hours post-transfection, cells were split into three separate dishes instead of preparing different transfection mixtures for each light exposure condition. This approach ensured that variations in protein expression due to differences in transfection efficiency in sister cultures would not affect the evaluation of protein degradation. Indeed, I preferred to treat each transfection as a single biological replicate from which three different conditions (two light exposure times and a dark one) were obtained. Then, 48 hours after the transfection, each dish was either kept in the dark or treated with light. At 4 hours the protein level was similar to that in the dark condition. Despite the fact that for both the TDP-43 and the optobody a reduction was evident after 6 hours of illumination, this was not statistically significant (shown in Figures R6D and E for both the optobody and the target).

Each experimental group, even focusing only on the dark, was affected by a strong variability; in other words, the biological replicates were very different in the protein expression levels. To better investigate this issue, I did immunofluorescence analysis to estimate the transfection efficiency in HEK293T cells transfected with the two plasmids coding for TDP-43 and for the optobody, respectively. As shown in Figure R6A there is a clear difference in the number of the TDP-43 positive cells, compared to the number optobody positive cells, thus, the transfection efficiency must be considered separately for one plasmid or the other. Indeed, 32% of the total cells were positive for TDP-43 while 5,6% were positive for the optobody (Figure R6B). These data provide insight into the issue of double transfection. Notably, 85% of the optobody-positive cells were also cotransfected, while only 14% of the TDP-43-positive were. This suggests that the plasmid containing TDP-43 is preferentially transfected on its own (Figure R6C). Thus, this bias in the co-transfection efficiency is responsible for the observed variability. I therefore sought a way to avoid the co-transfection, by constructing a single plasmid directing the expression of the two cDNAs.

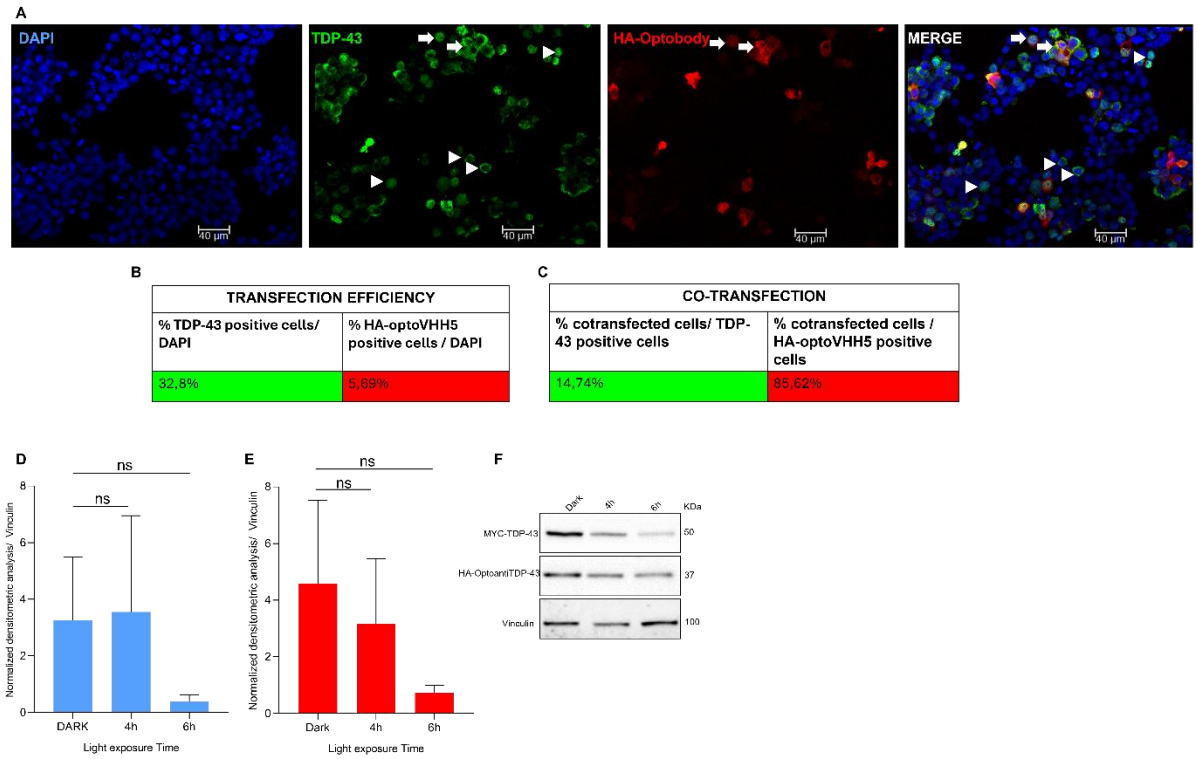

R6 ***Transfection efficiency issue. A)*** *Immunofluorescence on HEK293T double transfected with HA-optobody and MYC-TDP43, arrows indicate double-transfected cells, arrowheads indicate optobody-positive cells .* ***B)*** *quantification of transfection efficiency for the single construct and* ***C)*** *percentage of the TDP-43 or optobody positive cells among the cotransfected ones, of n=10 acquisitions.* ***D) E)*** *light induced degradation in co-transfection condition and* ***F)*** *representative*

*western blotting of the experiments shown in D and E. Statistical analysis D) and E) Bonferroni corrected One-way Anova; Error bar = mean with S.E.M.; p-value ns>0,05; *< 0,05; **<0,01; ***<0,001; ****< 0,00001.*

Single-Plasmid Strategy for Co-Expression of anti-TDP-43 optobody and TDP-43

Considering the double transfection efficiency issue, the solution I found was to modify the constructs used to transfect the cells. Indeed, MYC-TDP-43 and HA-optobody sequences were cloned into the same plasmid, including an auto-cleavage peptide sequence (P2A) to direct the expression of both proteins from a single mRNA transcript. Following translation, the two proteins are successfully cleaved and expressed as separate entities. Once the correct sequence of this new construct was confirmed, light-induced degradation experiments were performed. As a control for the cell viability upon light exposure, I performed an MTT assay on HEK293T cells exposed to 6h of light to check whether light itself could affect vitality; as shown in Figure 7D, no difference with the dark condition was detected. Furthermore, Figures R7A and R7B show that the new construct reduced within-group variability between different replicates, thus allowing for the demonstration of an effective light-dependent degradation pattern of both the optobody and its TDP-43 target. On the other hand, it also emerged that in the mammalian system, the light stimulation that is significant in protein reduction is the 6h. The same effective light-dependent degradation of TDP43 was further demonstrated in immunofluorescence analysis (Figure R8).

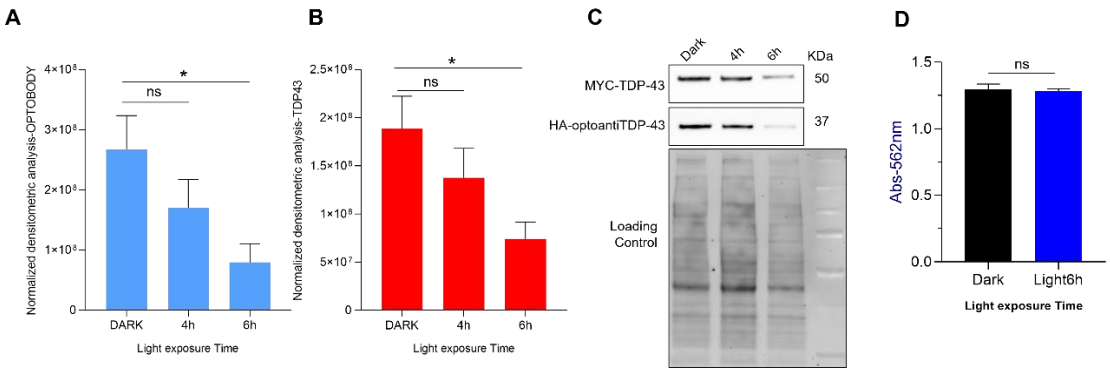

R4 ***Light-dependent targeted protein degradation in mammalian cells. A)*** *and* ***B)*** *quantification of light-dependent degradation of optobody and TDP-43, respectively by expressing them in HEK293T cells in a single vector.* ***C)*** *Representative western blotting of the experiments shown in A and B. Statistical analysis A) and B) Bonferroni corrected One-way Anova; Error bar = mean with S.E.M.; p-value ns>0,05; *< 0,05; **<0,01; ***<0,001; ****< 0,00001.*

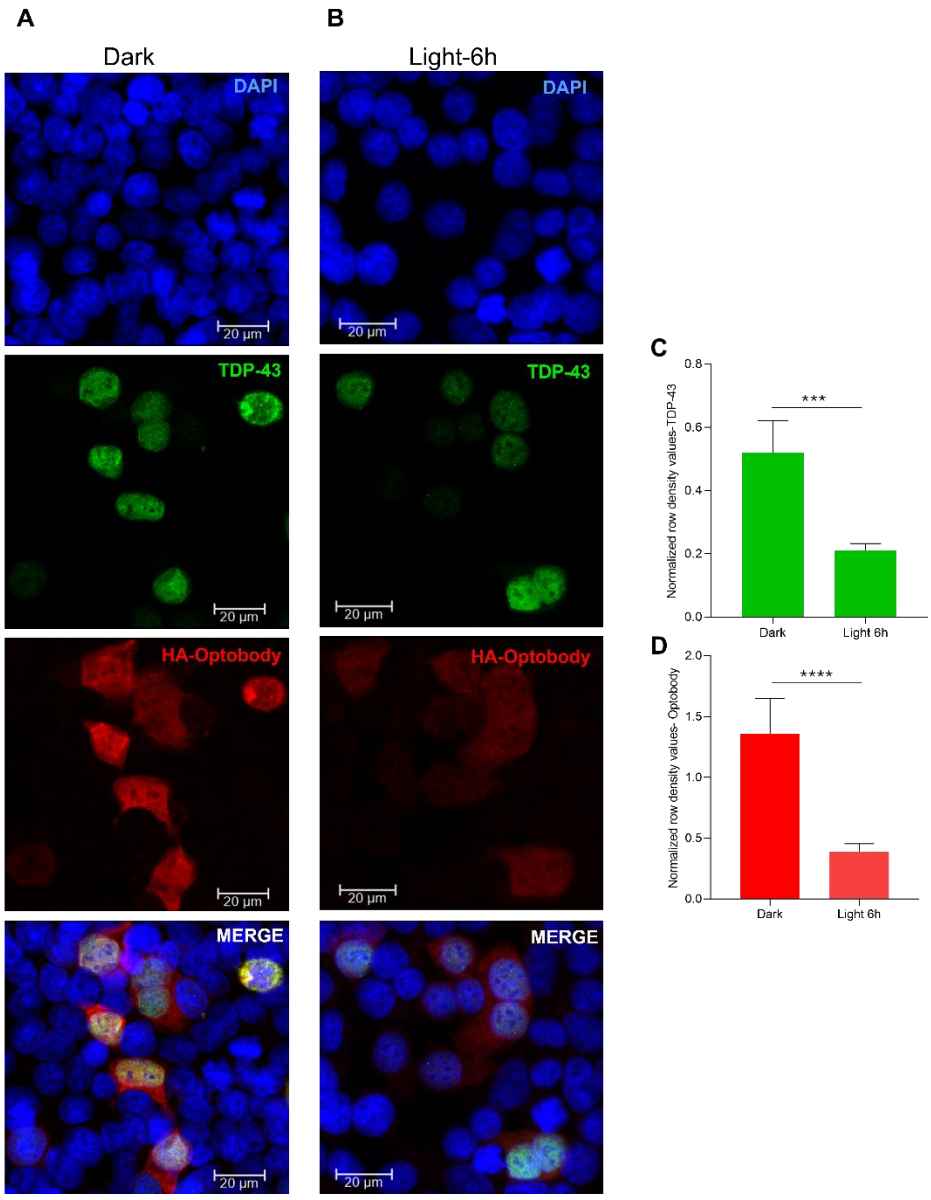

R5 ***Immunofluorescence analysis of targeted protein degradation in mammalian cells HEK293T.*** ***A)*** *HEK293T cells expressing MYC-TDP-43 and optobody anti-TDP-43 in dark condition, and* ***B)*** *in light condition.* ***C)*** *quantification of the fluorescence intensity of the TDP-43 and* ***D)*** *of the optobody in 6h of light stimulation. Statistical analysis C) and D) Unpaired t-test; Error bar = mean with S.E.M.; p-value ns>0,05; *< 0,05; **<0,01; ***<0,001; ****< 0,00001*

4.1.6 Targeted protein degradation of TDP-43: proteasome dependence

Having demonstrated an effective light-dependent Targeted Protein Degradation, I wanted to assess the proteasome involvement in the evident and significant protein level reduction demonstrated in the two cellular systems. The experiment aimed at pharmacologically inhibit the proteasome machinery and to evaluate the effect of blue light exposure on mammalian cells co-expressing both the optobody and TDP-43. To design these experiments, I decided to adapt the time window required to reach a significant reduction of the protein, with the inhibition of the proteasome system. I reasoned that to show the proteasome involvement in the light-dependent degradation, it was necessary to first apply a light stimulation protocol in cells

expressing both the partners, and to inhibit the 26S in the last two hours of the light protocol. The first preliminary experiment aimed at finding the ideal concentration of the MG132 proteasome inhibitor drug, considering that the cellular system was supposed to undergo also light stimulation. As shown in Figure R9 A and B, all the used concentrations of MG132 resulted in reduced cell viability if administered together with light exposure. Then, the best compromise for the experiment resulted to be the use of the minimal amount of MG132 found in literature (5 μM) during the selected time window of 2 hours. As illustrated in Figures R9C and D, the behaviour of TDP-43 and its optobody exhibits some differences. Specifically, a reduction in TDP-43 levels is observed after 6 hours of light in both the control condition and the MG132-treated sample, with no significant difference between the treated and untreated conditions (Figure R 9C). In contrast, for the optobody, inhibition of the 26S proteasome during the final two hours of light exposure leads to an increase in protein levels, with the difference from the control condition being statistically significant. Thus, while the 2 hours MG132 chase in the 4 to 6 light period appears to be sufficient to further inhibit the optobody degradation, this timing is not adequate to prevent the observed TDP-43 degradation. Different timing protocols might be required to observe an effect on the degradation of TDP-43. In any case, the experiment with the optoboy confirms that the light-dependent degradation mediated by the psd degron is proteasome-dependent.

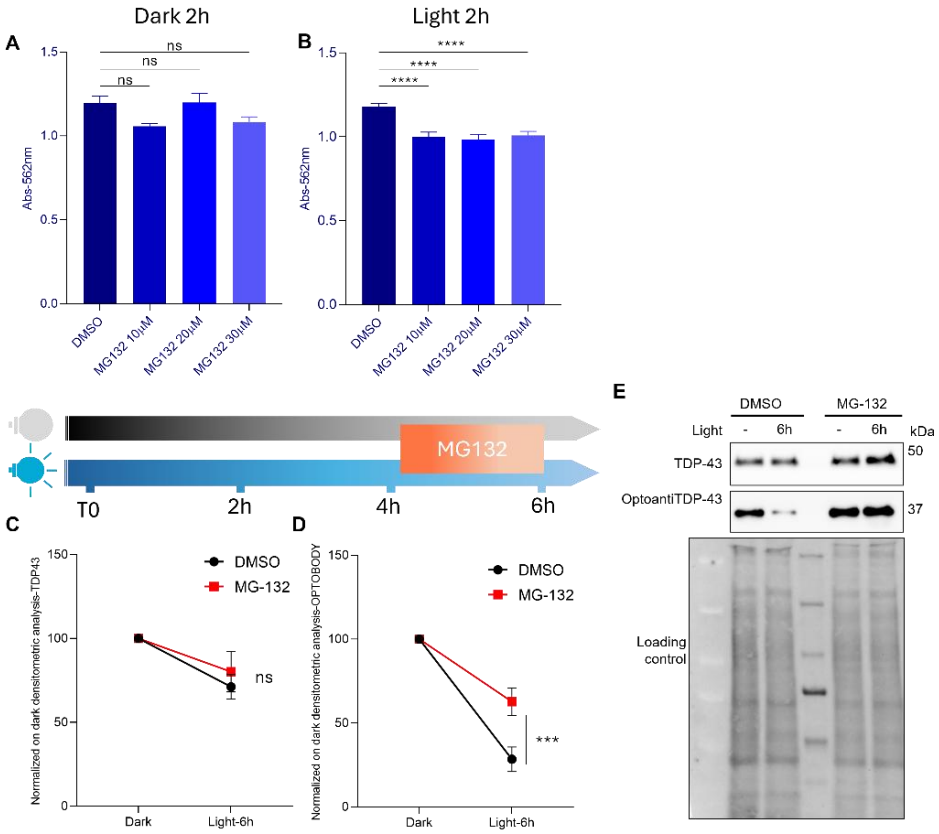

R 6 ***Proteasome inhibition chase experiments in HEK293T, A)*** *and* ***B)*** *MTT assay on HEK293T cells treated with MG132 in dark A and light B, n=5 replicates for A and n=12 replicates for B.* ***C)*** *and* ***D)*** *MG132 chase experiment in light-dependent degradation for the TDP-43 C and optobody D, n=8 independent experiments.* ***E)*** *representative western blotting of the quantification in C and D. Statistical analysis A) and B) Bonferroni corrected One-way Anova; C) D) Two-way Anova Sidak's multiple comparisons test; Error bar = mean with S.E.M.; p-value ns>0,05; *< 0,05; **<0,01; ***<0,001; ****< 0,00001*

4.1.7 Anti-TDP-43 optobody variants: delta degron and delta jα-chain

The second key feature of the optobody tool lies in the modularity of the construct. In addition to the intrinsic antigen-binding capability provided by the intrabody portion, two other essential conditions, light-dependence and degron dependence, are critical for enabling targeted protein degradation. To investigate these features, I cloned two variants of the optobody construct: one lacking the light-responsive element of the LOV domain, referred to as ΔJα, and the other lacking the degron signal, termed ΔODC1. These variants were co-expressed with TDP-43 in the format TDP-43-p2a-optobody to assess their effects on protein levels. The expectations for these constructs were a sort of light-insensitive constitutive degradation optobody for the Δjα , and a light-neutral optobody without the degradation activity for the ΔODC1 variant. In the dark, the Δjα anti TDP43 protein has a significantly lower expression than the control anti TDP-43 optobody (as shown in Figure R10D), and the same is true for the levels of TDP43 in the dark in the Δjα expressing cells than in the anti TDP-43 optobody expressing cells (as shown in Figure R10D). Upon light stimulation, the ΔJα optobody variant did not exhibit an additional

decrease in protein levels, which were already constitutively low in the dark (Figure R10A), and similarly for the TDP43 protein levels (Figure R10B). The ΔODC1 variant displayed no evidence for optobody degradation in the dark and a reduction trend similar to that of the full-length optobody, upon light stimulation (Figure R10 A). Conversely, no TDP-43 protein reduction was observed in the degron-deficient ΔODC1 optobody variant expressing cells, with respect to the control cells, either in the dark or upon light stimulation (Figure R10 B).

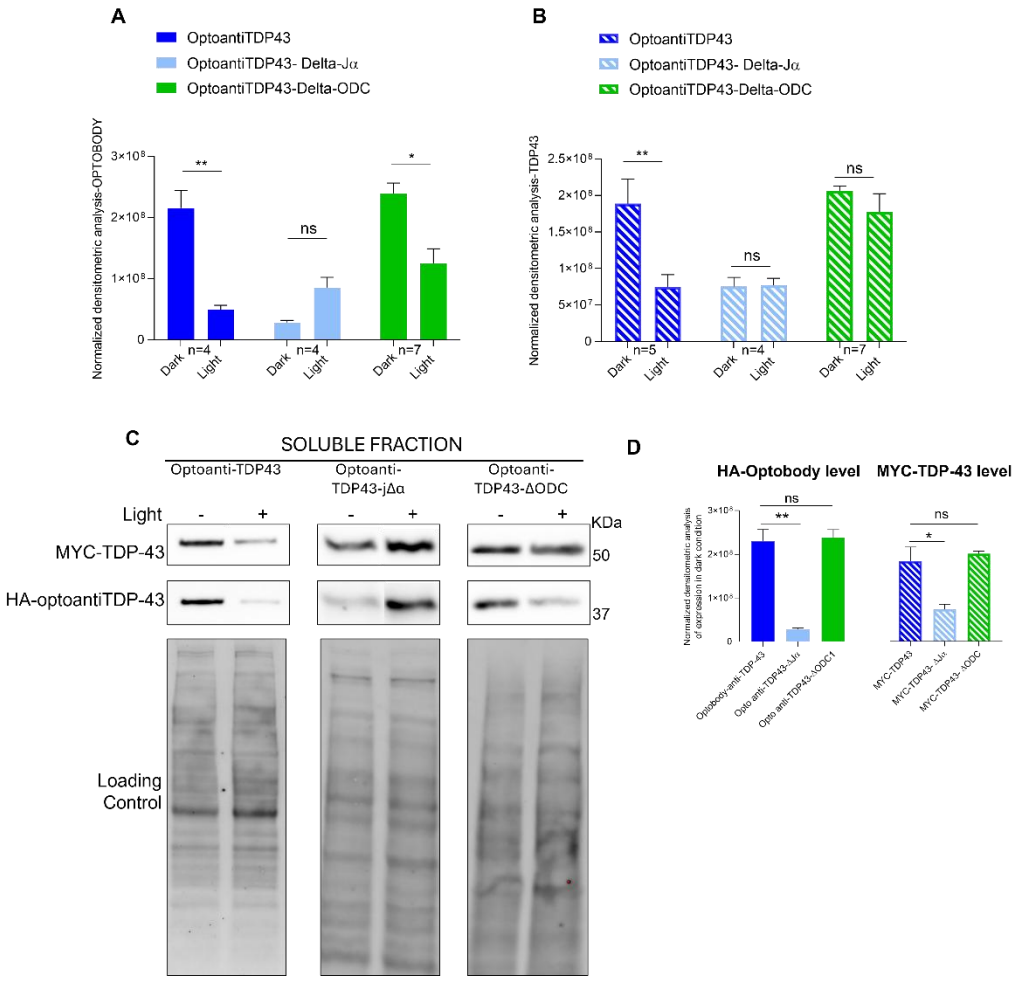

R 7 ***Comparisons between dark and light conditions among optobody variants.*** *A) B) Blue-light exposure experiments in HEK293T cells coexpressing the optobody and its variants together with TDP-43, quantification of optobody variation in A) and TDP-43 variation in B) in at least four independent experiments.* ***C)*** *Representative western blotting of the experiments shown in A and B and D.* ***D)*** *Quantification of the expression level of the optobody variants and TDP-43 in co-expression condition. Statistical analysis A) and B) Two-way Anova Sidak's multiple comparisons test; D) Dunnett's multiple comparisons test. Error bar = mean with S.E.M.; p-value ns>0,05; *< 0,05; **<0,01; ***<0,001; ****< 0,00001*

Having established that targeted protein degradation could only be achieved with the full-length version of the optobody was only half of the story. Indeed, the results shown so far have been obtained analysing the soluble fraction of the cellular extract. What about the partition in the insoluble cellular fraction? I sought to investigate further the behaviour of the optobody

formats in the insoluble fraction of the cellular protein extract. Figure R11 illustrates the trend of increase in the insoluble fraction for the optobody and its variants, even though this increase is not significant. Conversely, a prominent effect was found for the TDP-43 protein level, which undergoes a significant increase in the presence of the optobody lacking the degron signal (Figure R11B).

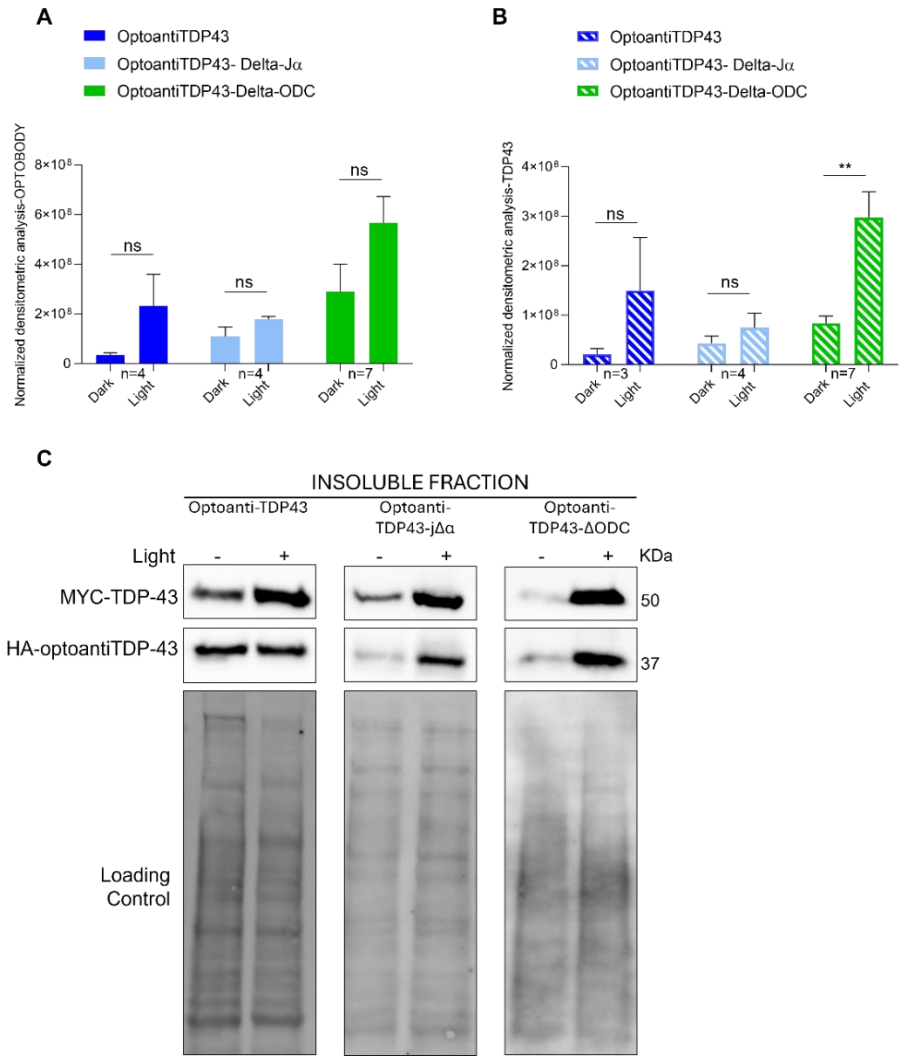

R8 ***Comparisons between dark and light conditions among the optobody variants in the insoluble fractions.*** ***A) B)*** *Blue-light exposure experiments in HEK293T cells coexpressing the optobody and its variants together with TDP-43, quantification of optobody variation in A) and TDP-43 variation in B) in at least four independent experiments.* ***C)*** *Representative western blotting of the experiments shown in A and B. Statistical analysis A) and B) Two-way Anova Sidak's multiple comparisons test; Error bar = mean with S.E.M.; p-value ns>0,05; *< 0,05; **<0,01; ***<0,001; ****< 0,00001.*

4.1.8 In vivo interaction between TDP43-NLS1mut and VHH5

Up to this point, the successful application of the intrabody-based optogenetic tool for the targeted protein degradation of TDP-43 has provided strong evidence of its validity and a

convincing proof of concept of the successful light-inducible degradation of the TDP-43 target protein.

Building on this successful proof of principle of the method, I shifted my focus towards exploring the targeted degradation of a disease-relevant mutant version of TDP-43, to investigate whether the light-inducible targeted degradation could interfere with specific biological pathways. To achieve this, I first assessed the in vivo interaction between the mutant TDP-43 and the optobody VHH5 in the yeast two-hybrid system, followed by co-immunoprecipitation assays in mammalian cells. Then I focused on the experiments to assess the different localizations of the mutant.

For the first part, L40 yeast cells were co-transformed with LexA-TDP-43 (K86S-R87S-K88S) in the pMicBD1vector, hereafter called TDP-43-NLS1mut, and the VHH5-anti-TDP-43-VP16 in the pLinker220 vector. As a positive control for the interaction, an intrabody anti-LexA protein was used. To better evaluate the interaction by monitoring the survival on the selective plates, 1,5 mM 3-AT was used in order to lower the transactivation and reduce false positive clones. As shown in Figure R12, although the mutations are in the N-terminal region of the TDP-43, where the VHH5 nanobody epitope is located, the binding with VHH5 is not affected, and is still effective. Indeed, the survival of the yeast cells expressing the VHH5 nanobody and TDP-43-NLS1mut in the selective medium is comparable to the growth of the WT TDP-43 strain (Figure R12).

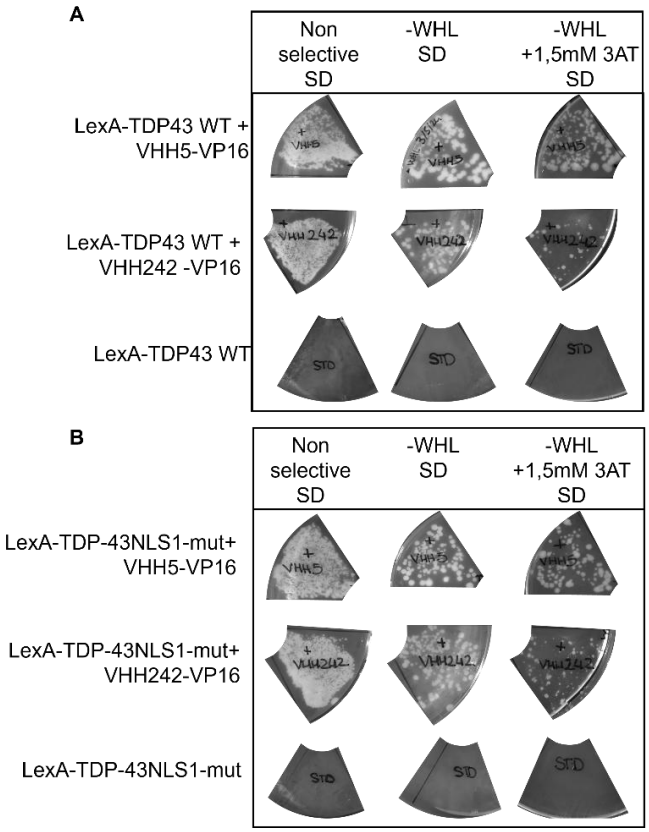

R 9 ***In vivo testing for the interaction between TDP-43 NLS1mut with VHH5 using the yeast two-hybrid system****. **A)** In vivo interaction between the LexA-TDP-43 WT and VHH5 compared to the positive control VHH242 anti-LexA. **B)** Interaction between LexA-TDP-43 NLS1 mutant and VHH5 compared to the VHH242 positive control of growth.*

Co-immunoprecipitation of TDP-43 WT and NLS1 mutant

The second validation step for the interaction was done by the co-immunoprecipitation of the TDP-43-NLS1mutant in mammalian cells expressing both the optobody anti-TDP-43 and its target. Figure R13B shows that in protein extract from HEK 293T cells expressing TDP-43 WT or the TDP-43-NLS1mutant and the HA-tagged-optobody, the immunoprecipitation of the optobodies with HA-beads allowed for the co-precipitation of both TDP-43 WT and TDP-43 NLS1mutant proteins , while the co-immunoprecipitation does not occur in cells expressing TDP-43 protein and an unrelated anti GFP optobody.

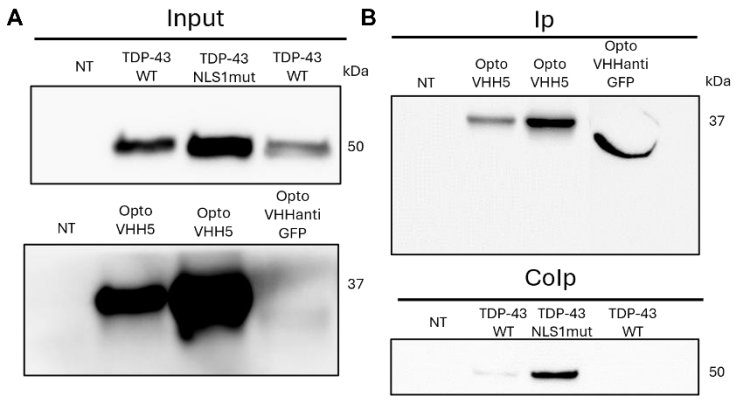

R10 ***Co-immunoprecipitation in HEK293T cells of MYC-tagged TDP-43 WT and TDP-43-NLS1mutant.*** *Immunoprecipitation of the optobodies from protein extract of the cells coexpressing TDP-43 WT and the mutant with the optobody5; an unrelated optobody was used as negative control. In* ***A) Input*** *shows the expression of TDP-43 and the optobody in the extract used for the co-IP;in* ***B) Ip*** *shows the blotting with anti-HA-antibody to check the pulled down proteins;* ***CoIP*** *shows the blotting with anti-MYC-antibody of the interacting proteins.*

Different localization of TDP-43 induced by disruption of NLS region

After confirming that disruption of the NLS1 region in TDP-43 does not abolish the epitope recognized by anti TDP-43 intrabody VHH5, the next step was to investigate its prominent localization in the cytosolic compartment, in comparison to the wild-type version. To this aim I investigated the fluorescence obtained using mouse anti-MYC-antibody and Alexa-Fluor-488 anti-mouse secondary antibody in HEK293T cells either transfected with the myc-tagged wild type TDP-43 or the TDP-43-NLS1mutant. As shown (Figure R14), the immunofluorescence experiment demonstrated that while for the wild-type the TDP-43 staining is mainly located into the nucleus, the fluorescence of the TDP-43-NLS1 mutant is equally distributed between the nucleus and the cytoplasm of the cell. Thus, the quantification of the fluorescence signal shows that almost 100% of the fluorescence detected for the wild type localises into the nucleus, while the fluorescence of the mutant is equally distributed between nuclear and cytosolic compartments.

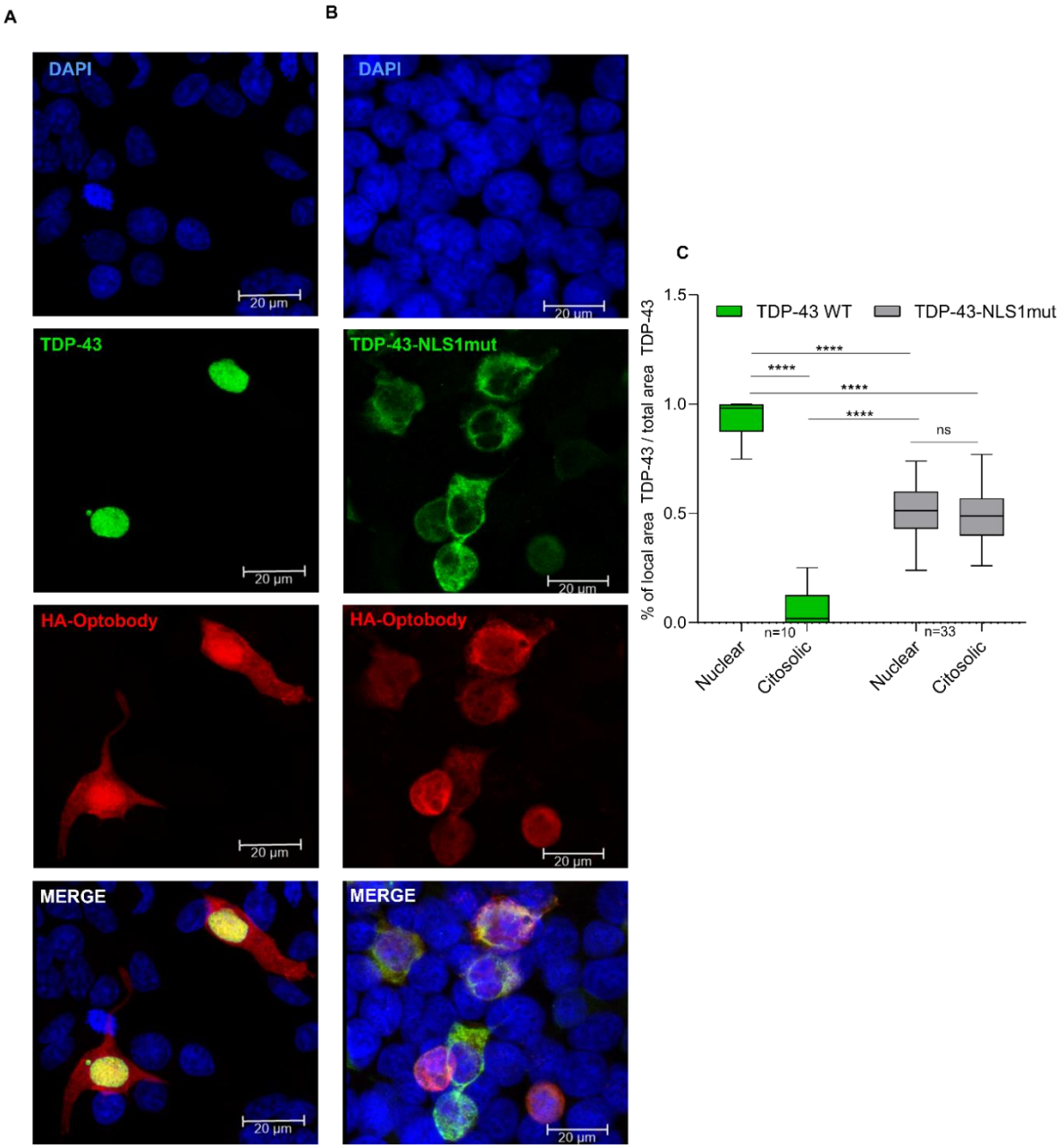

R 11 ***Different localization of TDP-43 NLS1 mutant variant. A)*** *and* ***B)*** *immunofluorescence on HEK293T cells expressing the MYC-TDP-43 wt or mutant (K86S-R87S-K88S).* ***C)*** *Quantification of the localization of the signal between the nucleus and the cytosol of individual cells. Statistical analysis C) Two-way Anova Sidak's multiple comparisons test; Error bar = mean with S.E.M.; p-value ns>0,05; *< 0,05; **<0,01; ***<0,001; ****< 0,00001.*

The last step in the validation of the tool was to check the light-induced degradation of the TDP-43-NLS1 mutant. Before this, I investigated whether the light stimulation alone could affect the solubility of the mutant version compared to that of the wild-type TDP-43. Again, the behaviour of the two variants is different, indeed, as shown in Figure R15B the mutant undergoes a significant increase in the insoluble fraction in light conditions, while the soluble fraction in 6h of dark does not change.

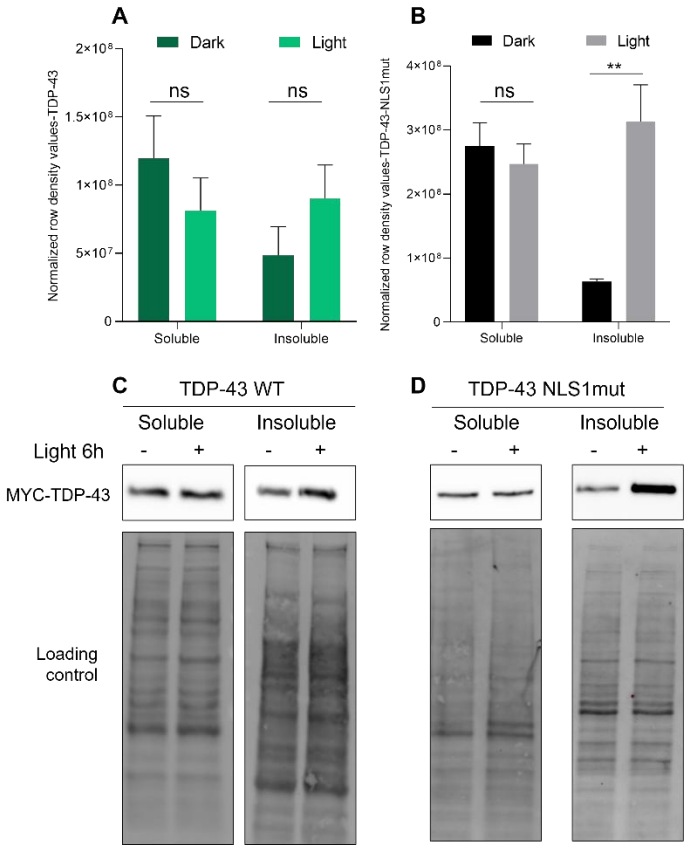

R 12 ***Effect of light exposure to TDP-43 soluble and insoluble fractions. A)*** *and* ***B)*** *quantification of the variation of the soluble and insoluble fractions of TDP-43 WT (A) or NLS1-mutant (B) due to light exposure, on n=5 independent experiments for A) and n=3 independent experiments for B).* ***C)*** *and* ***D)*** *Representative western blotting of the experiments shown in A and B, respectively. Statistical analysis Two-way-Anova -Sidak's multiple comparisons test; Error bar = mean with S.E.M.; p-value ns>0,05; *< 0,05; **<0,01; ***<0,001; ****< 0,00001*

Taking advantage of the information gained from the experiments on HEK293T cells with the wild type, I tested the optobody-dependent reduction of TDP-43 NLS1 mutant after 6 hours of light stimulation. To provide a more comprehensive analysis of the protein fractions, I quantified the variations in protein levels due to light-activated proteasomal degradation by performing western blotting on both the soluble and insoluble fractions of the cellular extracts (Figure R16). Despite the previous demonstration of cytosolic mislocalization (Figure R14), analysis of the soluble fraction following light stimulation revealed that the degradation pattern is maintained: I found a significant reduction for both the optobody (Figure R16A) and the TDP-43 mutant (Figure R16B). These results were further confirmed in the immunofluorescence experiments shown in Figure R17. In contrast, the insoluble fraction (Figure R16D-E-F) showed an increase under light conditions, though this change is not statistically significant.

Thus, I conclude that the targeted degradation of both WT TDP-43 and the TDP-43-NLS1 mutant, while leading to a decrease of the target in the soluble fraction, it concomitantly leads to a light-dependent increase of the two proteins in the insoluble fraction. This insoluble pool might correspond to the proteins associated to the proteasome compartments, and to their engagement in the degradation pathway.

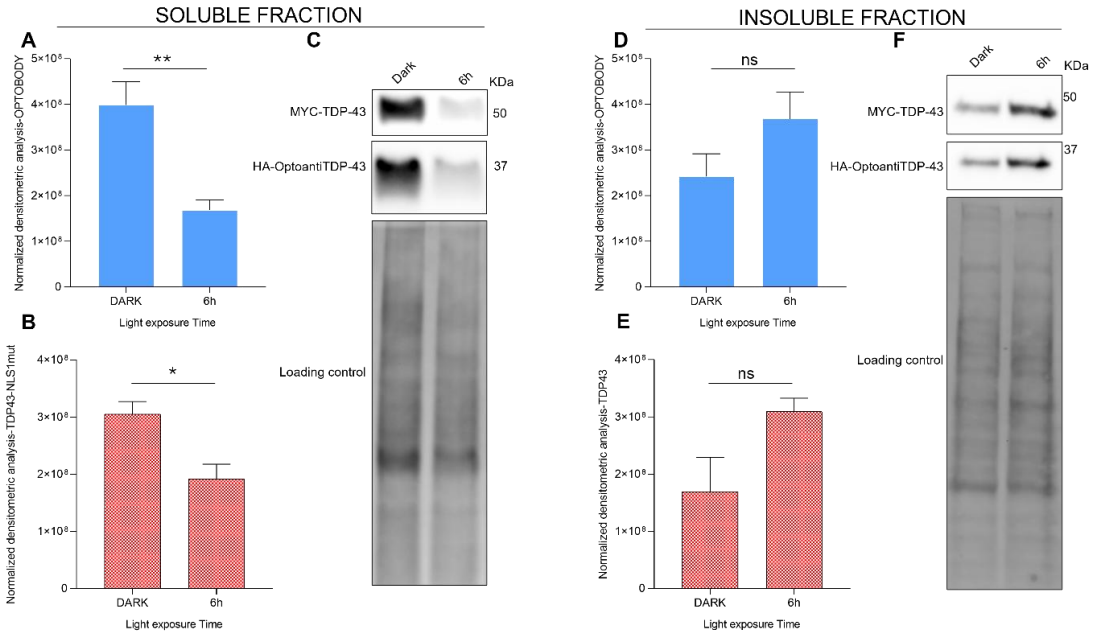

R 13 ***Light-dependent degradation of TDP-43 NLS1 mutant.*** ***A)*** *and* ***B)*** *quantification of the soluble extracts from HEK293T cells coexpressing MYC-tagged TDP-43 NLS1 mutant and the optobody in n=5 independent experiments,* ***C)*** *representative western blotting of the experiments in A) and B).* ***D)*** *and* ***E)*** *same quantification as A and B, performed in the insoluble extracts of n=5 independent experiments, F) representative western blotting of the experiments in D and E. Statistical analysis Unpaired t-test; Error bar = mean with S.E.M.; p-value ns>0,05; *< 0,05; **<0,01; ***<0,001; ****< 0,00001*

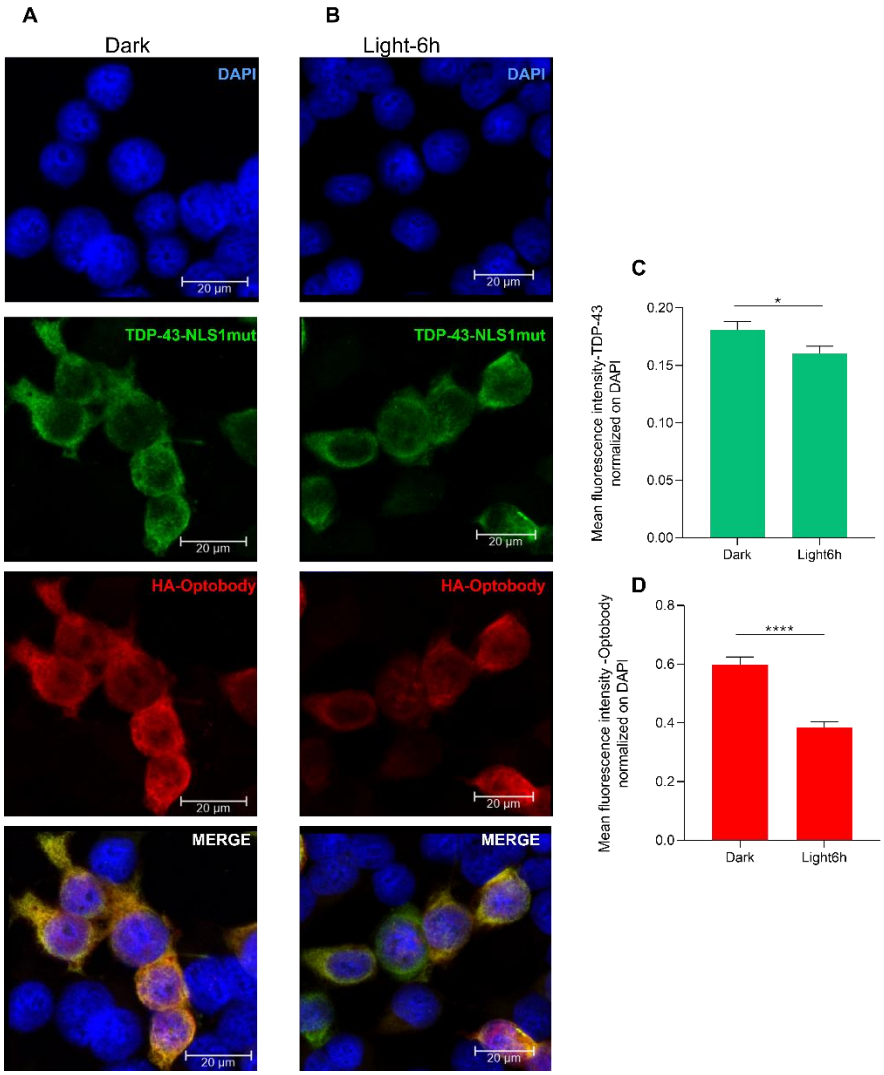

R 14 ***Immunofluorescence analysis of targeted protein degradation of TDP-43-NLS1 mutant in mammalian cells. A)*** *HEK293T cells expressing MYC-TDP-43 and optobody anti-TDP-43 in dark condition, and* ***B)*** *in light condition.* ***C)*** *quantification of the fluorescence intensity of the TDP-43 and* ***D)*** *of the optobody in 6h of light stimulation. Statistical analysis C) and D) Unpaired t-test; Error bar = mean with S.E.M.; p-value ns>0,05; *< 0,05; **<0,01; ***<0,001; ****< 0,00001*

4.1.8 TDP-43NLS1 mutant degradation-dependent variation of global translation

The positive results from the degradation of the mutant version of TDP-43 motivated me to further investigate the functional implications of both the expression and subsequent degradation of this mislocalizing variant.

Since it has been proposed that this particular mutant form of TDP-43 can affect global translation in HEK293T cells (Russo et al., 2017), I aimed to use this functional aspect to investigate whether the targeted degradation of the mislocalized TDP-43 mutant would affect the global translation profile in transfected cells.

Before examining global translation, I considered which proteins were most likely to interact with TDP-43 in the translation process. The literature highlighted RACK1 as a key interactor involved in this process (Russo et al., 2017). The experiments described below were designed to investigate how the degradation of the mislocalization-related version of TDP-43 might affect Rack1-dependent global translation. To monitor global translation levels, I employed the Surface Sensing of Translation (SUnSET) technique, which quantifies puromycin incorporation into the translation machinery of living cells. Before comparing global translation in HEK293T cells coexpressing mutant TDP-43 and optobody under light exposure, I first validated the SUnSET method in my hands and system. To do so, I assessed whether variations in puromycin incorporation, reflecting changes in global protein expression, could be detected by Western blotting. As shown in Figure R18, I tested puromycin incorporation in HEK293T cells treated or not with the translation inhibitor cycloheximide (CHX). In Figure R18B, two hours of CHX treatment resulted in a significant reduction in puromycin incorporation, with the signal from CHX-treated cells being as low as that from cells that did not receive puromycin, essentially matching the background signal of the technique.

.

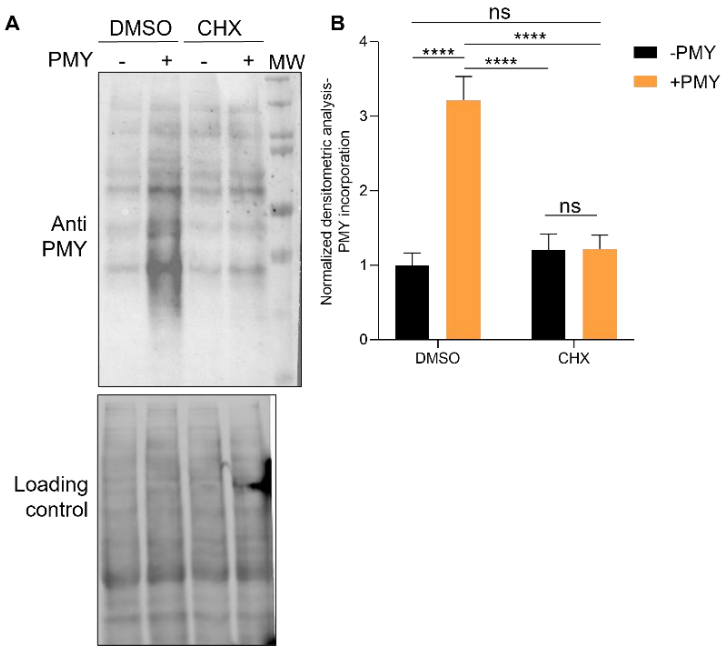

R 15 ***Surface Sensing of Translation (SUnSET)****. **A)** Representative SunSET western blot anti-puromycin for the **B)** quantification of the puromycin incorporation of untransfected HEK293T cells treated with CHX to induce protein synthesis shut off in n=3 independent experiments. Statistical analysis Two-way Anova Tukey's multiple comparisons test; Error bar = mean with S.E.M.; p-value ns>0,05; *< 0,05; **<0,01; ***<0,001; ****< 0,00001*

Another assessment to evaluate TDP-43-dependent changes in global translation upon degradation was to verify that the interaction with Rack1 was preserved in the presence of the optobody. In other words, the experiment requires that the epitope of the anti-TDP-43 VHH5 nanobody is different from the Rack1-TDP-43 protein-protein interaction domain. To achieve this, I did co-immunoprecipitation experiments on HEK293T cells transfected with MYC-TDP-43-NLS1 mutant and with the anti-TDP-43 optobody. On this protein extract, prepared in RIPA buffer, the same used for light-induced degradation quantification, I decided to pull down with anti-MYC antibody the mutant TDP-43, then, I checked whether endogenous Rack1 was still detectable. In Figure R19, the first experiment is shown: although the Rack1 band is clearly expressed both in the input extract and in the unbound extract, collected before the elution, no signal was found in the elution fraction. I then reasoned that there was a technical issue for the abolishment of this interaction; indeed, I assumed that the composition of the RIPA buffer could interfere with the interaction between Rack1 and TDP-43, thus I repeated the experiment using the milder extraction buffer PBS. In these conditions, as shown in Figure R20C, the immunoprecipitation of MYC-tagged TDP-43 allowed for the detection of Rack1 both in the presence of the optobody anti-TDP-43 and in the presence of an unrelated optobody anti-GFP.

Rack1 co-immunoprecipitation in RIPA

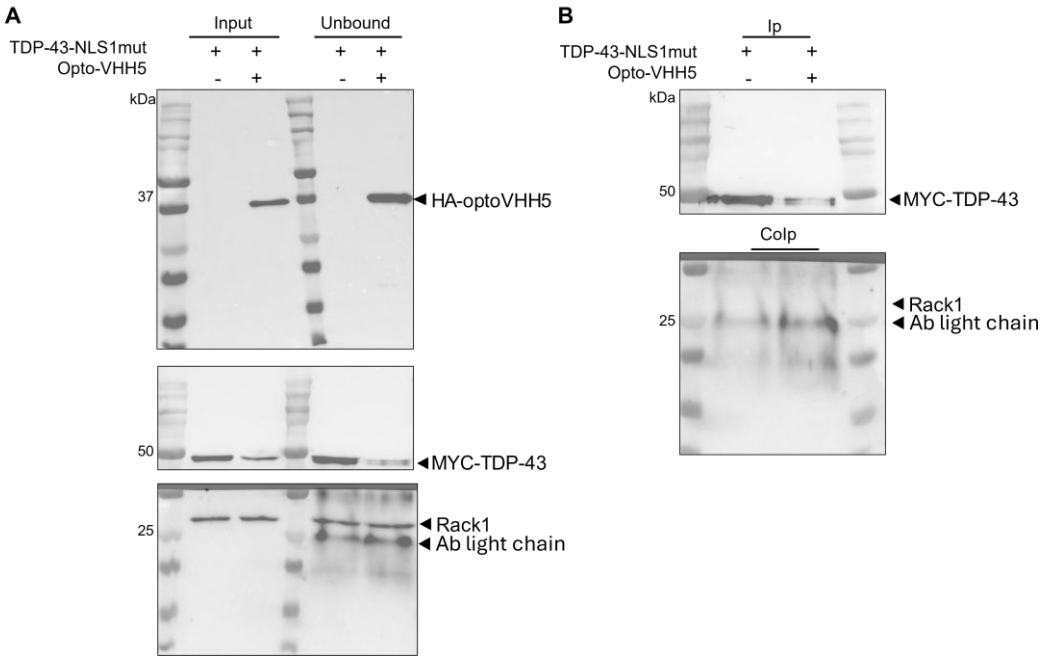

R 16 ***Co-immunoprecipitation of endogenous Rack1 in HEK293T expressing cells MYC-tagged TDP-43NLS1mutant and the optobody-antiTDP-43 RIPA buffer.*** *Immunoprecipitation of MYC-TDP-43 NLS1 with and without the optobody5;* ***A) Input*** *shows the expression of MYC- TDP-43 mut and the optobody in the extract used for the co-iP* ***Unbound*** *shows the extract after immunoprecipitation and before the elution; ;in* ***B) Ip*** *shows the blotting with anti MYC-antibody to check the pulled down proteins;* ***CoIP*** *shows the blotting with anti Rack1-antibody of the interacting proteins*

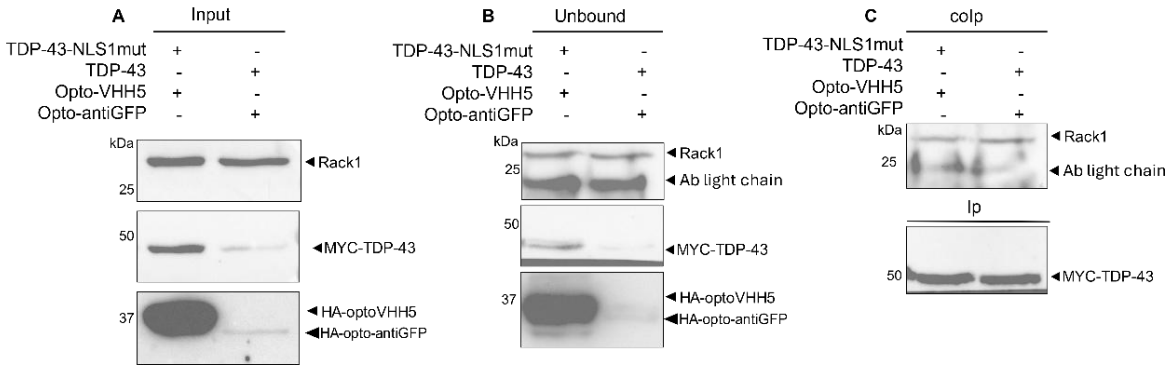

R 17 ***Co-immunoprecipitation of endogenous Rack1 in HEK293T expressing cells MYC-tagged TDP-43NLS1 mutant and the optobody-antiTDP-43 PBS buffer.*** *Immunoprecipitation of MYC-TDP-43 NLS1 with and without the optobody5 and with the unrelated optobody anti-GFP;* ***A) Input*** *shows the expression of MYC-TDP-43 mut and the optobody in the extract used for the co-iP;* ***B)Unbound*** *shows the extract after immunoprecipitation and before the elution; ;* ***C)CoIP*** *shows the blotting with anti-Rack1 antibody of the interacting proteins;* ***Ip*** *shows the blotting with anti-MYC antibody to check the pulled down proteins.*

Having established that the optobody does not interfere with the interaction between TDP-43 and Rack1, the subsequent experiment aimed to investigate the possible contribution of the TDP-43 NLS1 mutant to global translation changes. Figure R21 illustrates the impact of TDP-43 NLS1mutant degradation on global translation levels. Specifically, upon optobody-mediated light- induced degradation, there is a marked reduction in the levels of the TDP-43 NLS1 mutant protein (Figure 21A). Again, a reduction is found in the global protein synthesis level in the dark condition compared to the global translation monitored in the untransfected control dark condition (Figure 22C). When comparing the dark and light conditions of PMY incorporation in cells undergoing TDP-43 NLS1 mutant degradation, a significant increase in global translation was observed upon light-induced TDP-43 NLS1 mutant (Figure 21C). This demonstrates that degradation of TDP-43 NLS1 protein removes an inhibitory step of global translation.

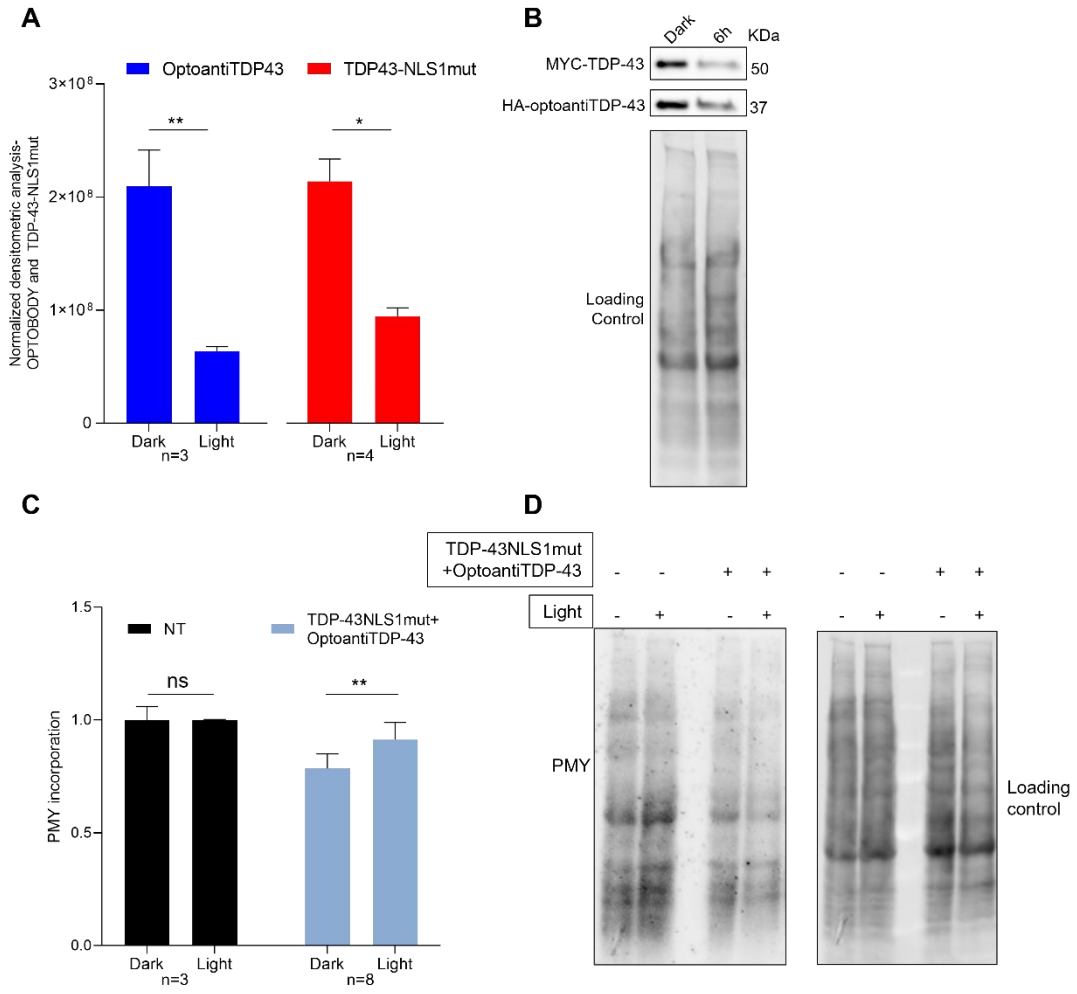

R 18 ***Degradation of mislocalized TDP-43 restores global translation A)*** *quantification of the light-induced degradation of the optobody and* ***B)*** *TDP-43NLS1 mutant in HEK293T cells coexpressing TDP-43 mutant and Optobody treated with PMY and* ***C)*** *representative western blotting of A) and B).* ***D)*** *quantification of puromycin incorporation of the same samples of A and B.* ***D)*** *representative western blotting of the experiments in C. Statistical analysis A) and B) Unpaired t-test; C) Two-way ANOVA Sidak's multiple comparisons test; Error bar = mean with S.E.M.; p-value ns>0,05; *< 0,05; **<0,01; ***<0,001; ****< 0,00001*

Having demonstrated the effect of the TDP-43NLS1 mutant degradation on protein synthesis, I further investigated the role of Rack1 in this process, given its well-documented involvement in translation. Since the interaction between Rack1 and TDP-43 in the presence of the optobody is preserved, I then asked whether the removal of Rack1 from the cellular system would lead to a more pronounced effect on the global translation activity. Thus, I explored a light-dependent TDP-43 NLS1 degradation experiment in HEK293T cells coexpressing TDP-43 NLS1 mutant and its optobody, upon co-transfection with a siRNA for Rack1, to obtain Rack1 protein knockdown. In Figure R22D, it is evident that Rack1 siRNA treatment reduces Rack1 levels, although this reduction is not statistically significant. However, the decrease in Rack1 levels leads to a reduction in global translation, which is not rescued by TDP-43 targeted

degradation, not even after light exposure (Figure R22E). These findings indicate that the role of TDP-43 in regulating global translation is dependent on Rack1 protein levels. Although the degradation of the TDP-43 NLS1 mutant is necessary to restore the global translation process, it is not sufficient when Rack1 is knocked down.

RACK1 contribution on global translation variation in light-induced degradation of TDP43-NLS1mutant

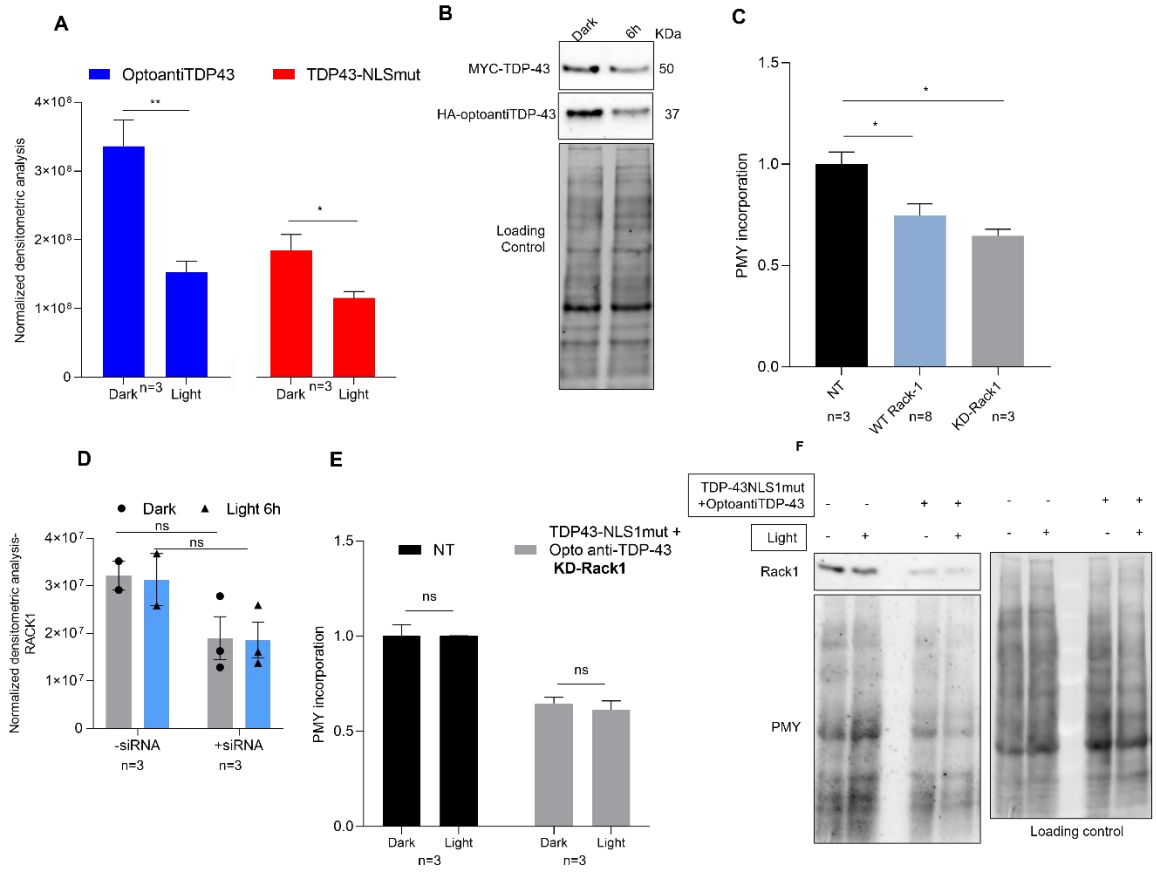

R 19 ***Rack1 involvement in TDP-43 degradation dependent rescue of global translation.*** ***A)*** *quantification of the light induced degradation of the optobody and TDP-43NLS1 mutant in HEK293T cells coexpressing TDP-43 mutant and Optobody in condition of Rack1 knockdown and treated with PMY and* ***B)*** *representative western blotting of A)* ***C)*** *comparison of PMY incorporation in dark conditions in RACK1 WT and KD in co-expression of TDP-43 mutant and optobody5.* ***D)*** *quantification of Rack1 reduction and* ***E)*** *quantification of puromycin incorporation in the same samples of A.* ***F)*** *representative western blotting of the experiments in C and D. Statistical analysis A) Unpaired t-test-; C) Dunnet multiple comparisons test, D) and E) Two-way ANOVA Sidak's multiple comparisons test; Error bar = mean with S.E.M.; p-value ns>0,05; *< 0,05; **<0,01; ***<0,001; ****< 0,00001.*

4.1.9 Ligand-induced degradation of VHH5-Ikβ

At this stage, after validating the Optobody system as a degradation tool, my research aimed to make a connection with previous foundational work from the lab, and to compare the degradation efficiency induced by blue light exposure with that achieved through another validated ligand-inducible degradation system for targeting proteins, developed in our lab using TNFα treatment as a degradation inducing signal (Melchionna & Cattaneo, 2007). To this end, I fused the anti-TDP43 intrabody VHH5 with the Ikβ domain and proceeded to design a degradation experiment using the "TNF-dependent suicide" intrabody. The experimental setup leveraged previously validated conditions for the Tau2 intrabody, as outlined in Melchionna et al.

Given that the goal was to compare two distinct degradation pathways triggered by the intrabody, I transfected HEK293T cells with VHH5-Ikβ. 24h after the transfection, the cells were split into two plates, one to be treated with TNFα and the second one without, as a negative control of the degradation. Thus, 48h after the transfection, the cells were treated with TNFα for 30 minutes. As shown in Figure R23A, TNFα treatment led to a certain reduction in VHH5-Ikβ levels, though this decrease was not statistically significant. Considering that the expression levels of the construct were relatively low even in the absence of the degradation inducer stimulation, I hypothesized that the Ikβ degron might have reduced the half-life of the entire construct, even in the absence of TNFα. To further explore this, I expressed the suicide intrabody and assessed the protein levels in the presence of a 2-hour proteasome inhibitor treatment, then administered the TNFα during the last 30 minutes of the treatment.

As depicted in Figure R23B, the trend observed in both the presence and absence of TNFα was similar: the protein levels of VHH5-Ikβ nearly tripled over 2 hours of MG132 treatment. Since the increase in protein levels under proteasome inhibition is expected, I sought to investigate the hypothesis that the VHH5-Ikβ construct may have a reduced half-life by performing a parallel MG132 chase experiment. This experiment involved HEK293T cells expressing the VHH5 intrabody, with or without the TNF-inducible degron. As shown in Figure R23C, when the intrabody was expressed without the degron signal, no significant increase in protein levels was observed upon proteasome inhibition. However, despite the increase in VHH5-Ikβ protein levels as seen in Figure R23B, the expression of the intrabody with the Ikβ degron was strongly lower than the expression level of the intrabody without the degron.

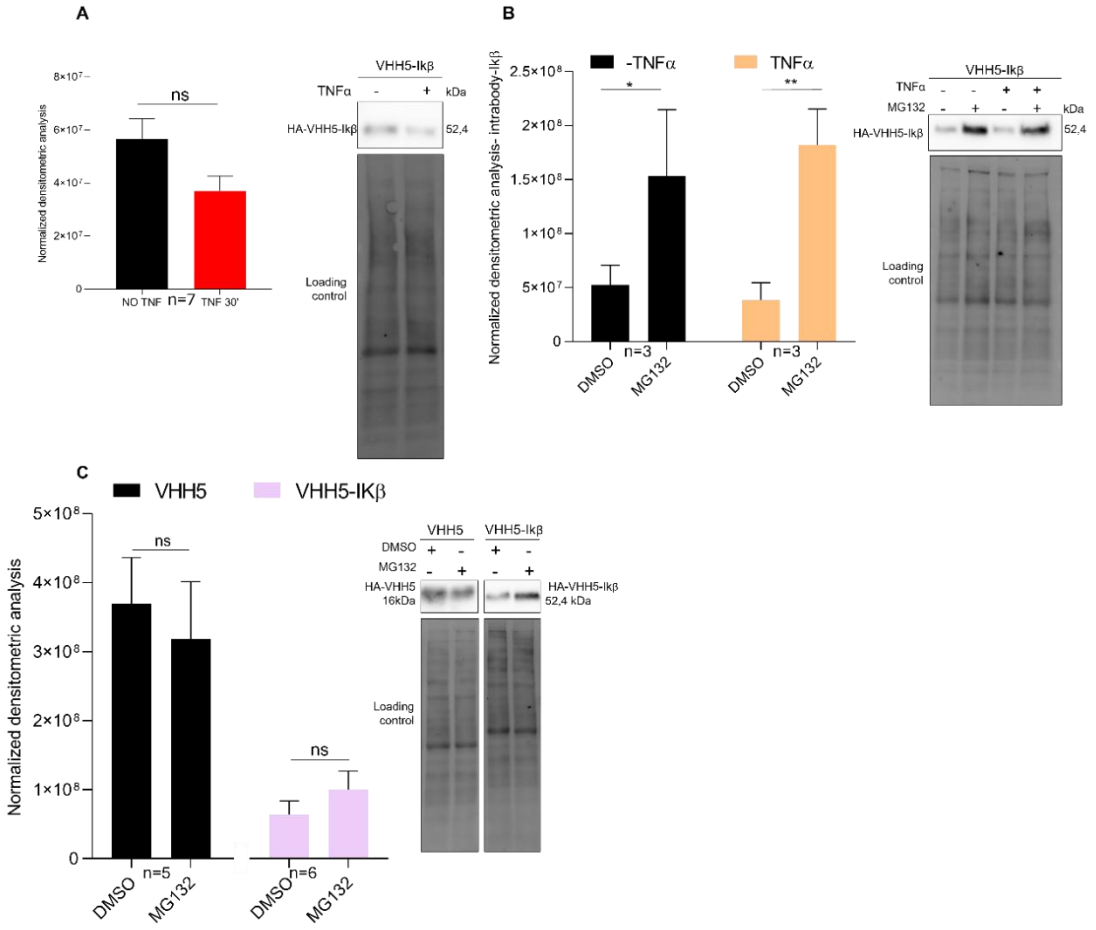

*R 20**Validation of VHH5-ikβ as a tool for TNFα mediated targeted degradation.** **A)** Quantification (barplot on the left) of intrabody reduction in HEK293T cells expressing VHH5-Ikβ induced with 30' of TNFα and representative western blotting (on the right). **B)** MG132-chase experiments in HEK293T cells expressing VHH5-Ikβ, were treated with 2h hours of MG132 and 30' of TNFα, representative western blotting on the right. **C)** MG132-chase experiments as in B, comparing the protein level in the absence or the presence of the Ikβ degron, representative western blotting on the right. Statistical analysis Unpaired t-test-; B) and C) Two-way ANOVA Sidak's multiple comparisons test; Error bar = mean with S.E.M.; p-value ns>0,05; *< 0,05; **<0,01; ***<0,001; ****< 0,00001.*

The second step to the comparison of the two systems was to effectively investigate the targeted protein degradation of TDP-43, mediated by the TNFα inducible suicide antibody. Before a real comparison, I aimed to assess the TDP-43 targeted protein degradation in HEK293T cells in co-expression conditions of both the antigen protein and its degron-fused intrabody as previously described. In the experiments in Figure R24, I tested the reduction of TDP-43 protein in co-expression conditions with anti-TDP-43 or unrelated anti-GFP intrabody fused to the Ikβ. Again, as shown in Figure R24A, neither the anti-TDP43 nor the anti-GFP is significantly reduced upon the treatment, and consequently, the TDP-43 protein level remains unaffected.

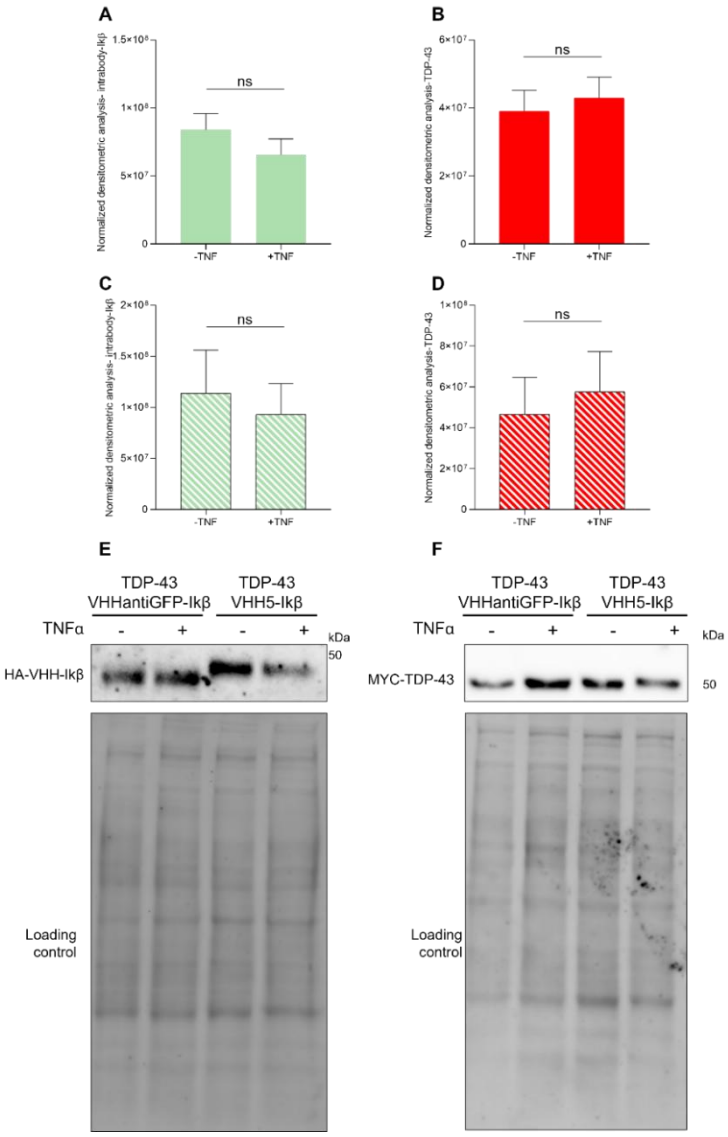

R 21 ***TNFα -induced targeted protein degradation of TDP-43. A)*** *Quantification of VHH5-Ikβ and* ***B)*** *TDP-43 upon TNFα treatment in HEK293T cells expressing both the suicide intrabody and its target;* ***C)*** *and* ***D)*** *same experiment in HEK293T cells coexpressing unrelated suicide intrabody anti-GFP, as control, and TDP-43, respectively.* ***E)*** *representative western blotting for the HA-tagged intrabodies in A and C, and* ***F)*** *for the MYC-tagged TDP-43 in B) and D). Statistical analysis: Unpaired t-test; Error bar = mean with S.E.M.; p-value ns>0,05; *< 0,05; **<0,01; ***<0,001; ****< 0,00001.*

Ligand-induced degradation of TDP-43 in HeLa cells

The last attempt to set the experimental condition for ligand-induced degradation was to change the cellular model to the HeLa cell line, to increase the TNF receptor expression, and therefore to raise the effect of the treatment. Again, the first experiment in HeLa cells was to check for the expression level of the intrabody and to compare it with the expression level in the proteasome inhibition condition. In this case, as expected, the trend for the increase of the protein level due to MG132 treatment is similar in both the absence and presence of TNFα (Figure R25).

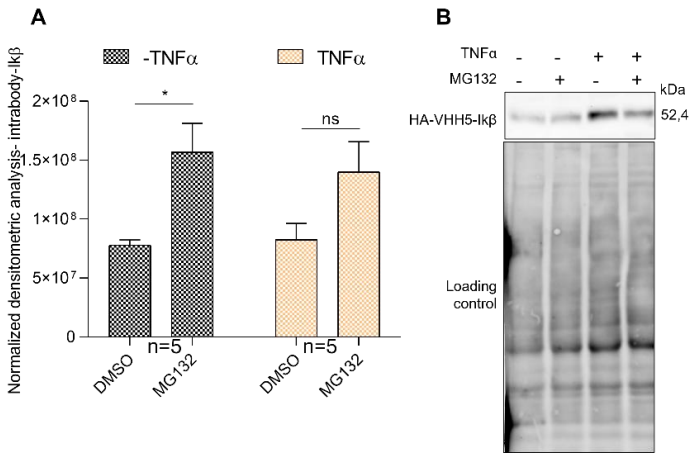

R 22 ***Validation of VHH5-ikβ in HeLa cell lines.*** *A) MG132-chase experiments in HeLa cells expressing VHH5-Ikβ, treated with 2 hours of MG132 and 30' of TNFα,* ***B)*** *representative western blotting. Statistical analysis: Two-way ANOVA Sidak's multiple comparisons test, Error bar = mean with S.E.M.; p-value ns>0,05; *< 0,05; **<0,01; ***<0,001; ****< 0,00001.*

Lastly, when HeLa cells were transfected to express TDP-43 along with the degron-intrabodies VHH5 or VHHanti-GFP, no significant reduction in intrabody levels (Figure R26 A-C) or targeted protein degradation (Figure R26 B) was observed upon treatment.

More experiments will be needed to compare the inducible targeted degradation systems mediated by TNFα or by light, in head-to-head experiments, taking however into consideration that TNFα is a highly bioactive ligand and certainly not an orthogonal synthetic regulating switch as light, that is certainly to be preferred.

Therefore, having successfully demonstrated that light-induced degradation is effective to achieve specific degradation with the corresponding anti-TDP-43 VHH5 optobody, I undertook to apply this strategy to the ambitious aim of achieving the targeted selective degradation of the post-translationally modified pool of a cellular protein.

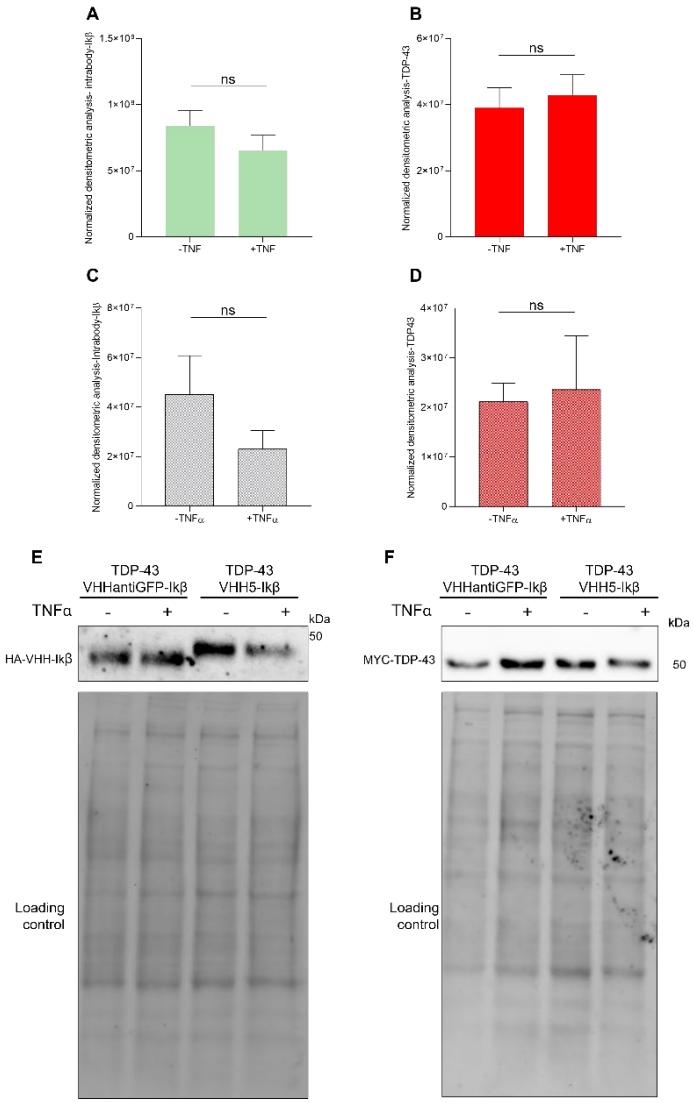

R 23 ***TNFα -induced targeted protein degradation of TDP-43. A)*** *Quantification of VHH5-Ikβ and* ***B)*** *TDP-43 upon TNFα treatment in HeLa cells expressing both the suicide intrabody and its target;* ***C)*** *and* ***D)*** *same experiment in HEK293T cells coexpressing unrelated suicide intrabody anti GFP, as control, and TDP-43, respectively.* ***E)*** *representative western blotting for the HA-tagged intrabodies in A and C and* ***F)*** *for the MYC-tagged TDP-43 in B and D. Statistical analysis: Unpaired t-test; Error bar = mean with S.E.M.; p-value ns>0,05; *< 0,05; **<0,01; ***<0,001; ****< 0,00001.*

4.2 Part II

4.2.1 Opto scFv against phosphorylated Tau protein at T231-S235

The chosen protein target, to attempt the targeted selective degradation of the post-translationally modified pool of a cellular protein, was the microtubule binding protein Tau. The chosen post-translational modification was tau Serine/Threonine phosphorylation, that is known to be pathologically altered Alzheimer's disease.

The second intrabody used in this work, to apply the optobody design to a case of great interest, was the scFv-p231-235, recognizing the phosphorylated form of Tau protein (Shih et al., 2012). To achieve the final goal of phosphorylation-state-dependent targeted protein degradation, the first assessment was to verify the antigen binding in the cellular system chosen to test the light-dependent degradation, namely the L40 yeast strain. The selected bait was the full-length Tau protein, hereafter called tau 2N4R, fused to LexA protein.

4.2.2 In vivo interaction of optoanti-p231-235 with Tau 2N4R in the LexA-fused format

To validate in yeast two-hybrid the interaction between scFv-p231-235 and Tau protein, the L40 strain was first transformed with the pMicBD1 vector, either coding for LexA-Tau-2N4R or, as a negative control for the interaction, the mutant LexA-Tau-2N4R-T231A-S235A, in which the bona fide phosphorylated Serine and Threonine residues are mutated to Alanines. For both constructs, two positive clones for the expression of the bait were plated onto a growing concentration of 3-AT to check for autoactivation of the HISIII gene (Figure R27A). Since no transactivation was detected, the minimal amount of 3AT was then used for the in vivo interaction assay. Thus, both the yeast strains were further transformed with the pLinker220 vector coding for the intrabody scFv-p231-p235.

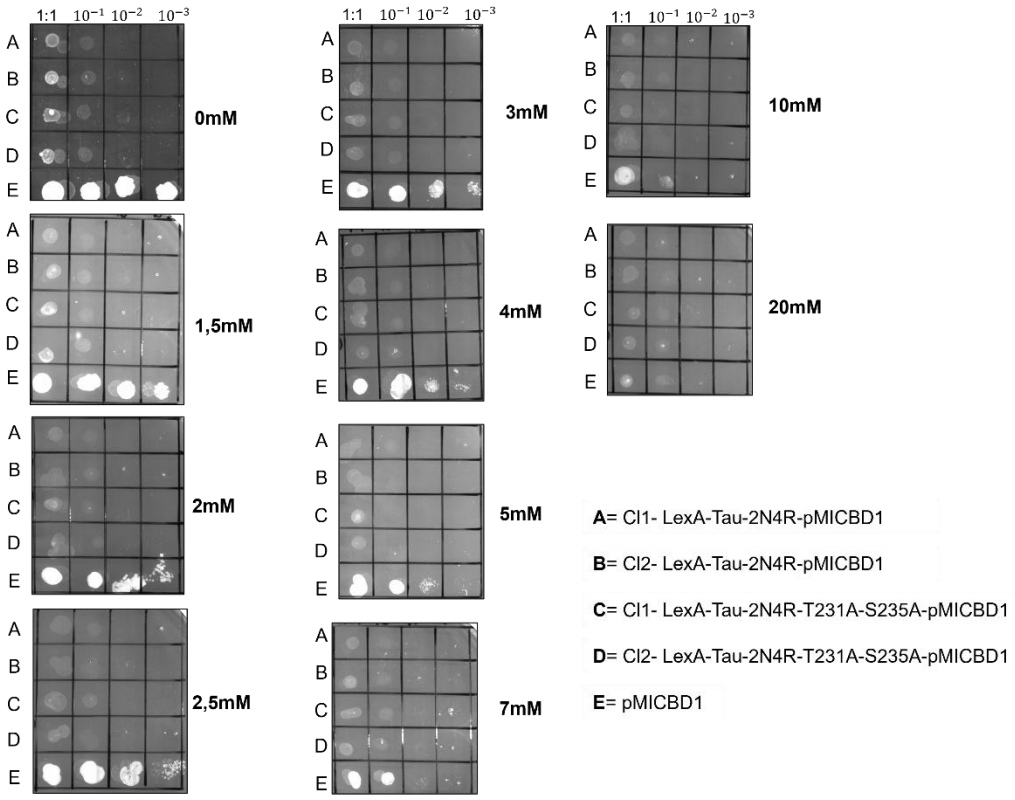

R 24 ***Transactivation curve of the Tau-2N4R bait in L40.*** *L40 transformed with pMicBD1 plasmid (constructs from A to E of the legend) plated on a growing concentration of 3-AT*

As shown in Figure R28A, onto selective media L40 expressing the Tau-2N4R and scFv-p231-p235 shows the same growth of the two positive controls, represented by an scFv anti-LexA domain of the bait, and the intrabody VHH98 anti-Tau. Conversely, no significant growth was present on selective plates when L40 coexpressed the double mutant of LexA-Tau2N4R-T231A-S235A and the scFv-pT231-pS235, although growth was supported by the two positive control intrabodies anti-LexA domain, and VHH98 anti-Tau. The failure of the double mutant of LexA-Tau2N4R-T231A-S235A to bind scFv-p231-p235, and thus to not support the yeast growth suggests the prevalent Tau phosphorylation dependence of scFv-p231-p235, at least in this yeast IACT assay. The bona fide Tau phosphorylation is likely achieved by endogenous kinases in yeast cells.

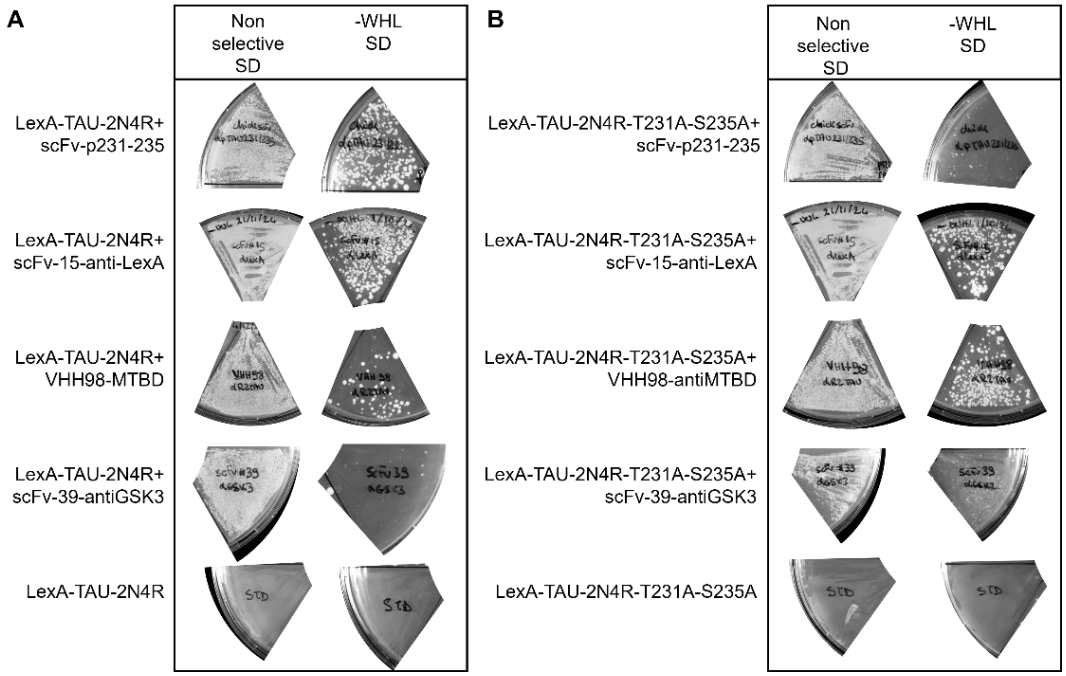

R 25 ***Yeast two-hybrid interaction between Tau-2N4R and scFv-p213p235 A)*** *L40 yeast strain expressing Tau-2N4R WT and scFv-pT231-pS235 plated into non-selective media (left side) and in selective media (right side) compared to three L40 strains expressing Tau-2N4R WT and control intrabodies against LexA domain of the bait, and Tau protein, and GSK3 kinases (negative control).* ***B)*** *L40 strains expressing Tau-2N4R-T231A-S235A and the scFv-pT231-pS235 compared with the same intrabodies described in A.*

4.2.3 Light-dependent degradation of phosphorylated Tau protein in L40 in the LexA-fused format

Having validated the interaction of the scFv-p231-235 with Tau, the second step was to add the photosensitive degron domain to the intrabody. After the cloning, the L40 strain was co-transformed with both the pMicBD2-LexA-Tau2N4R and the optobody-p231-p235. In the pMicBD2 vector, the LexA domain is mutated at R157G- K159E, which disrupts the nuclear localization signal, thus preventing the LexA-Tau bait from being targeted to the nucleus, thus facilitating the colocalization of the antigen and the optobody in the cytoplasm. The light-dependent degradation experiments were performed as previously described for TDP-43, by illuminating the culture for 4 hours and then splitting the culture for either being illuminated or being kept in dark conditions for the recovery.

In this case, the targeted protein degradation was finally aimed at selectively reaching the PTM version of the bait, but this objective was addressed in two steps.

In this first part, I focused on applying the optobody format to the new antigen thus, by blotting with anti-LexA antibody I monitored the variation of the total pool of Tau protein, fused to LexA, as a consequence of its degradation In Figure R29 A, it is shown that after 6h of light

stimulation, the optobody results strongly reduced, while in Figure R29 B, the highest reduction for the Tau target is reached after 4h of illumination.

This result extends the demonstration of the light-dependent degradation to a second optobody-target protein couple, namely anti Tau/Tau.

Another key feature of the optobody tool is the reversibility of the tool that can be maintained on the anti Tau/Tau couple. The recovery of protein levels for both the optobody and Tau reflects the distinct degradation dynamics shown in Figure R29A and B, respectively. Although a noticeable increase in optobody levels is observed after 2 hours of recovery in the dark following 4 hours of blue light exposure, this increase is not statistically significant. This is likely because the maximum light-induced degradation of the optobody occurs only after at least 6 hours of stimulation. In contrast, the same 2-hour recovery period results in a significant increase in Tau protein levels after 4 hours of blue light treatment (Figure R29B). These findings further demonstrate that reversibility is a robust and measurable property of the system, as shown by the recovery dynamics of the target proteins.

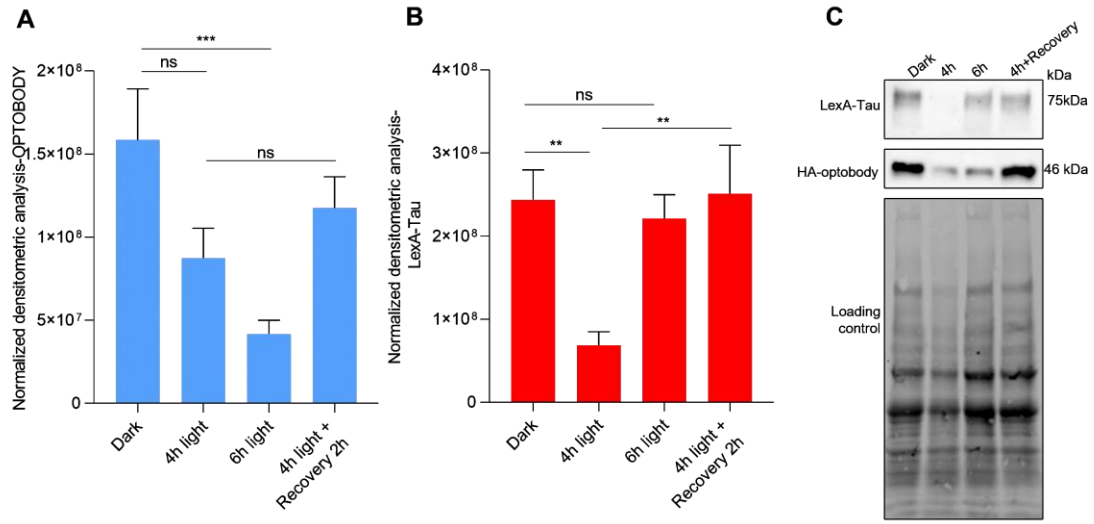

R 26 ***Light-induced and reversible Tau protein degradation in L40 yeast strain mediated by optoanti-p231-235. A)*** *Light-dependent degradation of the optobodyp231-235 and* ***B)*** *of Tau-2N4R in the LexA fusion format in L40 yeast strain.* ***C)*** *Representative western blotting of the quantification of the n=4 independent experiments shown in A. Statistical analysis A) Bonferroni-corrected one-way ANOVA; Error bar = mean with S.E.M.; p-value ns>0,05; *< 0,05; **<0,01; ***<0,001; ****< 0,00001*

I then addressed the question whether the bona fide prevalent phosphorylation dependence of the scFv-p231-235 antibody could be used to achieve the selective degradation of the specifically phosphorylated pool of Tau. Thus, the same illumination protocol was applied when the yeast strain expressed the optobody p231-p235 and the mutant 2N4R variant LexA-Tau2N4R-T231A-S235A (Figure R30). In this case, the degradation of the optobody was confirmed, even if the timing differed slightly from that previously observed when co-expressed with the wild-type Tau (Figure R29), being equally degraded after 4 and 6 hours. Surprisingly, however, also the mutant Tau2N4R-T231A-S235A was significantly degraded after 4 hours of illumination. This finding is unexpected, given the result reported in Figure R28B, which suggests the phosphorylation dependence of the interaction between the scFv-p231-235 antibody and Tau, assessed by the robust endpoint of growth and survival in the yeast two-hybrid assay. The unexpected finding of the equivalent targeted degradation of Tau2N4R and Tau2N4R-T231A-S235A by the scFv-p231-235 optobody raised new questions regarding the interaction between the optobody p231-235 and the target bait in both the wild-type and mutant forms.

To directly investigate this interaction in the protein extracts, I collected samples from the degradation experiments shown in Figures R29 and R30. These extracts were used to immunoprecipitate the HA-tagged optobody, and the bound antigen was detected with anti-LexA antibody. As shown in Figure 30E, a band corresponding to LexA-Tau2N4R was present in both samples, confirming that the immunoprecipitation of the HA-tagged optobody allowed the detection of two bands corresponding to both the wild-type and mutant forms of Tau.

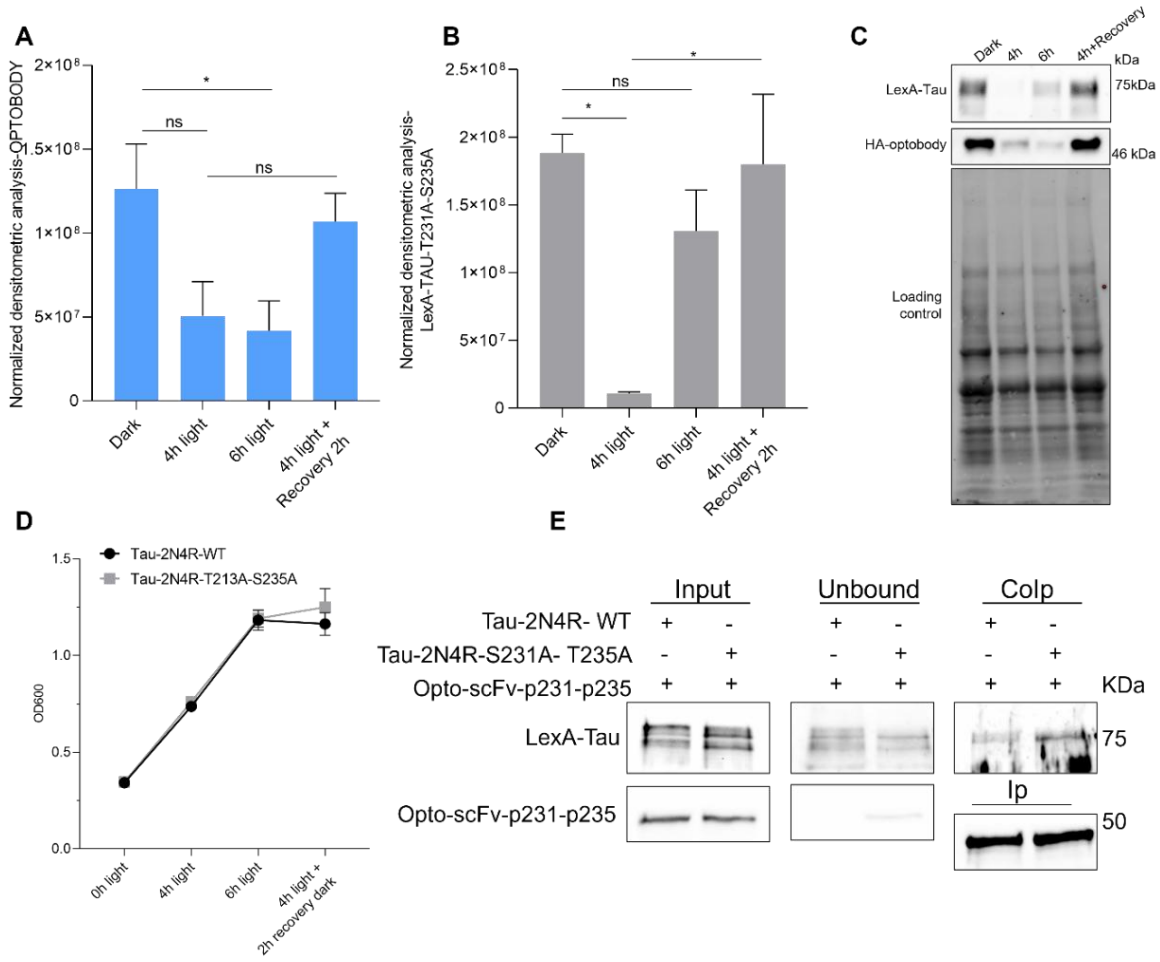

R 27 ***Light-induced and reversible Tau protein degradation in L40 yeast strain mediated by optoanti-p231-235. A)*** *Light-dependent degradation of the optobodyp231-235 and* ***B)*** *of Tau-2N4R-T231A-S235A in the LexA fusion format in L40 yeast strain.* ***C)*** *Representative western blotting of the quantification of the n=4 independent experiments shown in A and B.* ***D)*** *Growth curve during degradation experiments in coexpression condition optobody+2N4RWT and optobody+2N4Rmutant.* ***E)*** *co-immunoprecipitation of 2N4R WT and mutant by opto-p231-p235. Statistical analysis A) and B) Bonferroni-corrected one-way Anova; Error bar = mean with S.E.M.; p-value ns>0,05; *< 0,05; **<0,01; ***<0,001; ****< 0,00001*

Taken together, the two experiments aimed at investigating the interaction between opto-scFv-p231-p235 and Tau in both the wild-type and mutant forms, namely the *in vivo* interaction in the yeast two-hybrid system and the coimmunoprecipitation assay, gave opposite results. The former excludes the interaction with the mutant Tau, while the second one confirms it.

Since in this section of my project my aim was to assess the selective targeted degradation of phosphorylated Tau protein, it was imperative to address the phosphorylation state of bona fide Tau epitope and the stringency of the phosphorylation dependence of the scFvp231-p235 binding. I further investigated whether the Tau pool, whose levels were affected by light-dependent degradation, contained phosphorylation at specific residues. Although Tau

phosphorylation involves numerous serine and threonine residues susceptible to such post-translational modifications, for my thesis, I specifically analyzed, using western blotting, the phosphorylation of the optobody epitope, at threonine 231. As shown in Figure R31, extracts from the light-induced degradation experiments were analyzed by immunoblotting with anti-p231-TAU antibodies. The densitometric analysis of the samples before and after light dependent degradation revealed a comparable degradation profile to that observed in Figure R29A, where total Tau degradation was assessed using anti-LexA. However, the differences between the dark condition and the 4-hour or 6-hour light exposures in this case were not statistically significant.

On the other hand, when blotted on the extracts of the mutant Tau, no signal was detected with the anti-p231-TAU antibodies, confirming the absence of phosphorylation on the epitope in the Tau2N4R-T231A-S235A mutant.

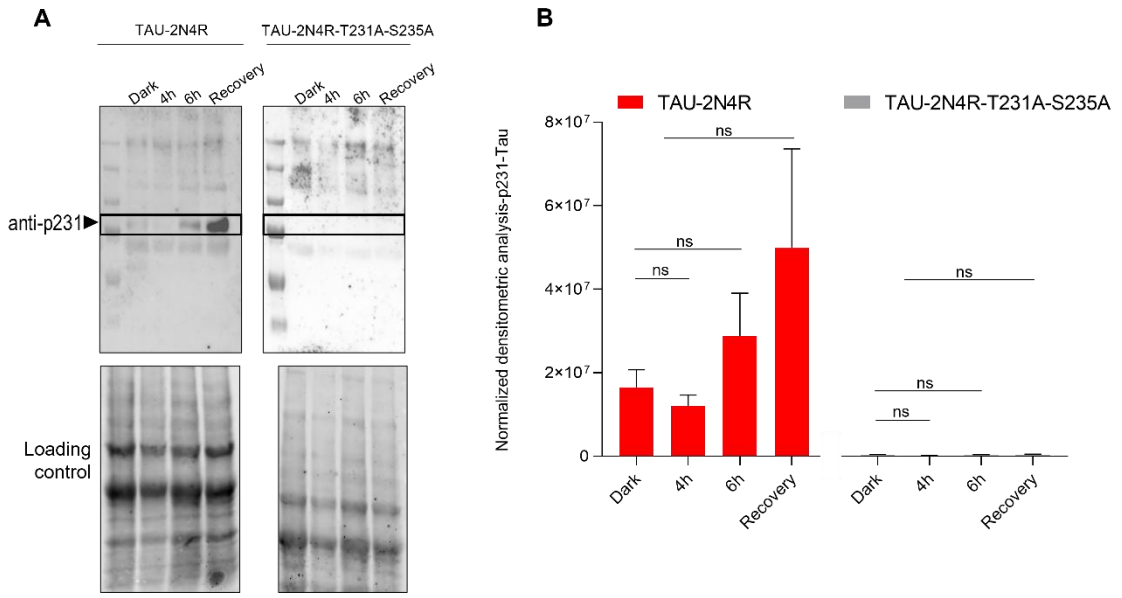

R 28 ***Light-dependent degradation of the phosphorylated Tau mediated by opto-p231-235 A)*** *Representative western blotting with the antibody anti-phospho-threonine231 on light degradation experiments in L40 expressing opto-pT231-pS235 and Tau2N4R WT (left panel) n=4 independent experiments or T231A-S235A (right panel), n=3 independent experiments* ***B)*** *densitometric analysis of the western blotting in A. Statistical analysis B) Bonferroni-corrected one-way Anova; Error bar = mean with S.E.M.; p-value ns>0,05; *< 0,05; **<0,01; ***<0,001; ****< 0,00001*

4.2.4 Evaluation of phosphorylation state of Tau-2N4R in L40

Although no statistically significant reduction in phosphorylated Tau levels upon light exposure was detected using anti-phospho-Tau immunoblotting, I decided to further investigate the proportion of phosphorylated versus non-phosphorylated Tau within the total protein extract.

In the light degradation experiments, Tau degradation was assessed either by evaluating the reduction of the total pool, or the variation of the phosphorylated form on threonine 231. To put these data together and then to split the total Tau protein in its two components, I chose to use the phos-tag technology (O'-Donoghue & Smolenski, 2024). This strategy allows to distinguish between the band corresponding to the phosphorylated form, that is affected by a delay in the run, and the one corresponding to the non-phosphorylated form, that migrates at in a lower position. Thus, the protein extracts of the L40 yeast strain expressing the two variants of Tau-2N4R were treated with phosphatase as a negative control for the phosphorylation. As shown in Figure R32A and B, samples were run in parallel in either the phos-tag gel or the stain-free gel, respectively, and the band corresponding to LexA-Tau was identified with the antibody anti-LexA.

Figure R32C displays a magnified view of the bands detected on the phos-tag gel. As anticipated, the blot reveals multiple bands, as the objective is to differentiate between various forms of the same protein. While it is not possible to directly compare individual bands or specific Tau species between conditions (indeed, the color code for the bands changes in each bar), it is evident that treatment with phosphatase causes a downward shift in the bands, confirming that the overall signal for Tau-2N4R corresponds to a phosphorylated form. Additionally, as shown in Figure R32D, in lane two, the upper band splits into two distinct bands in the presence of the T231A and S235A mutations in lane 4. In these cases, the mutant Tau migrates into six separate bands, whereas the wild-type protein clearly shows only five. These observations confirm that the Tau-2N4R isoform predominantly exists in a phosphorylated state under the tested conditions, and that specific mutations at T231 and S235 alter its phosphorylation pattern, leading to distinct migration profiles on the phos-tag gel. This highlights the sensitivity of the assay in detecting phosphorylation-dependent changes in Tau mobility. However, a more precise evaluation of the relative abundance of specific phosphorylated forms could be achieved by probing individual phospho-epitopes through targeted immunoblotting, allowing for quantitative estimation of each phosphorylation state.

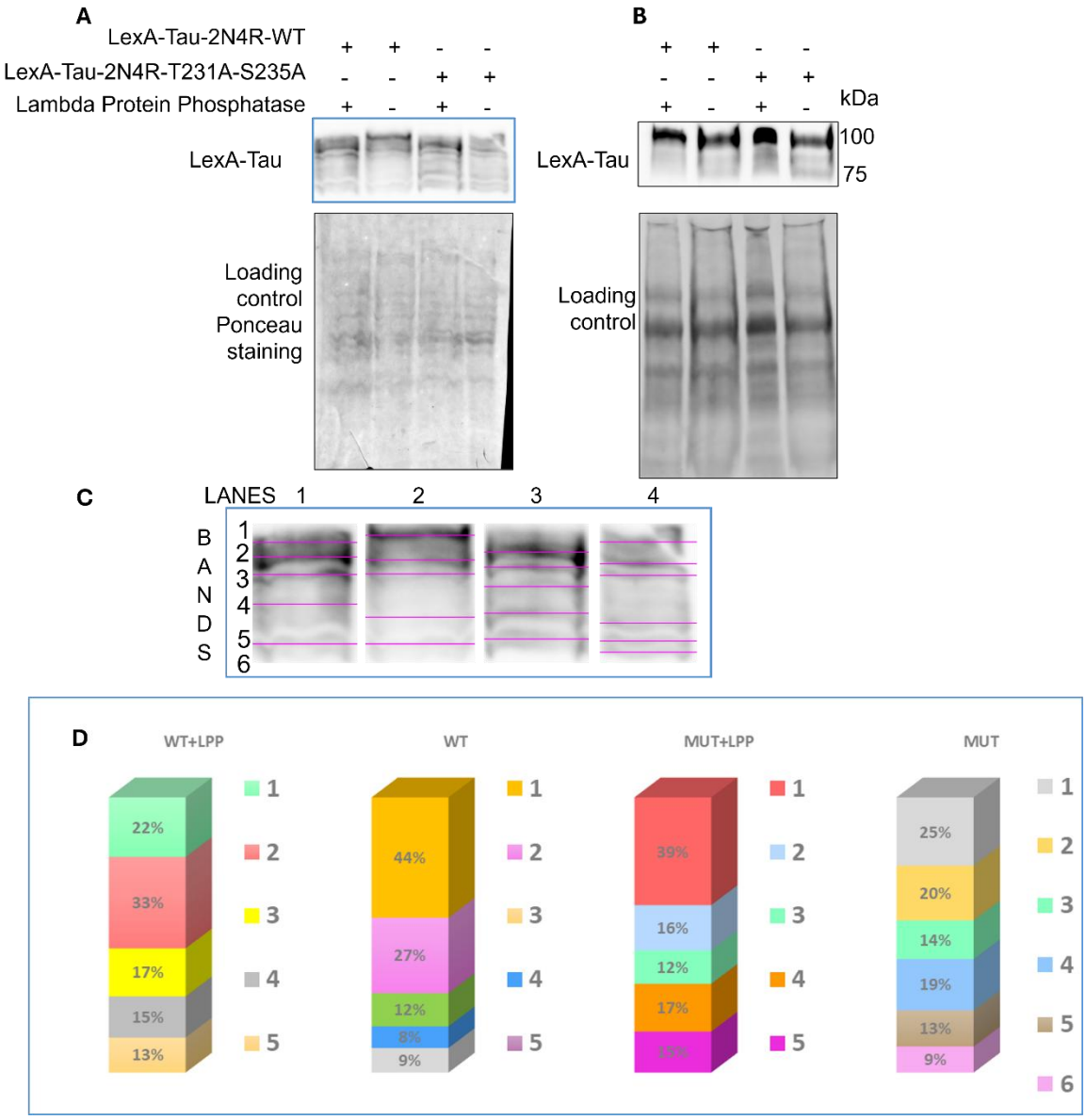

*R 29**Phosphorylation pattern on SDS-page and phos-Tag gel A)** Phos-tag and **B)** stain-free gel and western blotting of LexA-Tau2N4R WT and T231A-S235A in L40 yeast culture. **C)** magnification of A, **D)** quantification of the blot signal in the four conditions, the percentage shows the ratio among all the bands of each lane.*

4.3 Part III

4.3.1 IACT for Arc protein

The aim of this part of my thesis is to extend the targeted degradation strategy that I am developing to a protein target whose function is relevant for the physiological study of synaptic plasticity, namely the Arc/Arg 3.1 (activity-regulated cytoskeleton-associated protein, in short Arc protein). To this aim, using IACT I selected a panel of intrabodies against the N-lobe domain of Arc (N-terminus of mArc protein (1-140).

Bait validation- transactivation curve

The IACT selection platform enables the identification of binders from the L40 yeast strain expressing the antigen-bait fusion protein and the intrabody and growing in histidine-lacking media. The first step in validating the antigen-bait expression in the strain was to check for activation of the HISIII gene mediated solely by the LexA-antigen (the N-terminus of mArc protein (1-140) bait). Thus, the L40 transformed with the LexA-Arc protein was plated into growing concentrations of 3-AT and the growth was compared to a positive control for the transactivation represented by the LexA protein itself. As shown in Figure R32 a minimal amount of 3-AT, 5mM, was sufficient to abolish the transactivation.

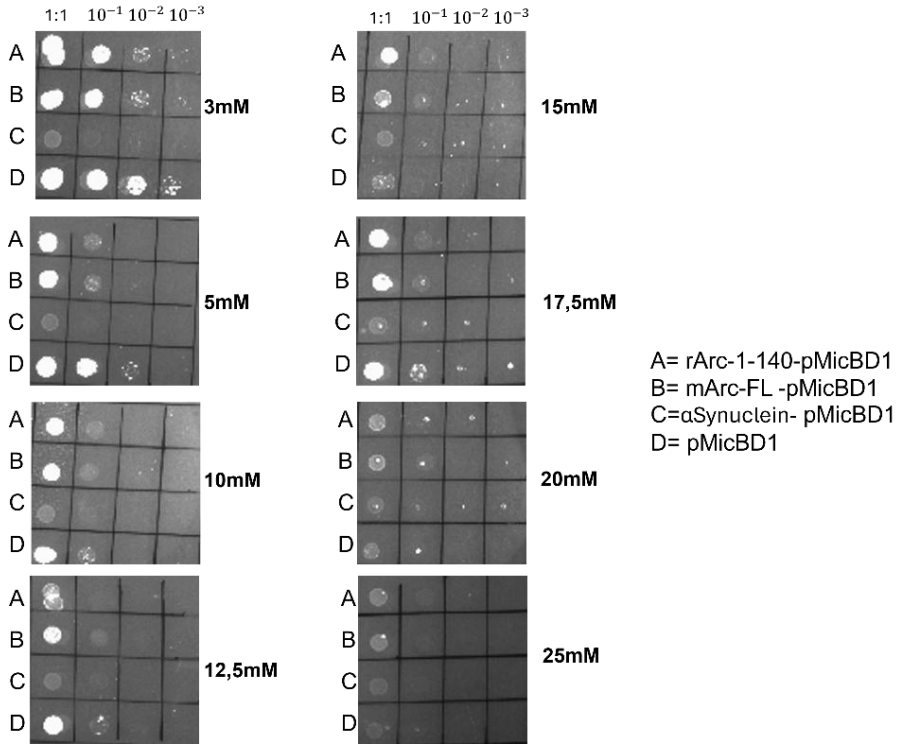

R 30 ***Transactivation curve for Arc-bait****. Serial dilutions of the culture of the five clones of L40 transformed with rArc-1-140-LexA* ***(A)****, mFL-Arc-LexA* ***(B)****, α-Synuclein-LexA* ***(C)****, LexA* ***(D)****, all in the pMicBD1 vector, were plated into -WH media with 3-5-10-12,5-15-17,5-20-25 mM 3-AT.*

The L40 yeast strain was then transformed on a large scale to perform IACT using the N-terminus of mArc protein (1-140). The naïve Llama library (Gilodi et al., 2022) was screened for interactors as described in the Materials and Methods section (please see Section 3.1.1). The transformation efficiency of the screening was $2 * 10^8$, while 337 clones were re-streaked onto -WHL plates (Figure R34A), and 80 of them resulted in being double positive. After the fingerprinting analysis (not shown) and the secondary screening (Figure R34 B-C), clone 213 turned out to be the best candidate for the yeast two-hybrid interaction

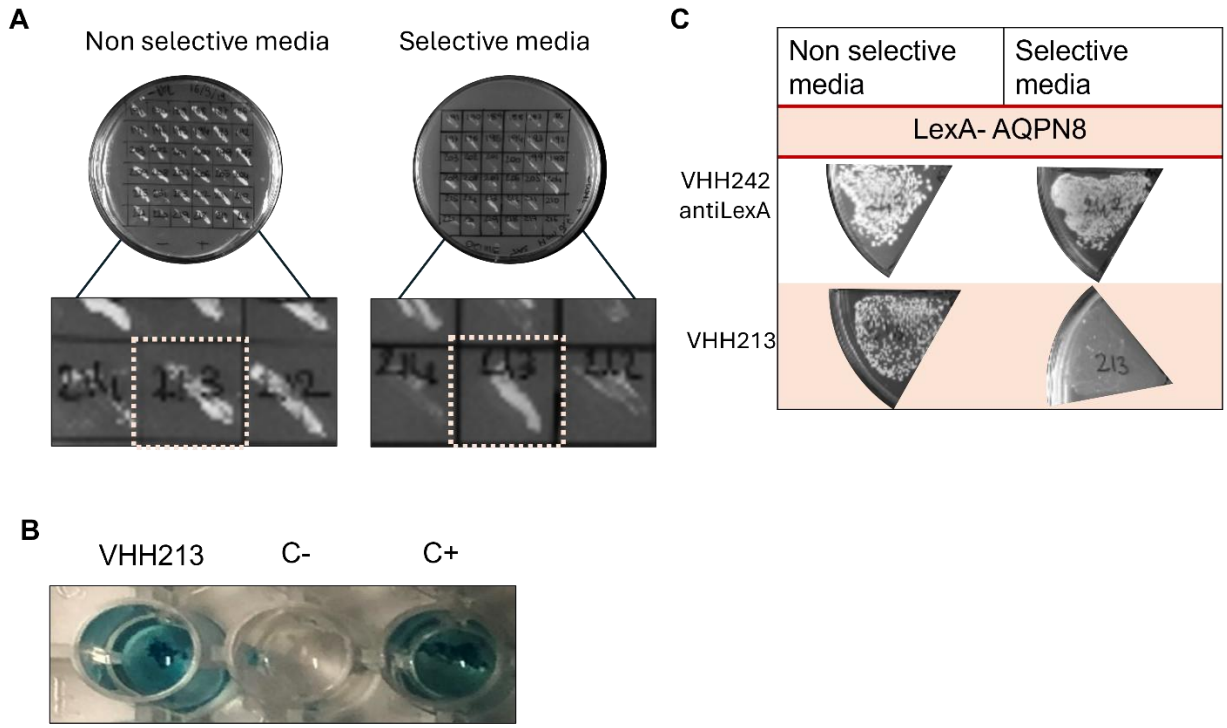

R 31 ***IACT selection of intrabody anti-Arc****. **A)** Positive clones after the first round of selection against rArc-LexA bait. **B)** β-Gal assay for the clone expressing intrabody 213. **C)** Secondary screening of intrabody 213 against the unrelated LexA-AQPN8 protein, intrabody 242 anti-LexA used as a positive control.*

In-vivo epitope mapping (IVEM)

The in vivo interaction was then applied to set the in vivo epitope mapping experiment, testing the binding of the VHH213 against specific regions of the original bait used for the selection. The LexA-Arc bait was subcloned into smaller regions, namely: N-coil amino acids 1-76, the inter-coil 31-108 aa, and the C-coil from 77 to 140. As results from the experiment in Figure R35 the recognition of a smaller portion of the original bait used in the selection did not occur properly since no growth in selective media was observed. On the other hand, the recognition of the bigger Arc fragment 1-140 was confirmed.

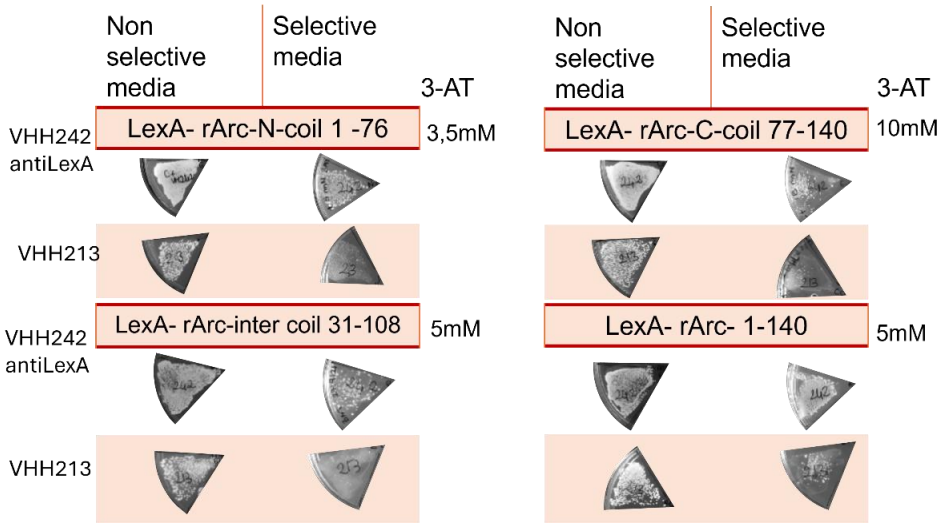

R 32 ***In vivo epitope mapping- VHH213****. Different L40 yeast strains expressing different regions of the original bait rArc (aa 1-76; 77-140; and inter coil were screened for the interaction with the intrabody 213.*

4.3.2 Optoanti-Arc and light-induced targeted protein degradation

Co-immunoprecipitation of Arc protein in HEK293T cells expressing optobody 213

After validating the interaction between intrabody 213 and Arc protein in the in vivo L40 yeast strain, I proceeded to directly fuse the previously validated PSD module to the intrabody sequence to create the optobody targeting Arc protein. Given that the goal of the Arc protein project was to apply the optobody to neuronal cell lines, I cloned the construct into a plasmid designed for mammalian expression, resulting in the Arc-p2a-optobody-213 format. I then used this construct for co-immunoprecipitation experiments on HEK293T protein extracts, where I pulled down HA-tagged optobodies and immunodetected MYC-tagged Arc protein. These experiments were performed in the presence of optobody 213 or of the unrelated optobody VHH5 targeting TDP-43. As shown in Figure R36D, the MYC-Arc band was only detected in

the lane corresponding to the immunoprecipitation of the optobody targeting Arc, providing further validation of the interaction in cells.

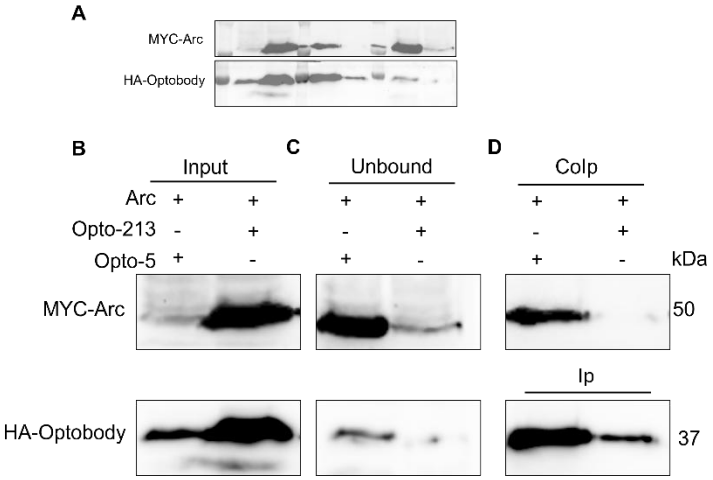

R 33 ***Coimmunoprecipitation of Arc protein with VHH213. A)*** *Western blotting showing the co-immunoprecipitation of MYC-Arc in HEK293T expressing MYC-Arc with optobody213 or optobody 5 (anti-TDP43);* ***B) C)*** *and* ***D)*** *magnification of A. In B) The protein extract input of the co-Ip showing the expression of Arc protein and both the optobody; C) Unbound fraction collected before the elution; D) fraction eluted from the HA-beads and blotting of the immunoprecipitation (lower panel) HA-tagged optobodies and coimmunoprecipitation (upper panel) of MYC-Arc.*

Light-induced degradation of Arc protein in mammalian cells

Taking advantage of these results, I then tested the degradation activity of the optobody in mammalian cells expressing MYC-Arc and the anti-Arc optobody231. Again, taking into account the previous results on targeted protein degradation, I decided to apply four and six hours of illumination protocol to investigate Arc degradation. As shown in Figure R37, 6 hours of light stimulation were sufficient to induce optobody degradation. However, while a clear trend toward reduced Arc protein levels was observed, the decreases at both 4 and 6 hours did

not reach statistical significance.

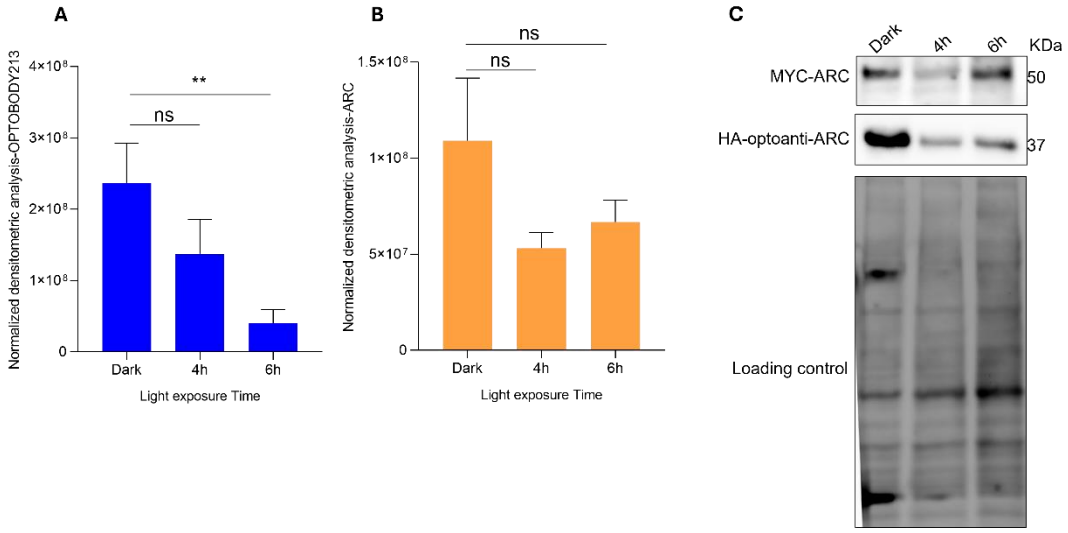

R 34 ***Light-dependent degradation experiment using anti-Arc optobody in mammalian cells. A)*** *and* ***B)*** *quantification of light-dependent degradation of optobody and Arc, respectively by expressing them in HEK293T cells in a single vector.* ***C)*** *Representative western blotting of the experiments shown in A and B. Statistical analysis A) and B) Bonferroni corrected One-way Anova; Error bar = mean with S.E.M.; p-value ns>0,05; *< 0,05; **<0,01; ***<0,001; ****< 0,00001.*

Opto-anti GFP and GFP light-induced degradation in mammalian cells

To optimize the experimental design for testing Arc-targeted degradation in neuronal cell culture, I prepared an optobody construct targeting the GFP protein, which would serve as an unrelated optobody in subsequent experiments. The chosen intrabody was a VHH format (Fridy et al., 2014). To assess its efficacy as an optobody, I began by cloning both the GFP and anti-GFP optobody into the same plasmid, separated by a P2A signal peptide, as previously validated for other optobody-target pairs. I then tested light-induced degradation of the GFP protein in HEK293T cells expressing the anti-GFP optobody and subject to light stimulation. As shown in Figure R37B, 6 hours of light exposure effectively reduced the optobody signal. However, the GFP signal (Figure R37A) showed only a non-significant decrease in protein levels, indicating that the light-induced degradation was not as pronounced for GFP.

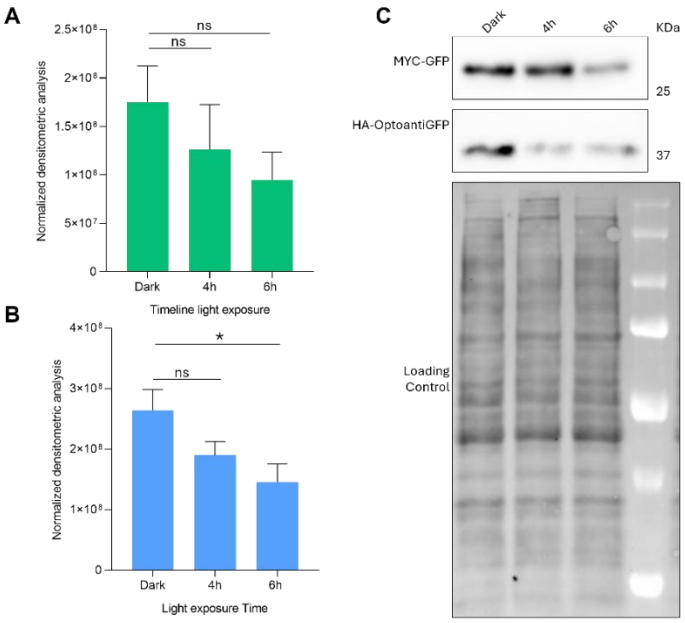

R 35 ***Light-dependent degradation experiment using optoanti-GFP in mammalian cells. A)*** *and* ***B)*** *quantification of light-dependent degradation of GFP and optobody anti-GFP, respectively, by expressing them in HEK293T cells in a single vector.* ***C)*** *Representative western blotting of the experiments shown in A and B. Statistical analysis A) and B) Bonferroni corrected One-way Anova; Error bar = mean with S.E.M.; p-value ns>0,05; *< 0,05; **<0,01; ***<0,001; ****< 0,00001.*

4.3.3 Endogenous Arc light-dependent degradation in mouse embryonic stem cells-derived cortical neurons

The first step in assessing the targeted protein degradation within the physiological environment was represented by the experiments aimed at targeting endogenous Arc in cortical neurons derived from mouse embryonic stem cells (mESCs) (Tonelli et al., 2025). Briefly, upon activation of MAP/ERK signaling, mESCs differentiate into neuronal progenitors (NPs). Furthermore, as demonstrated from Tonelli *et al*, inhibition of MEK and BMP (MiBi) pathways promotes a pronounced cortical identity in these neurons, which are thus referred to as MiBi cultures.

A first step in assessing Arc expression in MiBi neurons was the Real Time PCR mRNA extracted from MiBi culture at different maturation stages (Figure R38) DIV 25, 35, and 50. Thus, as illustrated in Materials and Methods Figure M2, the experimental design was planned to transduce the MiBi neurons at DIV 14 and to induce the expression of the optobody-213 with doxycycline at DIV34, while at DIV35 the light stimulation was performed.

.

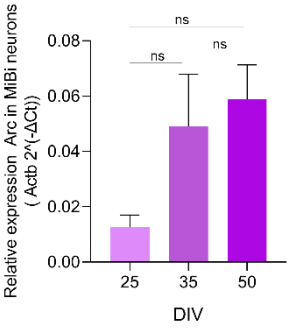

R 36 ***Real-time PCR on MiBi cortical neurons for Arc expression.*** *Real-time PCR on Arc mRNA in MiBi neurons at different stages, normalized on actinβ. n=3 independent experiments, each corresponding to 2 technical replicates. Statistical One-way Anova – Bonferroni correction; Error bar = mean with S.E.M.; p-value ns>0,05; *< 0,05; **<0,01; ***<0,001; ****< 0,00001*

Twelve hours after doxycycline induction of either the optobody-213 or the opto-anti-GFP, the cells were fixed for immunofluorescence analysis following the light stimulation protocol. As shown in Figure R398 A and B, the optobody signal significantly decreased after 4 hours of light stimulation, while the green fluorescence of endogenous Arc remained unaffected. A similar pattern was observed in MiBi cultures transduced to express the anti-GFP optobody negative control, where the optobody signal was reduced to nearly zero following light exposure (Figure R39).

I have established the conditions to effectively degrade the optobody in MiBi neuronal cultures, but the degradation of the constitutive endogenous pool of Arc still remains to be demonstrated. The levels of Arc mRNA and Arc protein are known to be regulated at manyfold different levels (Eriksen & Bramham, 2022), as a function of neuronal and synaptic activity. It will be of interest to assess the ability of the anti-Arc optobody to degrade the de novo pool of neo-translated Arc protein.

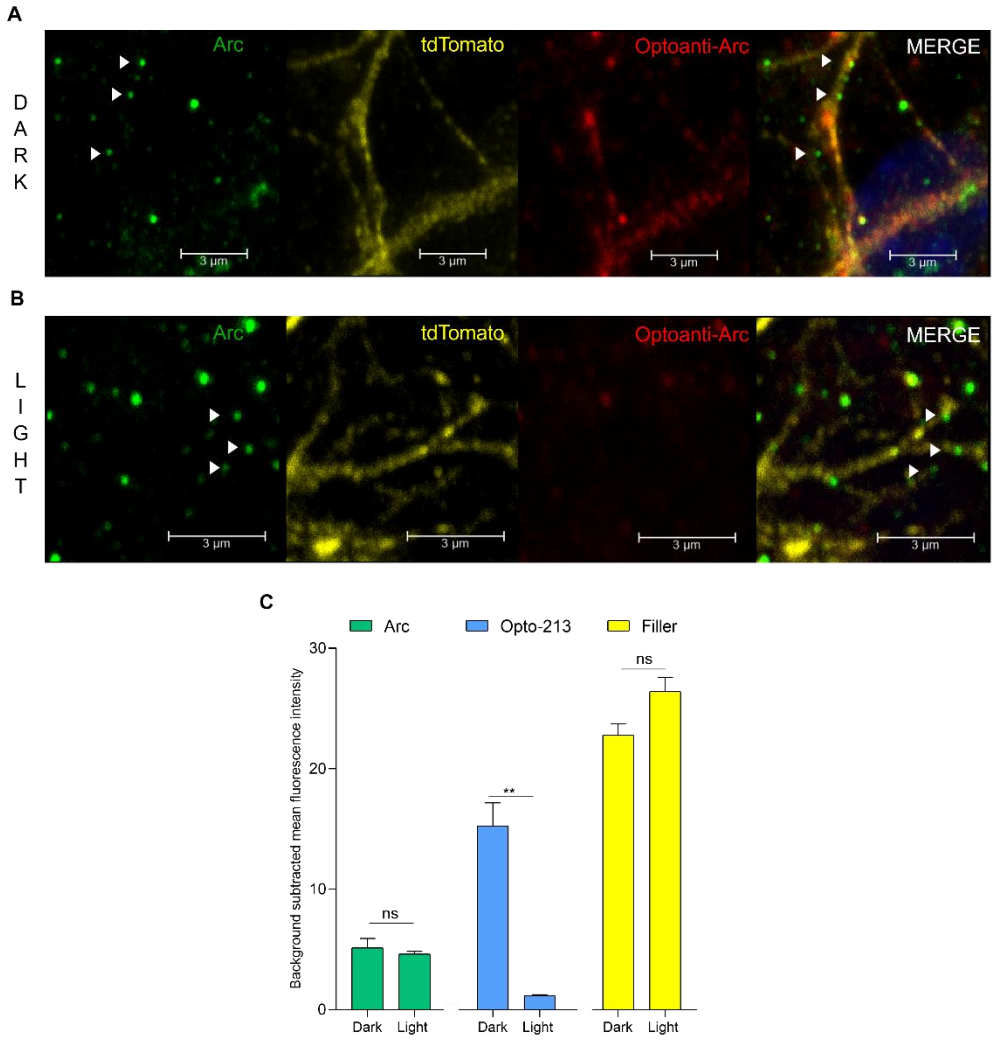

R37 ***Light-dependent degradation of endogenous Arc using optoanti-Arc in MiBi cortical neurons. A)*** *and* ***B)*** *immunofluorescence of MiBi culture induced for the expression of the optobody213 in dark and light conditions respectively.* ***C)*** *Quantification of mean fluorescence of Arc, optobody213, and tdTomato staining of the IF shown in A and B. n=3 independent experiments; 10 field each condition, at least 5 ROIs each field. Statistical analysis A) and B) unpaired t test; Error bar = mean with S.E.M.; p-value ns>0,05; *< 0,05; **<0,01; ***<0,001; ****< 0,00001.*

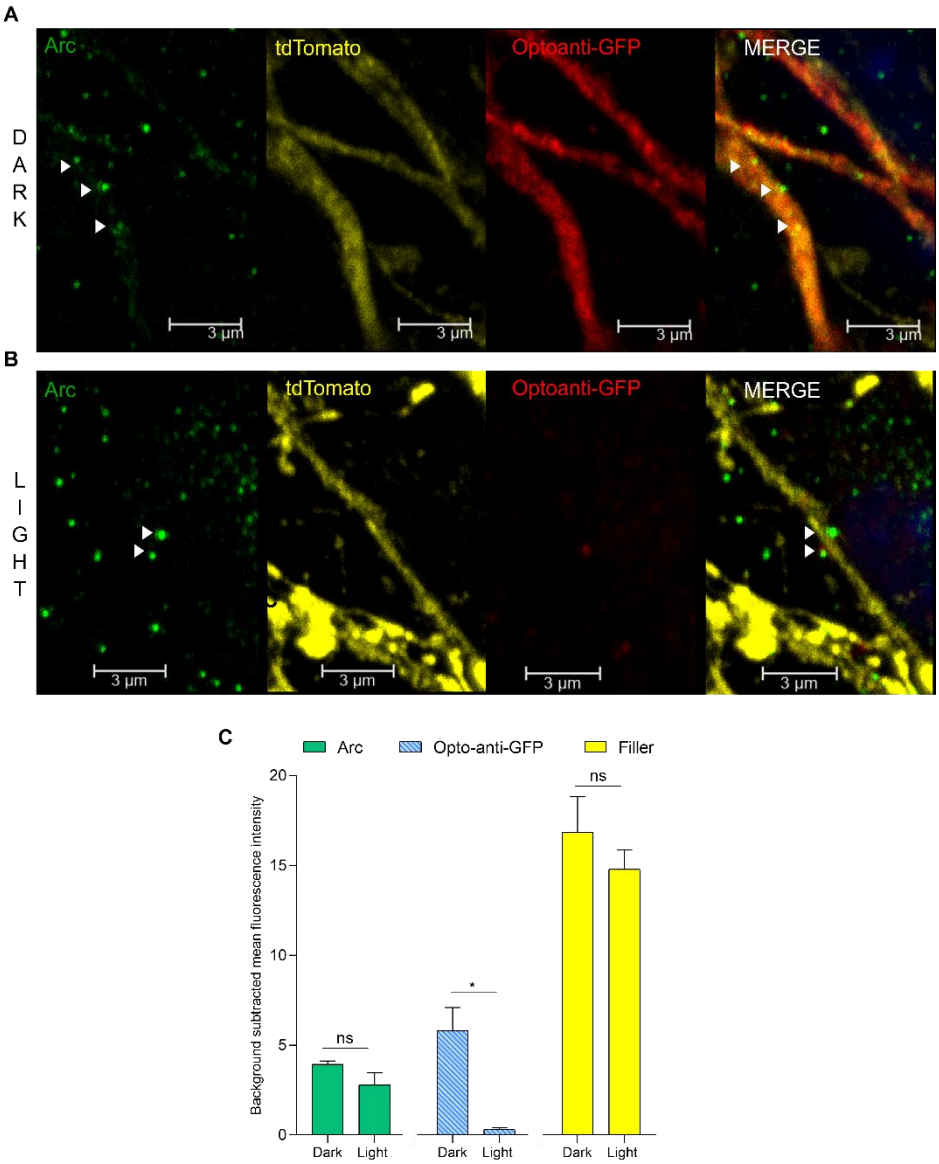

R38 ***Light-dependent degradation of endogenous Arc optoanti-GFP in MiBi cortical neurons. A)*** *and* ***B)*** *immunofluorescence of MiBi culture induced for the expression of the optobody anti-GFP in dark and light conditions, respectively.* ***C)*** *Quantification of mean fluorescence of Arc, optobody213 and tdTomato staining of the IF shown in A and B. n=3 independent experiments; 10 field each condition, at least 5 ROIs each field Statistical analysis A) and B) unpaired t test; Error bar = mean with S.E.M.; p-value ns>0,05; *< 0,05; **<0,01; ***<0,001; ****< 0,00001.*

5. Discussion

5.1 Part I: Intrabody-mediated targeted protein degradation of TDP-43

Protein homeostasis, known as proteostasis, is a tightly regulated process that allows for the correct concentration, conformation, and binding interaction of proteins. When abnormal or long-lived proteins occur, degradation is the route to maintain proteostasis (Hipp et al., 2019). Many neurodegenerative diseases show as a common feature a failure of proteosasis, with abnormal and generally misfolded proteins that escape the degradation pathway and accumulate in the cytoplasm of neuronal cells in the form of insoluble aggregates (Dugger & Dickson, 2017). Another key aspect of all these aggregation-based neurodegenerative disorders is that many of these can rather be considered proteinopathies since, although the overall pathophysiology of the disorders is very complex, they often arise from a single or a small number of aberrant proteins that become prone to accumulate and mislocalize, thus driving neurodegeneration. Since aggregation is a concentration-dependent process, it is clear that a strategy that selectively targets the specific misfolded or aggregation-prone proteins to directly interfere with them would be very useful, first of all from the research standpoint. To work at the protein level, the way to reach high specificity for the target protein within the cellular environment is to apply intracellular antibodies technology (Biocca & Cattaneo, 1995; Visintin et al., 2002b) . The modulation of such intracellular technology is another key element to properly control the intracellular activity. To obtain a precise timing, duration and spatial resolution of the modulation activity, I explored the light stimulation as the best-fitted strategy to control the intrabody actions. Thus, genetically coded expression of photosensitive proteins, or optogenetics, resulted to be an option worthwhile exploring for our purpose of developing targeted degradation regulated by orthogonal signals (Tischer & Weiner, 2014). We selected Light oxygen voltage domain from Arabidopsis thaliana as the genetically encoded photosensitive protein to be fused with VHH intrabody sequence to obtain a controlled optogenetic intracellular antibody. The last key feature is then to reach the degradation activity through the ubiquitin-independent proteasome activation system, in my case via the ornithine decarboxylase degradation sequence (Murakami et al., 1992). When fused to a light activated protein, the construct is defined as a photosensitive degradation module or psd (Renicke et al., 2013). In this work I present an intracellular antibody-based strategy to create a selective tool to reach inducible targeted protein degradation. In the first proof of principle study, it was already demonstrated that equipping an intrabody with a ligand-induced degron can be effectively used as inducible degraders of endogenous proteins (in that case the microtubule

associated protein Tau) (Melchionna & Cattaneo, 2007). However, our idea is not only to create a degradation targeting intrabody tool but even to modulate reversibly through a light-sensitive degradation domain (Figure D1).

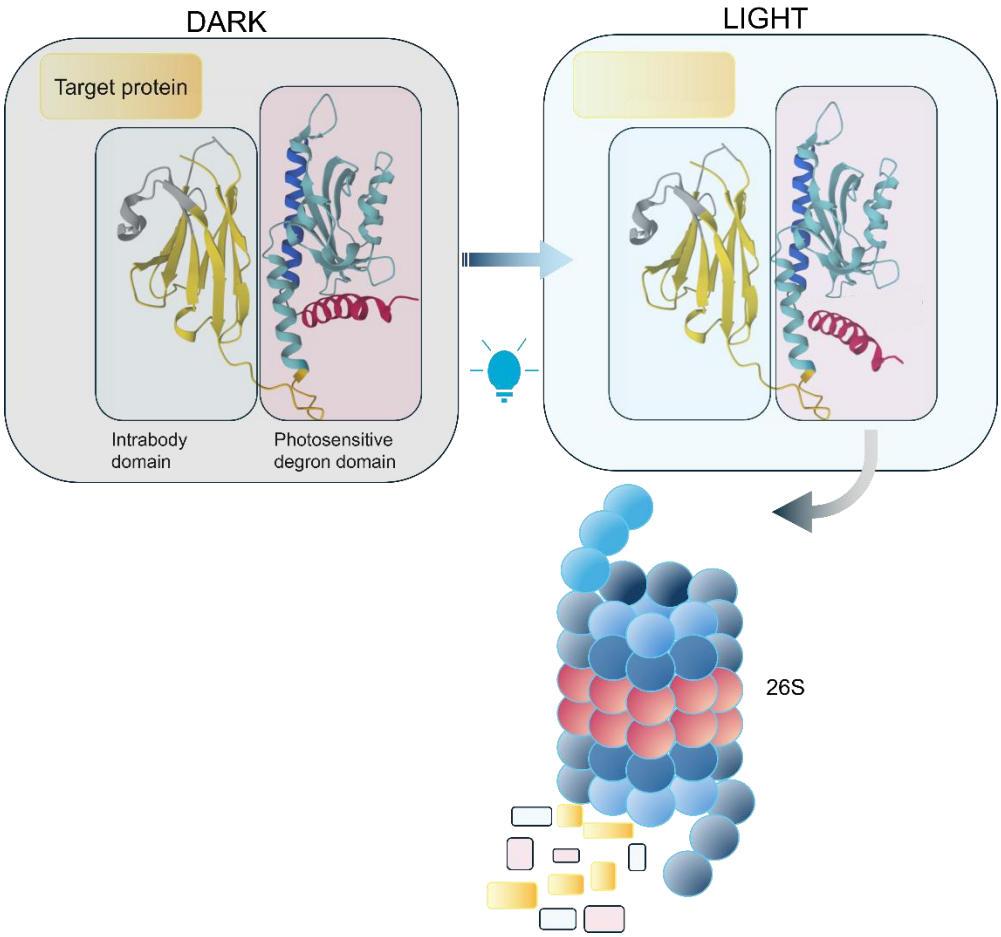

D 1 ***Overview of the mechanism of the intrabody-based light-activated targeted protein degradation mediated by the proteasome***

To first assess the activity of the psd, I generated a fluorescent photosensitive degron domain by fusing AtLov2 (3m)-c-OCD1 to the YFP protein. The opto-YFP construct represents the proof of concept of the applicability of psd module in a yeast model and a mammalian cell line. The yeast strain is the cellular system used for the intrabody capture technology, the tool to select intrabodies based on their binding to the corresponding antigen. In other words, intrabodies reach their proper folding and recognize and bind the antigen-bait to allow for the selection, so it represents the best cellular environment in which to start the evaluation of an intrabody-based degrading system.

5.1.1 Modulated targeted protein degradation with optobody

Light is a very convenient orthogonal stimulus to control the activity of synthetic proteins for many reasearch applications. I have investigated the use of light to control the activity of intracellular antibodies, a technology that was pioneered in the lab (Biocca & Cattaneo, 1995, 1997). The application of light-sensitive effectors to the intrabody and nanobody technology is emerging, and the definition of optobody was only very recently introduced, associated to photo-stimulated intracellular antibodies whose antigen-binding function was activated upon light exposure (Yu et al., 2019). This optogenetic intracellular antibody tool has the main initial goal to assess the efficacy of targeted protein degradation of the antigen bait upon light stimulation. The candidate that I selected as a first target of optobody-mediated degradation was the TDP-43 protein. By using VHH5 anti-TDP-43 protein, isolated through IACT (Gilodi et al., 2022), I could address two different questions at the same time: the first was to prove that the intracellular antibody domain can gain the degradation function through the fusion with the psd, and the second was whether the intracellular binding of the antigen epitope mediated by the VHH domain can be combined with the degradation activity mediated by the optobody, thereby targeting the complex, formed by both the optobody and the target, to the degradation machinery. The first purpose, shown in Figure R3A, was reached by applying the same stimulation protocol that resulted effective on opto-YFP. The reduction trend from the dark condition, after a light period of 6h, appears to be coherent with the expectation that a constantly expressed optobody, when exposed to blue light, is getting degraded in a fashion that reflects the stimulation protocol; in other words, a continuous degradation-inducing stimulus triggers a continuous degradation pathway. It is reasonable to argue that the balance between physiological protein synthesis and degradation shifts toward degradation upon light exposure. Given the promising light-dependent reduction trend observed, we next investigated whether a similar behaviour could be seen in the co-transformed yeast strain that also expresses the corresponding antigen. The protein reduction patterns for the target, differ notably with respect to the corresponding target (and also differ for different optobody-target couples, as we shall discuss below). After 4 hours of light exposure, the reduction of the optobody is more pronounced than that of the TDP-43 protein. Furthermore, while the optobody level drops dramatically after 6 hours of light, the reduction of TDP-43 at 6 hours remains comparable to the 4-hour time point. This relative balance in TDP-43 levels between 4 and 6 hours could be attributed to the diminishing efficacy of the optobody, likely due to its extremely low amount, combined with the ongoing synthesis of TDP-43 itself. In other words, while the optobody is

primarily degrading itself in response to light exposure, it maintains its target degradation activity during the first 4 hours. However, once the optobody level falls below a certain threshold, its ability to remove TDP-43 is compromised, halting further reduction. An important consideration regarding the different light-dependent degradation trends observed in LexA-TDP-43 is that the construct used in these experiments was the one validated for the IACT selection. In this format, although TDP-43 is overexpressed at high levels, it is specifically targeted to the nucleus to exploit the DNA-binding activity of the LexA domain. Therefore, a significant portion of the overexpressed bait protein is localised in the nucleus, while the optobody, present in the cytoplasm, binds the antigen and, upon light activation, facilitates target degradation. Although the degradation process significantly impacts the protein levels in the cytoplasm, as shown in Figure R3D for the optobody and R3E for the antigen, the western blot analysis focuses on the total protein extract from L40 cells. In this context, even though LexA-TDP-43 continues to be expressed and subjected to degradation during light exposure, a substantial portion of the protein is excluded from optobody-mediated TDP-43 degradation, due to its localisation in the nucleus, thus affecting the analysis. In other words, although the optimal approach for achieving target degradation would be a co-expression system that ensures the synchronised colocalization of both the optobody and its antigen, TDP-43 degradation remains significant after 4 hours of light exposure and becomes more pronounced after 6 hours of blue light.

5.1.2 Reversibility of the tool

Another layer for investigating the optogenetic tool was the assessment of its reversible efficacy after turning on the targeted protein degradation. As shown in Figure R4, the reversibility was demonstrated in the L40 yeast strain with a 2h period of dark after 4h of blue light stimulation. Again, the behaviour of the two proteins during recovery after light-induced degradation differs. As expected, upon removal of the light, the optobody protein level increases significantly within 2 hours, while the antigen protein shows no such increase. This discrepancy could be explained by several factors. First, the recovery of protein levels after removing the degradation stimulus depends on the balance between the physiological rates of protein synthesis and degradation at any given time. Therefore, if the rates of synthesis for the optobody and its antigen differ, removing the light stimulus will result in distinct recovery timelines for each protein. Second, if degradation affects the two proteins to varying extents, and in this case, the target protein synthesis results in being slower, significant rescue will only occur if either the degradation can be amplified, or the recovery time is adjusted to match the

synthesis rate of each target protein. Given that 2 hours of recovery in the dark are sufficient for the optobody to increase its expression, it suggests that its synthesis rate is higher than that of the antigen.

Furthermore, because the PSD module is fused to the intrabody sequence, degradation primarily impacts the optobody's half-life. As shown in Figure R3E, the degradation of TDP-43 is less pronounced compared to the optobody after 6 hours of light stimulation. Consequently, if the translation rate of LexA-TDP-43 is slow, the recovery of TDP-43 levels after 2 hours of dark may be minimal, despite a slight increase being observed.

In summary, all these factors are essential for selecting the optimal system to detect targeted protein degradation. The ideal design would synchronize the synthesis rates of both the optobody and the antigen, creating not only a tool whose activity can be modulated, but also one whose expression is induced from the outset. A kinetic mathematical model will be useful to carefully titrate the induction time, the synthesis and degradation rates and the dark/light/recovery periods for an optimal effect (work in progress). The quantitative modelling will also have to take into account the partitioning of the target protein between the soluble and the insoluble pool, due to intrinsic aggregation properties (for misfolding proteins) and the association to the 26 proteasome (that would be part of the effective degradation).

Targeted protein degradation in the yeast cellular model represents the consolidation of our optogenetic tool in the model organism used for intrabody selection, even though, as discussed in the previous section, this approach is not the most efficient design. When I moved into the HEK293T cellular system, although the experimental design was similar to that used in the yeast system, the degradation trend in HEK293T cells changed significantly for both the optobody and its antigen. The pattern of protein level reduction during light exposure showed considerable variability across experimental replicates. This variability can be explained by several factors: first, despite achieving overexpression conditions through transfection, the percentage of cells effectively expressing both the optobody and the target protein is inconsistent in different experimental replicates. The representative quantification of transfection efficiency reveals that a substantial number of cells are only expressing one of the two plasmids, which can be either the optobody or the antigen. On the other hand, since the protein level of TDP-43 is reduced after 6 hours, there is no reason to believe that the plasmid encoding TDP-43 is consistently transfected alone. If that were the case, no reduction in protein

levels would have been observed. The fact remains, however, that the percentage of cells expressing both plasmids is variable and also ill defined.

Thus, to evaluate the protein reduction in cells expressing both the optobody and its target, I prepared a construct for the transient expression of both proteins. Targeted protein and optobody degradation were reached after 6h of light stimulation, and this data emerged yet on western blotting analysis but was also evident by monitoring the difference of fluorescence intensity in immunofluorescence. Thus, in the mammalian cells, the degradation pattern for the optobody reflects more closely that of the target; indeed, in both cases, the reduction is significant after 6h of light exposure.

5.1.3 Proteasome involvement

So far, the first strong evidence of the efficacy of the tool comes from its confirmation in different cellular systems and with two different techniques, demonstrating that the reduction of protein levels can be achieved after induction by light exposure. The logical expectation and interpretation of this reduction is that both the optobody and TDP-43 are directed to the 26S proteasome upon light activation of the degron domain. To further investigate this, I examined the protein reduction under proteasome inhibition conditions. Although it has already been shown that the light exposure does not affect cell viability, when applying 2h of proteasome inhibitor, the cell viability was impacted. As a result, the experimental design for the evaluation of protein reduction had to be adapted to the time window for the administration of MG132. I reasoned that performing proteasome inhibition in the last two hours of light exposure could be the best compromise to monitor the variation in protein degradation patterns in yet healthy cells.

The rationale was to give the HEK293T cells co-expressing the optobody and its target enough time to reach the previously validated light-dependent degradation, six hours, and then to monitor the protein levels after MG132 addition. While the degradation pattern in HEK293T cells was confirmed to be similar for both the optobody and TDP-43, the MG132-chase experiment revealed different behaviours for the two proteins. As shown in Figure R9C, the reduction of TDP-43 after 6 hours of light exposure with MG132 is comparable to the reduction observed in the control condition. In contrast, the reduction of the optobody in the light+MG132 condition is significantly lower than in the control condition. This more pronounced effect on the optobody level aligns with the findings from experiments focused on

the reversibility of the tool. Given that the synthesis rate of the optobody appears higher than that of TDP-43, even after 4 hours of being targeted for degradation, inhibiting the proteasome machinery leads to a significant increase in protein levels. Furthermore, as the yeast cell experiments concluded, if the synthesis rate of TDP-43 is slow, 2 hours of MG132 treatment can only produce a small increase in protein levels that is not significant.

5.1.4 Modularity of the tool

After investigating how the pathway involved in the reduction of protein contributes to the validation of the intrabody-based TPD tool, I shifted my focus to assessing the role of specific regions required for degradation activity. I created two variants of the optobody tool: the first one, lacking the region involved in the blue-light sensitivity, and the other one, lacking the degradation signal downstream of the LOV domain. The rationale was that, in the absence of the degron, any observed residual reduction in protein levels in the soluble fraction might reflect cellular degradation events not directly linked to the engineered degron and might likely indicate accumulation in the insoluble fraction. Conversely, removing the jα chain could potentially affect the solubility of the optobody.

The exposure to blue light of these two variants generates two distinct scenarios when monitoring the optobody level or the TDP-43 in the soluble protein extract (Figure R10). As expected, blue light exposure did not induce a reduction in the soluble fraction for either optobody-Δjα or TDP-43. Furthermore, while the insoluble fraction did not increase (Figure R11), confirming that this variant is relatively stable even in light conditions, the expression levels were lower compared to full-length (Figure R10D). This suggests that the removal of the α-chain compromises optobody stability enough to reduce its half-life, even in the dark.

The second scenario involves the ΔODC1 variant, which unexpectedly shows a decrease after 6 hours of light exposure, while the target remains unaffected (Figure R10). This may be explained by the fact that, although removing the degron should eliminate the link to the proteasomal pathway, the jα unfolding and light exposure are unaffected and may still be sufficient to induce degradation. This could explain why the optobody variant undergoes a significant reduction in the soluble fraction, while the insoluble fraction remains relatively stable (Figure R11). Thus, even though the ΔODC1 variant shows light-induced degradation, it is incapable of degrading the target.

When evaluating the insoluble fractions, light exposure resulted in a significant increase in the insoluble fraction for both the optobody variant and the target protein. This increase was particularly pronounced for TDP-43 when co-expressed with the ΔODC1 variant, almost confirming that light exposure in the TDP-43 expression condition must be carefully controlled. Otherwise, it could become a toxic stimulus by promoting the accumulation of the protein in an insoluble form. This is further confirmed by the different trend shown in HEK293T cells expressing only the TDP-43 WT or the NLS1 mutant version. As shown in Figure R15A-B, the variation of the protein level due to light exposure is significant only when looking at the increase in the insoluble fraction of the mutant. This might reflect the pool of the target protein localized to the proteasomes, on its way to be degraded. Also, this could be due to a double-stress condition for the cell, the mislocalization of the protein, and the administration of an exogenous stimulus.

Up until this point, the approach for monitoring the reduction of protein levels in the presence of an optobody and its activating stimulus has been focused on establishing a clear pipeline to assess the efficacy of the tool. Each module is crucial for the optobody to effectively guide the target to the 26S proteasome. However, it is equally important to distinguish between the reduction in the soluble fraction due to the degradation pathway and that resulting from the natural tendency of a soluble monomer to lose solubility and become part of the insoluble fraction under stress conditions. When the TDP-43 mutant was overexpressed without the optobody, a marked increase in the insoluble fraction was observed, which suggests that the targeted protein degradation seen after 6 hours of light stimulation in co-expression conditions could have also been attributed solely to an increase in the insoluble pool of the protein, in addition to its association with the 26S proteasome. Surprisingly, experiments revealed that the soluble fraction of the protein was significantly reduced alongside the optobody. In contrast, the insoluble portion of the mutant target protein increased only slightly upon light stimulation, with this increase not reaching statistical significance (Figure R16). These results indicate that the optobody precisely limits the transition of the mislocalizing-prone target from the soluble to the insoluble fraction. In other words, while 6 hours of light exposure may constitute a stress stimulus for HEK293T cells expressing the TDP-43 mutant alone sufficient to detect an increase in the insoluble fraction, this increase is significantly modulated by the presence of the optobody.

5.1.5 Targeted degradation of TDP-43 variant and global translation variation

TDP-43 is involved in a wide range of cellular functions, from mRNA transport to stress granule formation and translational control. In this thesis, I focused on its role in the translation process. The mutant form of TDP-43, which is prone to mislocalization, has been shown to induce the co-aggregation of the RACK1 protein (Receptor for Activated Kinase 1) RACK1 disrupting the global translation pathway in the cell (Russo et al., 2017). RACK1 is a component of the 40S ribosome (Sengupta et al., 2004) and is a crucial translation regulator. Furthermore, Russo and collaborators found that co-overexpression of RACK1 can rescue the global translation level that is affected by the mislocalization of the TDP-43 mutant protein. Interestingly, the knockdown of RACK1 in the presence of the mutant TDP-43 also appears to restore global translation (B. Zhao et al., 2023), further confirming the role of both TDP-43 and RACK1 in regulating translation. These findings highlight the critical role of TDP-43 abundance and its interaction with RACK1 in modulating the translation machinery. Motivated by these insights, my research aimed to explore the impact of targeted degradation of TDP-43 mutant on global translation in greater detail. Specifically, I sought to evaluate changes in translation patterns before and after light-induced targeted degradation of TDP-43, providing further insights into how TDP-43 dysregulation affects the translation process.

Paving the way for global translation variation due to light-induced degradation of mutant TDP-43 and taking into account the required interaction with RACK1, I checked if the presence of the optobody could affect the TDP-43-RACK1 interaction. Thus, once confirmed that the presence of the optobody, whose epitope resides between RRM1 and RRM2 domains of TDP-43 (Gilodi et al., 2022), preserves the capacity of MYC-tagged TDP43 to co-immunoprecipitate the RACK1 (in-cell co-immunoprecipitation), I proceeded with the investigation of monitoring the PMY incorporation during light-dependent TDP-43 mutant degradation. As expected, on one side I gained the confirmation of the hypothesis that TDP-43 mutant is affecting the global translation process since, in dark condition the PMY incorporation is significantly reduced as shown in figure R21C, but on the other side, the targeted protein degradation obtained by the light activation of the optobody tool is sufficient to rescue the global translation in HEK293T cells.

Although it was not the primary focus of this thesis to delve into the detailed interaction between TDP-43 and RACK1, I sought to investigate whether there was a light-dependent rescue of PMY incorporation under conditions where global translation was impaired by both

the overexpression of the mislocalizing TDP-43 mutant and the silencing of RACK1. In these experiments, while PMY incorporation levels in HEK293T cells were reduced when RACK1 was silenced, no significant changes in translation suppression were observed following light-dependent degradation of the TDP-43 NLS1 mutant (Figure R22E). One possible explanation for this result is that only the physiological levels of RACK1 can offset the imbalance caused by TDP-43 overexpression up to a certain threshold, beyond which further quantifiable effects are not observed.

Based on the experimental setup, it was anticipated that simultaneous optobody-mediated removal of the TDP-43 mutant and RACK1 silencing would lead to an even more pronounced reduction in global translation compared to the dark condition. However, this was not the case. In contrast, Figure R22D shows that, despite a measurable reduction in RACK1 protein levels across experimental replicates, the knockdown achieved through RACK1 siRNA transfection did not yield statistically significant results. This could be attributed to technical challenges associated with siRNA transfection, where transfection efficiency can vary significantly between individual cells. Nonetheless, the trend observed in protein silencing does suggest that the reduction in RACK1 levels affects PMY incorporation in HEK293T cells.

Interestingly, when TDP-43 levels were also affected by light-dependent degradation, the removal of the mislocalized TDP-43 mutant was insufficient to restore global translation. This finding aligns with the known direct interaction between RACK1 and the ribosomal machinery within the 40S subunit. In contrast, the role of TDP-43 appears to be more indirect, relying on the presence of RACK1 for its effects on translation.

5.1.6 Comparison with ligand-induced degradation methods

The confirmed strength of the optobody-mediated targeted protein degradation offered the opportunity to compare the degradation methods with another validated stimulus induced intrabody based degradation tool previously validated for Tau protein degradation. Taking into account the TPD mediated by scFvTau2-Ikβ in Melchionna *et al.*, to compare two technologies whose activity involves a third component, which is the reduction of the target, the first step is to validate the ligand-induced degradation of TDP-43 protein in the cellular system. When tested in HeLa cells, TNFα-induced degradation of TDP-43 by the VHH5-Ikβ was not detectable, despite MG132 chase experiments clearly showing the involvement of the proteasome upon TNFα treatment. In studies using intrabody-based tools, the first step in

troubleshooting a loss of effect on the antigen side is to investigate the activity of the intrabody itself. In this case, no protein reduction was observed following degron stimulation (Figure R26A). The fusion of a nanobody, such as VHH5, to a full-length protein like Ikβ significantly shortens per se the protein's half-life. Notably, in the absence of the degradation inducer, protein levels nearly doubled when the proteasome was inhibited, suggesting that the fusion of VHH5 to Ikβ may destabilize the protein per se, hindering its degradation activity on the antigen (Figure R25).

Concluding this part, although the goal of this study was to compare light- and ligand-dependent degradation of TDP-43, the expected proof of efficacy for ligand-mediated TDP-43 degradation was not achieved using the VHH anti-TDP-43 approach. The results indicated that the VHH5-Ikβ levels were insufficient for effective binding to its target. This was likely due to a sort of constitutive degradation of VHH5-Ikβ itself, which prevented it from accumulating at adequate levels to properly escort TDP-43 to the proteasome machinery. More work will be needed to compare the two methods, but, in any case, the light inducing stimulus is much better than the TNFα ligand-inducing stimulus.

5.2 Part II: Tau protein degradation mediated by anti-phospho-specific intrabody

5.2.1 Phospho-specific scFv format equipped with psd

In this second part of my work I sought to extend to another neurodegeneration-linked protein (namely the microtubule-associated-protein Tau) the successful proof of principle obtained for the light-induced targeted degradation of TDP-4.3. In particular, I undertook work to ask the ambitious question as to whether the light-induced degradation of Tau protein could be selectively restricted to a post-translationally modified subset of the Tau protein. To this aim I engineered the photosensitive degron domain on an ultra-specific scFv specifically targeting the phosphorylated form of Tau at a specific epitope (Shih et al., 2012). Thus, having the optobody format for targeted protein degradation with the TDP-43 antigen, the next step was to extend the strategy by making it able to target an early form of toxic Tau protein, focusing on its post-translational modifications. The development of an optobody tool mediating the phospho-specific Tau variant degradation could help understanding the pathological processes behind misfolding and aggregation.

The results discussed in section 5.1.4 demonstrate a scenario in which the presence of the optobody can interfere with the function of the target protein, specifically by influencing the increase in the insoluble fraction, a critical step in the aggregation process. Thus, I tried to reach the phospho specific target protein degradation through the optobody tool, and again in this case, I started from the cellular model in which I tested for the in vivo interaction between the Tau protein and the scFv-pT231-pS235. Yeast two-hybrid system allowed me to assess that the scFv-pT231-pT235 could discriminate between the Tau WT and the T231A-S235A version so much that the growth in selective media is abolished in the latter case. The binding was further confirmed by the degradation trend shown in Figure R29, which strongly suggests that while the degron signal primarily affects the half-life of the optobody upon light stimulation, the degradation of Tau reaches its highest efficacy when the optobody concentration exceeds a certain threshold, specifically within the first 4 hours of light stimulation. Notably, even with continuous light exposure between 4 and 6 hours, Tau protein levels begin to rise. This may occur because, during this time window, the optobody concentration falls below the level necessary to effectively escort the target to the degradation pathway.

5.2.2 Light-induced degradation reveals different kinetics of dark recovery for the optobody and Tau

Furthermore, the trend observed during the 2-hour recovery period in the dark following 4 hours of light exposure reveals distinct behaviours for the optobody and the target protein. The

intrinsic rates of synthesis and half-lives of both the optobody and the target play a crucial role in explaining these trends. While the recovery of the optobody is not substantial, the recovery of Tau is significant. This suggests that, while the degradation of the optobody is gradual, reaching its maximum reduction after 6 hours (at least under the experimental conditions designed to align with the log phase of the growth curve), the difference between 4 hours of light exposure with and without recovery is not significant. In contrast, Tau degradation reaches its peak efficacy within 4 hours, and the recovery phase is sufficient to significantly increase its protein concentration. This can be attributed to the synthesis rate aligning with the duration of the recovery period. Therefore, the behaviour observed during the recovery phase is closely linked to the intrinsic properties of each protein.

5.2.3 Phospho specificity of the optobody-mediated degradation

The first aim of this part of the work was therefore reached: the light-induced targeted degradation approach could be extended to a second protein of huge physiological and pathological importance, the neuronal microtubule-associated protein Tau.

The targeted protein degradation approach, in the case of this proteini, at evaluating the phosphorylated pool of the Tau protein, asking whether this pool might be selectively affected by the reduction due to optobody activity. Importantly, two theoretical preconditions need to be fulfilled in order to expect seeing a specific signal read-out for a selective degradation of the post-translationally modified protein, with respect to the total pool of the protein. First, the binding affinity difference between the phosphorylated epitope, with respect to the same unphosphorylated epitope on Tau, needs to be large enough to account for a differential binding, under the conditions (and the concentrations) of the experimental system in cells. Second, the fraction of the phosphorylated pool, with respect to the total pool, should be small enough to be able to measure a differential signal. These considerations need to be clearly taken into account when interpreting the results of the experiments.

When the experiments were conducted in the co-expression condition of the optobody with the mutant Tau, an unpredictable scenario emerged. The mutant tau protein, lacking the serine or Threonine residues putatively phosphorylated in the wild type tau protein, showed the same degradation trend as the wild type format, although no evidence of interaction with the phospho-specific intrabody was observed in the yeast two-hybrid assay. This, the biological read-out, provided evidence for a phosphorylation-specific interaction, while the degradation

assay read-out showed no such selectivity. Possible explanations reside in the different concentration range of the optobody-Tau antigen couple in the two assays. Although a non-univocal result was obtained using the mutant version of the antigen, I further elucidated whether the Tau portion affected by light-induced protein reduction was indeed phosphorylated on threonine 231. Due to time constraints in completing my project, I could not obtain more than three replicates, but it was still possible to obtain a degradation pattern of the Tau-p231 on yeast extract expressing the opto-p231-253 treated with light. As shown in Figure R31 in 4h of light, a reduction trend emerged, although not statistically significant. On the other hand, it is impressive that even if the expression level of the phosphorylated form is lower than the one obtained for the total Tau, since the densitometric values are an order of magnitude lower, compared to Figure R29B y axes, the pattern of the bands recapitulates the one of the total Tau. Thus, I can assume that the degradation assessed for the total Tau also affects the phosphorylated form.

Going back to the result on the mutant Tau, I focused on the two conditions required for the phospho-specific degradation: the phospho specificity of the optobody and the phosphorylation status of the target. When considering the specificity of the scFv-p231-p235, I reasoned that the explanation for the dual behaviour of the intrabody, failing to promote growth on selective plates when co-expressed with the mutant but inducing degradation activity on the mutant when grown in non-selective medium for protein degradation experiments, may be due to protein overexpression (and hence on the relative concentrations of the interacting proteins). The Tau-2N4R mutant was expressed fused to LexA protein for the yeast two-hybrid assay and fused to NLS mutant-LexA protein for the degradation experiments to increase the cytosolic concentration of the protein, which must be recognized, bound, and retargeted by the optobody within the same cellular compartment. It became apparent that the overexpression of the mutant Tau-2N4R, when fused with LexA WT, prevented yeast growth on selective media. However, it cannot be ruled out that, in small amounts, the scFv-pT231-pS235 might still bind some monomers of the mutant form.

The in vivo readout based on yeast survival relies on the activation of a pathway that allows removal of auxotrophy for histidine, transforming the strain into a new version able to activate the biosynthesis pathway thanks to the expression of HISIII gene. In this view, only the reconstitution of the transcription factor, DNA binding domain, and activation domain in close proximity, upstream the HISIII gene, can guarantee the final experimental read out; in other

words, only strong interactors can significantly impact yeast survival. On the other hand, as clarified by Shih *et al*., the epitope of scFv-pT231-pS235 resides in a 7-amino acid region from lysine 225 to phosphothreonine 231 (KVAVVRpT), with a dissociation constant (kd) of 0.35 nM, giving it the quality of an "ultra-specific" antibody domain. However, in the presence of the mutant T231A, the affinity decreases by three orders of magnitude, yet it still maintains a kd of 500 nM. Furthermore, although a real comparison between the affinity of different intrabodies is not intended in this discussion session, the kd of 500 nM remains ten times higher the dissociation constant measured for other intrabodies selected in our laboratory against the N-protein of Sars-cov2 (Lisi et al., 2024). Thus, one assumption can be that 500nM of kd, the presence of six out of seven residues of the original epitope, and the over expression conditions of the antigen and may be sufficient to degrade the unwanted antigen, while the only first two conditions were not enough to allow for yeast survival on selective medium.

5.2.4 Consideration on the phosphorylated pools of Tau protein

When evaluating the phosphorylation state of the Tau-2N4R WT compared to the mutant protein by investigating the migration on phos-tag western blotting, a few considerations could be given. Although the aim was to distinguish between the two pools of the Tau protein, at least five bands can be detected in each lane (Figure R32D). Moreover, the migration pattern of each band varies together with the position of the bands, indicating that while the number of Tau isoforms is consistent across lanes, the level of phosphorylation differs. Furthermore, between lane 2 and lane 4, there is a reduction of the highest band, which confirms that the pool of Tau highly phosphorylated is reduced when T231 and S235 are mutated to alanine. Therefore, it is reasonable to draw only general conclusions about the phosphorylation state of the Tau-2N4R used in this study. Based on the quantification of the relative intensity of each band, it is evident that multiple phosphorylated forms exist, even after phosphatase treatment. Indeed, the phosphatase treatment did not completely remove phosphorylation from the protein, as both the number and relative intensities of the bands remained similar to those in the untreated samples, even if the absolute intensities are lower. Considering that the Tau isoforms used in this work contains 85 potential serine (Ser), threonine (Thr), and tyrosine (Tyr) phosphosites (Basheer et al., 2023), and that the combination of the phosphorylation on these residues can produce different pattern of migration, the six different bands in this view represent even a simplified view of the complexity of the issue. While optimizing the phosphatase protocol could potentially eliminate all phosphorylated sites, reducing the Tau

protein to a single 68 kDa band (fused with LexA), this would not provide additional insights into the precise number of phosphorylated sites on the baits in the L40 yeast strain. Additionally, each band in lanes two and four likely represents a mixture of LexA-Tau forms, phosphorylated at different sites but affected by the same migration delay, resulting in similar band patterns.

In conclusion, on one hand, a positive result was obtained for TPD on the Tau protein antigen; on the other hand, promising, although not yet conclusive, results have been obtained for Post Translational Modification-selective Targeted Protein Degradation (PTM-TPD) of Tau phosphorylated at Threonine 231. I can only infer that the light-dependent degradation mediated by the optobody affects the phosphorylated pool, even though no significant reduction was detected in the experimental replicates shown in this thesis. Moreover, the ratio between the non-phosphorylated and phosphorylated pools of the protein, considered as total Tau, could not be accurately assessed. This limitation arose from the presence of multiple phosphorylated forms of Tau in the L40 strain used for the degradation experiments, which made it challenging to precisely distinguish the band corresponding to p231.

In any case, this thesis offered the opportunity to carefully understand the critical points, the need for attention on crucial aspects and parameters to be considered.

Part III: Targeting the Activity-regulated cytoskeletal protein at the protein level

In this work, targeted protein degradation has emerged as a key downstream application of the intracellular antibody selection platform, providing a novel solution to the challenge of undruggable proteins. By enabling precise interference with protein function, this approach operates at the molecular level, allowing for the specific targeting and modulation of proteins that are difficult or impossible to address with traditional small-molecule drugs. On the other hand, the power of the optogenetic tool presented in the previous sessions, together with the potential of owning a selection platform that allows for isolation of intrabody binders against any antigen, enhances the applicability of the photosensitive degradation tool.

I explored the intracellular antibodies capture technology to isolate the intrabody domain against the activity-regulated cytoskeletal protein, Arc, that represents the perfect target to bind within the intracellular environment, where its function is not yet fully understood, despite being a crucial protein for synaptic plasticity and memory studies. While this was not the primary focus of the current work, it is worth noting that targeting such a protein with high spatial precision can lead to the development of a tool to map activated neurons at a dendritic resolution. The intrabody-like domains, isolated from a library of 10th Fibronectine typeIII (10FnIII) screened with RNA display (FingRs) have already been used to create reagents to label excitatory and inhibitory synapses in live neurons by targeting PSD-95 and Gephyrin, respectively (Gross et al., 2013). Briefly, the FinGRs approach allows for the isolation of intrabody-like binders that recognize intracellular targets to map excitatory and inhibitory synapses in living neurons by fusing FingRs with EGFP. The fluorescent antibody-like domain is further coupled with two additional partners that establish a negative feedback loop. In this system, when the FingR-EGFP-ZF-KRAB(A) construct binds to its target protein, into an activated synapse, the KRAB(A)-ZF component is prevented from entering the nucleus and binding to the ZF binding sequence located upstream of the promoter controlling FingR expression. When all the target is bound, the KRAB(A)-ZF can migrate into the nucleus where it can act as a transcriptional repressor of the FingR coding region. This mechanism effectively addresses the common issue of overexpression, which can lead to mislocalization of target signals due to unbound intrabodies. By ensuring that expression is tightly regulated, the system minimizes potential artifacts caused by nonspecific binding and mislocalization, providing a more accurate and reliable tool for cellular studies. The work of Gross *et al.* represents an example of the power of intrabody-like domains against activity-dependent targets to elucidate their localization and function. In this view, the Arc protein becomes a brilliant candidate to

investigate protein function and, trafficking using an intrabody-based approach. Thus, one application of an intrabody base tool targeting Arc protein could map with a precise temporal and spatial resolution the activated spines of a specific neuron; moreover, a degradation tool can help the understanding of its role in synaptic plasticity. Understanding the molecular functions of Arc has proven challenging due to its unique nature as a single-copy gene, regulated at all possible molecular regulation levels, from transcriptional, RNA processing, RNA transport, RNA degradation, protein translation and post-translational levels, and degradation, lacking identifiable family members or clearly defined biochemical domains (W. Zhang et al., 2015).

5.3.1 Optobody213 as a TPD tool against activity-regulated cytoskeletal protein

Aiming at increasing the range of applicability of the optobody format, I focused my work on the targeted protein degradation of the Arc protein in the mammalian cell line HEK293T, and then I moved into neuronal cell lines. The IACT selection platform allowed to isolation of VHH213 as a the best candidate against the N-terminal region of Arc protein, and then the IVEM confirmed the isolation of a conformation-sensitive intrabody, interacting with the full-length Arc format both in vivo and through co-immunoprecipitation experiments. On the other hand, when the epitope used in the primary screening, composed of two coils divided by an inter-coil region, was further divided into three distinct structural portions, namely N-coil, C-coil and inter-coil region, no binding was detected. In this view, the conformational sensitive intrabody against the N-terminal region of Arc protein was modified with the addition of the photosensitive degron domain. The targeted protein degradation experiments in this part of the work took advantage of the previous results obtained with the optobody-anti-TDP-43, thus, the experimental pipeline applied was the same. Indeed, when tested in mammalian cell lines, the Arc and the optobody213 sequence, although a clear reduction trend shown by the optobody upon light exposure, significant in 6h, the Arc protein did not undergo a significant reduction. In Figure R37B it is shown that 4h of stimulation are enough to reduce the Arc protein level, while in the next two hours of light exposure it the protein level may increase. For Arc protein light-induced degradation in HEK293T cells, only a few considerations can be made from the results I showed in the previous session. Despite Although the co-expression condition in the same transcript of the optobody-213, the expression level of Arc protein was difficult to detect by immunoblotting, as demonstrated by the different range of values present on the y axes in Figure R37A and B. The lower densitometric values of the MYC-tagged Arc protein band may be due to a lower concentration of the soluble portion of the Arc protein in the HEK293T

cellular system. It cannot be excluded that Arc overexpression in transfection conditions can lead to instability of the soluble portion itself.

5.3.2 Targeted degradation of endogenous Arc mediated b

Aiming at increasing the range of applicability of the optobody format, I focused my work on the targeted protein degradation of the Arc protein in the mammalian cell line HEK293T, and then I moved into neuronal cell lines. The IACT selection platform allowed to isolation of VHH213 as the best candidate against the N-terminal region of Arc protein, and then the IVEM confirmed the isolation of a conformation-sensitive intrabody, interacting with the full-length Arc format both in vivo and through co-immunoprecipitation experiments. On the other hand, when the epitope used in the primary screening, composed of two coils divided by an inter-coil region, was further divided into three distinct structural portions, namely N-coil, C-coil and inter-coil region, no binding was detected. In this view, the conformational sensitive intrabody against the N-terminal region of Arc protein was modified with the addition of the photosensitive degron domain. The targeted protein degradation experiments in this part of the work took advantage of the previous results obtained with the optobody-anti-TDP-43, thus, the experimental pipeline applied was the same. Indeed, when tested in mammalian cell lines, the Arc and the optobody213 sequence, although a clear reduction trend shown by the optobody upon light exposure, significant in 6h, the Arc protein did not undergo a significant reduction. In Figure R37B it is shown that 4h of stimulation are enough to reduce the Arc protein level, while in the next two hours of light exposure it the protein level may increase. For Arc protein light-induced degradation in HEK293T cells, only a few considerations can be made from the results I showed in the previous session. Although the co-expression condition in the same transcript of the optobody-213, the expression level of Arc protein was difficult to detect by immunoblotting, as demonstrated by the different range of values present on the y axes in Figure R37A and B. The lower densitometric values of the MYC-tagged Arc protein band may be due to a lower concentration of the soluble portion of the Arc protein in the HEK293T cellular system. It cannot be excluded that Arc overexpression in transfection conditions can lead to instability of the soluble portion itself.

5.3.3 Targeted degradation of endogenous Arc mediated by optobody213 in neuronal cells

Despite initial efforts, HEK293T cells did not prove to be the most suitable in vitro model for investigating Arc-targeted protein degradation. Therefore, to overcome this issue, a shift to a more appropriate in vitro neuronal model appeared to be the solution. The MiBi cortical

neurons provided a more relevant physiological context for studying activity-induced Arc expression and its reduction via optobody-mediated degradation.

The idea was to use MiBi culture to obtain Arc expression through stimulation protocols, while optobody expression was controlled via a tetracycline-responsive element (TRE) promoter, allowing for temporal regulation. A key consideration in this experimental design was the synchronization of two distinct but interdependent events: (1) activity-induced expression and subcellular localization of endogenous Arc, particularly within dendritic spines, and (2) the accumulation of the optobody to a steady-state level, the dark condition, sufficient for antigen recognition. Achieving temporal overlap between these two processes was essential to enable light-inducible optobody activation to effectively target Arc protein for degradation.

Before optimizing the Arc induction protocol in cortical neurons, I focused on validating the functionality of the optobody system within a biologically relevant environment. MiBi cultures were particularly advantageous in this regard, as they allow for baseline expression of Arc due to the presence of brain-derived neurotrophic factor (BDNF) in the culture medium. BDNF is a well-characterized physiological inducer of Arc, and its presence facilitated the testing of the optobody under near-endogenous conditions without relying on overexpression artifacts. This validation step was crucial in establishing the feasibility of applying the optobody system for activity-dependent degradation of Arc in neurons, thereby setting the stage for subsequent protocol optimization and experimental evaluation of the temporal dynamics of the system. On the other hand, the doxycycline induction allowed for avoiding the optobody constitutive overexpression that may interfere with the normal Arc activity even in dark conditions.

Despite this controlled design, light-induced degradation experiments in MiBi cortical neurons expressing endogenous Arc did not yield a detectable reduction in Arc protein levels. In contrast, both opto-213 and the control anti-GFP optobody showed significant decreases in their protein levels upon light stimulation (Figures R40 and R41). These findings suggest several possible explanations. First, the optobody itself may be subject to rapid degradation during the four-hour light stimulation period, potentially before it has sufficient opportunity to bind to Arc. This would hinder both antigen recognition and subsequent targeted degradation.

Second, it is possible that the endogenous Arc levels induced by BDNF exceeded the available pool of optobody, thereby shifting the stoichiometric balance in favour of the target and limiting the efficiency of degradation. This again highlights the importance of finely tuning the ratio

between optobody and antigen as a critical parameter for successful protein knockdown in neuronal systems. A pulse of de novo Arc protein synthesis, as opposed to a long steady state induction by BDNF might be a better strategy to achieve the targeted degradation of the de novo synthetized Arc pool.

Furthermore, when considering the role of Arc's N-terminal (NT) domain in its synaptic functions, another layer of complexity emerges. Under endogenous expression conditions, Arc is trafficked to dendritic spines where it interacts with multiple protein partners. Given that the optobody epitope lies within amino acids 1–140 of Arc at its N-terminal, it is plausible that this region becomes sterically occluded or masked by binding partners in vivo, thereby impeding recognition by the optobody. This potential epitope shielding would limit the accessibility required for optobody binding and subsequent degradation, even in the presence of light activation.

Another layer of investigation arises when focusing on synchronizing the inducible expression of the anti-Arc optobody and the light degradation window, with the half-life of the target. Since newly synthesized Arc undergoes rapid ubiquitination and proteasomal degradation with an estimated half-life between 30 and 60 minutes (Eriksen & Bramham, 2022), a truly orthogonal degrader tool must exert its effect within a similarly short timeframe, ideally under one hour.

The light exposure durations employed in this study were initially optimized in lower-order cellular models and subsequently applied to more complex neuronal systems. This approach was based on the assumption that light functions as the primary external factor modulating proteasomal activity in this system. However, it cannot be excluded that the cellular context itself significantly influences the efficiency of the degradation pathway. Therefore, the application of the same optobody system across distinct cellular environments may necessitate specific adjustments to the degradation protocol, including light exposure parameters and timing.

These considerations point to a broader need for systematic optimization within the optobody platform. While prior studies in mammalian cells have demonstrated maximal optobody degradation after six hours of continuous light exposure, the results obtained in this project show that the anti-Arc optobody undergoes substantial degradation already within four hours of blue light illumination. However, if the light exposure required to activate targeted protein

degradation cannot precede the physiological turnover of Arc, then the system's resolution and efficiency are inherently limited.

In conclusion, while the MiBi cortical neuron model offered a more physiologically relevant platform for studying Arc degradation, several biological and technical challenges limited the effectiveness of optobody-mediated targeted protein degradation. The need for precise temporal coordination between Arc expression and optobody availability, combined with the rapid turnover of Arc and potential epitope masking within dendritic spines, likely contributed to the absence of measurable Arc reduction despite successful optobody degradation. These findings underscore the complexity of applying optogenetic degrader systems in neuronal environments and highlight the importance of optimizing not only the timing and dosage of expression but also the design of the optobody itself to ensure efficient target engagement and degradation. This would include engineering optobodies with improved stability, faster activation kinetics, and enhanced target-binding under physiological conditions, ultimately enabling precise temporal control over protein function in complex neuronal systems. Although clearly defined, this objective could not be fully realized within the timeframe of this project.

6. Conclusions

Becoming part of the intrabody group, I could exploit the Intracellular antibodies capture technology at many different levels, from the isolation of intrabody domains to engineering already validated intrabodies by creating and optimizing what we define as optobody technology for degradation. The biological question I could address with my work was the targeted protein degradation mediated by the most potent binders in nature, the antibody domains. In this view, the targeted protein degradation can represent the downstream application that addresses the issue of undruggable proteins, with the need for a tool to interfere with the protein function, working exquisitely at the protein level. Protein interference is rapidly emerging as a powerful approach for dissecting protein function. While RNA interference (RNAi) can block protein production at the translational level, and antisense oligonucleotides (ASOs) can disrupt mRNA processing, these strategies are ineffective against long-lived proteins that have already been synthesized. Also, RNA-based strategies are by definition ineffective for a post-translational selective interference with a PTM pool of a given protein target. In this context, targeted protein degradation represents a more direct and efficient solution. A key advantage lies in the use of a modulable, bifunctional intrabody capable of recruiting the proteasome machinery without relying on the complex ubiquitination cascade. This approach offers a compelling alternative to conventional E3 ligase-based degradation systems (such as the PROTACs).

This study comprehensively evaluates an innovative optobody-mediated strategy for targeted protein degradation, leveraging intracellular antibodies fused to a light-sensitive degron to selectively modulate protein levels in various cellular contexts. The tool successfully demonstrated precise, light-dependent degradation of both TDP-43 and Tau, with promising results on its phosphorylated form, highlighting its versatility and temporal control in both yeast and mammalian systems. While the degradation of TDP-43 effectively restored translation homeostasis disrupted by its mislocalization, the Tau experiments, albeit with limitations in quantifying phosphorylation states, clearly demonstrate the applicability of the optobody format on post-translational modifications (PTMs).

The extension of this technology to the Arc protein revealed critical constraints imposed by the rapid turnover and potential epitope masking in neurons, emphasizing the necessity for enhanced design optimization and synchronization between optobody activation and target availability. Overall, this work not only validates optobody-based TPD as a powerful tool to

probe protein function with spatial and temporal precision but also underscores key considerations for its application in complex biological systems, paving the way for future refinements in degrader technology.

Furthermore, the potential of our optobody as a TPD tool can be significantly enhanced by isolating intrabodies that specifically recognize the desired post-translational modification (PTM) of the target protein, enabling a tunable and PTM-specific degradation of the target.

Finally, a thorough understanding of the optobody technology presented in this study necessitates a critical examination of its inherent limitations. Although TPD is mainly exploited for therapeutic application, indeed, the molecules currently in the clinical trial process are PROTAC or molecular glues (Zhong et al., 2024), TPD technologies, undoubtedly, will also provide powerful tools for biomedical research. The current optobody system is intended exclusively as a molecular research tool for in vitro applications, enabling targeted protein degradation to dissect protein function in controlled cellular environments. While the use of light provides an orthogonal and temporally precise activation mechanism, this feature is not translatable to therapeutic contexts in its present form. Specifically, the prolonged blue light exposure required to induce degradation is compatible with in vitro models but infeasible for in vivo use, particularly in therapeutic settings. Additionally, the design is not optimized for pharmacological delivery or systemic modulation and therefore is not intended for drug discovery or clinical application. Instead, the platform is best suited for mechanistic studies aimed at understanding protein dynamics, interaction networks, and functional outcomes of acute protein loss.

7. References

Abbas, A. K., Lichtman, A. H., & Pillai, S. (2011). *Molecular and Cellular Immunology* (7th ed.). Elsevier. https://books.google.it/books?id=qtJY05rIUKQC&printsec=copyright&redir_esc=y#v=onepage&q&f=false

Balch, W. E., Morimoto, R. I., Dillin, A., & Kelly, J. W. (2008). Adapting Proteostasis for Disease Intervention. *Science*, *319*(5865), 916–919. https://doi.org/10.1126/science.1141448

Banik, S. M., Pedram, K., Wisnovsky, S., Ahn, G., Riley, N. M., & Bertozzi, C. R. (2020). Lysosome-targeting chimaeras for degradation of extracellular proteins. *Nature*, *584*(7820), 291–297. https://doi.org/10.1038/s41586-020-2545-9

Barbas, C. F., Kang, A. S., Lerner, R. A., & Benkovic, S. J. (1991). Assembly of combinatorial antibody libraries on phage surfaces: The gene III site. *Proceedings of the National Academy of Sciences*, *88*(18), 7978–7982. https://doi.org/10.1073/pnas.88.18.7978

Bartel, B., Wünning, I., & Varshavsky, A. (1990). The recognition component of the N-end rule pathway. *The EMBO Journal*, *9*(10), 3179–3189. https://doi.org/10.1002/j.1460-2075.1990.tb07516.x

Basheer, N., Smolek, T., Hassan, I., Liu, F., Iqbal, K., Zilka, N., & Novak, P. (2023). Does modulation of tau hyperphosphorylation represent a reasonable therapeutic strategy for Alzheimer's disease? From preclinical studies to the clinical trials. *Molecular Psychiatry*, *28*(6), 2197–2214. https://doi.org/10.1038/s41380-023-02113-z

Békés, M., Langley, D., & Crews, C. (2022). PROTAC targeted protein degraders: The past is prologue. *Nature Reviews Drug Discovery*, *21*(3), 181–200. https://doi.org/10.1038/s41573-021-00371-6

Biocca, S., & Cattaneo, A. (1995). Intracellular immunization: Antibody targeting to subcellular compartments. *Trends in Cell Biology*, *5*(6), 248–252. https://doi.org/10.1016/S0962-8924(00)89019-4

Biocca, S., & Cattaneo, A. (1997). Intracellular Antibodies. In *Intracellular Antibodies, Development and Application* (pp. 119–120). Springer Verlag.

Biocca, S., Neuberger, M. S., & Cattaneo, A. (1990). Expression and targeting of intracellular antibodies in mammalian cells. *The EMBO Journal*, *9*(1), 101–108. https://doi.org/10.1002/j.1460-2075.1990.tb08085.x

Bird, R. E., Hardman, K. D., Jacobson, J. W., Johnson, S., Kaufman, Bennet. M., Lee, S.-M., Lee, T., Pope, S. H., RIoRDAN, G. S., & Whitlow, M. (1988). *Single-Chain Antigen-Binding Proteins*. *242*.

Bliss, T. V. P., & Lømo, T. (1973). Long-lasting potentiation of synaptic transmission in the dentate area of the anaesthetized rabbit following stimulation of the perforant path. *The Journal of Physiology*, *232*(2), 331–356. https://doi.org/10.1113/jphysiol.1973.sp010273

Bourdenx, M., Martín-Segura, A., Scrivo, A., Rodriguez-Navarro, J. A., Kaushik, S., Tasset, I., Diaz, A., Storm, N. J., Xin, Q., Juste, Y. R., Stevenson, E., Luengo, E., Clement, C. C., Choi, S. J., Krogan, N. J., Mosharov, E. V., Santambrogio, L., Grueninger, F., Collin, L., … Cuervo, A. M. (2021). Chaperone-mediated autophagy prevents collapse of the neuronal metastable proteome. *Cell*, *184*(10), 2696-2714.e25. https://doi.org/10.1016/j.cell.2021.03.048

Butler, D. C., & Messer, A. (2011). Bifunctional Anti-Huntingtin Proteasome-Directed Intrabodies Mediate Efficient Degradation of Mutant Huntingtin Exon 1 Protein Fragments. *PLoS ONE*, *6*(12), e29199. https://doi.org/10.1371/journal.pone.0029199

Cao, F., De Weerd, S., Chen, D., Zwinderman, M. R. H., Van Der Wouden, P. E., & Dekker, F. J. (2020). Induced protein degradation of histone deacetylases 3 (HDAC3) by proteolysis targeting chimera (PROTAC). *European Journal of Medicinal Chemistry*, *208*, 112800. https://doi.org/10.1016/j.ejmech.2020.112800

Cattaneo, A., & Chirichella, M. (2019). Targeting the Post-translational Proteome with Intrabodies. *Trends in Biotechnology*, *37*(6), 578–591. https://doi.org/10.1016/j.tibtech.2018.11.009

Cattaneo, A., & Neuberger, M. S. (1987). Polymeric immunoglobulin M is secreted by transfectants of non-lymphoid cells in the absence of immunoglobulin J chain. *The EMBO Journal*, *6*(9), 2753–2758. https://doi.org/10.1002/j.1460-2075.1987.tb02569.x

Chatterjee, D., Bhatt, M., Butler, D., De Genst, E., Dobson, C. M., Messer, A., & Kordower, J. H. (2018). Proteasome-targeted nanobodies alleviate pathology and functional decline in an α-synuclein-based Parkinson's disease model. *Npj Parkinson's Disease*, *4*(1), 25. https://doi.org/10.1038/s41531-018-0062-4

Chirichella, M., Lisi, S., Fantini, M., Goracci, M., Calvello, M., Brandi, R., Arisi, I., D'Onofrio, M., Di Primio, C., & Cattaneo, A. (2017). Post-translational selective intracellular silencing of acetylated proteins with de novo selected intrabodies. *Nature Methods*, *14*(3), 279–282. https://doi.org/10.1038/nmeth.4144

Christie, J. M., Gawthorne, J., Young, G., Fraser, N. J., & Roe, A. J. (2012). LOV to BLUF: Flavoprotein Contributions to the Optogenetic Toolkit. *Molecular Plant*, *5*(3), 533–544. https://doi.org/10.1093/mp/sss020

Clift, D., McEwan, W. A., Labzin, L. I., Konieczny, V., Mogessie, B., James, L. C., & Schuh, M. (2017). A Method for the Acute and Rapid Degradation of Endogenous Proteins. *Cell*, *171*(7), 1692-1706.e18. https://doi.org/10.1016/j.cell.2017.10.033

Cohen, T. J., Lee, V. M. Y., & Trojanowski, J. Q. (2011). TDP-43 functions and pathogenic mechanisms implicated in TDP-43 proteinopathies. *Trends in Molecular Medicine*, *17*(11), 659–667. https://doi.org/10.1016/j.molmed.2011.06.004

Collins, G. A., & Goldberg, A. L. (2017). The Logic of the 26S Proteasome. *Cell*, *169*(5), 792–806. https://doi.org/10.1016/j.cell.2017.04.023

Cotton, A. D., Nguyen, D. P., Gramespacher, J. A., Seiple, I. B., & Wells, J. A. (2021). Development of Antibody-Based PROTACs for the Degradation of the Cell-Surface Immune Checkpoint Protein PD-L1. *Journal of the American Chemical Society*, *143*(2), 593–598. https://doi.org/10.1021/jacs.0c10008

Cotton, T. R., & Lechtenberg, B. C. (2020). Chain reactions: Molecular mechanisms of RBR ubiquitin ligases. *Biochemical Society Transactions*, *48*(4), 1737–1750. https://doi.org/10.1042/BST20200237

Cowan, A. D., & Ciulli, A. (2022). Driving E3 Ligase Substrate Specificity for Targeted Protein Degradation: Lessons from Nature and the Laboratory. *Annual Review of Biochemistry*, *91*(1), 295–319. https://doi.org/10.1146/annurev-biochem-032620-104421

Crosson, S., Rajagopal, S., & Moffat, K. (2003). The LOV Domain Family: Photoresponsive Signaling Modules Coupled to Diverse Output Domains. *Biochemistry*, *42*(1), 2–10. https://doi.org/10.1021/bi026978l

De Wispelaere, M., Du, G., Donovan, K. A., Zhang, T., Eleuteri, N. A., Yuan, J. C., Kalabathula, J., Nowak, R. P., Fischer, E. S., Gray, N. S., & Yang, P. L. (2019). Small molecule degraders of the hepatitis C virus protease reduce susceptibility to resistance mutations. *Nature Communications*, *10*(1), 3468. https://doi.org/10.1038/s41467-019-11429-w

Deisseroth, K. (2011). Optogenetics. *Nature Methods*, *8*(1), 26–29. https://doi.org/10.1038/nmeth.f.324

Dugger, B. N., & Dickson, D. W. (2017). Pathology of Neurodegenerative Diseases. *Cold Spring Harbor Perspectives in Biology*, *9*(7), a028035. https://doi.org/10.1101/cshperspect.a028035

Eriksen, M. S., & Bramham, C. R. (2022). Molecular physiology of Arc/Arg3.1: The oligomeric state hypothesis of synaptic plasticity. *Acta Physiologica*, *236*(3), e13886. https://doi.org/10.1111/apha.13886

Fan, X., Jin, W. Y., Lu, J., Wang, J., & Wang, Y. T. (2014). Rapid and reversible knockdown of endogenous proteins by peptide-directed lysosomal degradation. *Nature Neuroscience*, *17*(3), 471–480. https://doi.org/10.1038/nn.3637

Fletcher, A., Clift, D., De Vries, E., Martinez Cuesta, S., Malcolm, T., Meghini, F., Chaerkady, R., Wang, J., Chiang, A., Weng, S. H. S., Tart, J., Wong, E., Donohoe, G., Rawlins, P., Gordon, E., Taylor, J. D., James, L., & Hunt, J. (2023). A TRIM21-based bioPROTAC highlights the therapeutic benefit of HuR degradation. *Nature Communications*, *14*(1), 7093. https://doi.org/10.1038/s41467-023-42546-2

Fridy, P. C., Li, Y., Keegan, S., Thompson, M. K., Nudelman, I., Scheid, J. F., Oeffinger, M., Nussenzweig, M. C., Fenyö, D., Chait, B. T., & Rout, M. P. (2014). A robust pipeline for rapid production of versatile nanobody repertoires. *Nature Methods*, *11*(12), 1253–1260. https://doi.org/10.1038/nmeth.3170

Fulda, S., & Vucic, D. (2012). Targeting IAP proteins for therapeutic intervention in cancer. *Nature Reviews Drug Discovery*, *11*(2), 109–124. https://doi.org/10.1038/nrd3627

Gallardo, G., Wong, C. H., Ricardez, S. M., Mann, C. N., Lin, K. H., Leyns, C. E. G., Jiang, H., & Holtzman, D. M. (2019). Targeting tauopathy with engineered tau-degrading intrabodies. *Molecular Neurodegeneration*, *14*(1), 38. https://doi.org/10.1186/s13024-019-0340-6

Gebauer, F., & Hentze, M. W. (2004). Molecular mechanisms of translational control. *Nature Reviews Molecular Cell Biology*, *5*(10), 827–835. https://doi.org/10.1038/nrm1488

Gilodi, M., Lisi, S., F. Dudás, E., Fantini, M., Puglisi, R., Louka, A., Marcatili, P., Cattaneo, A., & Pastore, A. (2022). Selection and Modelling of a New Single-Domain Intrabody Against TDP-43. *Frontiers in Molecular Biosciences*, *8*, 773234. https://doi.org/10.3389/fmolb.2021.773234

Gross, G. G., Junge, J. A., Mora, R. J., Kwon, H.-B., Olson, C. A., Takahashi, T. T., Liman, E. R., Ellis-Davies, G. C. R., McGee, A. W., Sabatini, B. L., Roberts, R. W., & Arnold, D. B. (2013). Recombinant Probes for Visualizing Endogenous Synaptic Proteins in Living Neurons. *Neuron*, *78*(6), 971–985. https://doi.org/10.1016/j.neuron.2013.04.017

Guo, D., Hazbun, T. R., Xu, X.-J., Ng, S.-L., Fields, S., & Kuo, M.-H. (2004). A tethered catalysis, two-hybrid system to identify protein-protein interactions requiring post-translational modifications. *Nature Biotechnology*, *22*(7), 888–892. https://doi.org/10.1038/nbt985

Hallin, E. I., Eriksen, M. S., Baryshnikov, S., Nikolaienko, O., Grødem, S., Hosokawa, T., Hayashi, Y., Bramham, C. R., & Kursula, P. (2018). Structure of monomeric full-length ARC sheds light on molecular flexibility, protein interactions, and functional modalities. *Journal of Neurochemistry*, *147*(3), 323–343. https://doi.org/10.1111/jnc.14556

Hamers-Casterman, C., Atarhouch, T., Muyldermans, S., Robinson, G., Hammers, C., Songa, E. B., Bendahman, N., & Hammers, R. (1993). Naturally occurring antibodies devoid of light chains. *Nature*, *363*(6428), 446–448. https://doi.org/10.1038/363446a0

He, H., Zhou, C., & Chen, X. (2023). ATNC: Versatile Nanobody Chimeras for Autophagic Degradation of Intracellular Unligandable and Undruggable Proteins. *Journal of the American Chemical Society*, jacs.3c08843. https://doi.org/10.1021/jacs.3c08843

Hinz, M., & Scheidereit, C. (2014). The IκB kinase complex in NF -κB regulation and beyond. *EMBO Reports*, *15*(1), 46–61. https://doi.org/10.1002/embr.201337983

Hipp, M. S., Kasturi, P., & Hartl, F. U. (2019). The proteostasis network and its decline in ageing. *Nature Reviews Molecular Cell Biology*, *20*(7), 421–435. https://doi.org/10.1038/s41580-019-0101-y

Hu, Y.-B., Dammer, E. B., Ren, R.-J., & Wang, G. (2015). The endosomal-lysosomal system: From acidification and cargo sorting to neurodegeneration. *Translational Neurodegeneration*, *4*(1), 18. https://doi.org/10.1186/s40035-015-0041-1

Huala, E., Oeller, P. W., Liscum, E., Han, I.-S., Larsen, E., & Briggs, W. R. (1997). *Arabidopsis* NPH1: A Protein Kinase with a Putative Redox-Sensing Domain. *Science*, *278*(5346), 2120–2123. https://doi.org/10.1126/science.278.5346.2120

Inobe, T., & Matouschek, A. (2014). Paradigms of protein degradation by the proteasome. *Current Opinion in Structural Biology*, *24*, 156–164. https://doi.org/10.1016/j.sbi.2014.02.002

Ito, C., Saito, Y., Nozawa, T., Fujii, S., Sawa, T., Inoue, H., Matsunaga, T., Khan, S., Akashi, S., Hashimoto, R., Aikawa, C., Takahashi, E., Sagara, H., Komatsu, M., Tanaka, K., Akaike, T., Nakagawa, I., & Arimoto, H. (2013). Endogenous Nitrated Nucleotide Is a Key Mediator of Autophagy and Innate Defense against Bacteria. *Molecular Cell*, *52*(6), 794–804. https://doi.org/10.1016/j.molcel.2013.10.024

Itoh, Y., Ishikawa, M., Naito, M., & Hashimoto, Y. (2010). Protein Knockdown Using Methyl Bestatin−Ligand Hybrid Molecules: Design and Synthesis of Inducers of Ubiquitination-Mediated Degradation of Cellular Retinoic Acid-Binding Proteins. *Journal of the American Chemical Society*, *132*(16), 5820–5826. https://doi.org/10.1021/ja100691p

James, L. C., Keeble, A. H., Khan, Z., Rhodes, D. A., & Trowsdale, J. (2007). Structural basis for PRYSPRY-mediated tripartite motif (TRIM) protein function. *Proceedings of the National Academy of Sciences*, *104*(15), 6200–6205. https://doi.org/10.1073/pnas.0609174104

Ji, C. H., Kim, H. Y., Lee, M. J., Heo, A. J., Park, D. Y., Lim, S., Shin, S., Ganipisetti, S., Yang, W. S., Jung, C. A., Kim, K. Y., Jeong, E. H., Park, S. H., Bin Kim, S., Lee, S. J., Na, J. E., Kang, J. I., Chi, H. M., Kim, H. T., … Kwon, Y. T. (2022). The AUTOTAC chemical biology platform for targeted protein degradation via the autophagy-lysosome system. *Nature Communications*, *13*(1), 904. https://doi.org/10.1038/s41467-022-28520-4

Jo, M., Lee, S., Jeon, Y.-M., Kim, S., Kwon, Y., & Kim, H.-J. (2020). The role of TDP-43 propagation in neurodegenerative diseases: Integrating insights from clinical and experimental studies. *Experimental & Molecular Medicine*, *52*(10), 1652–1662. https://doi.org/10.1038/s12276-020-00513-7

Kargbo, R. B. (2019). PROTAC Degradation of IRAK4 for the Treatment of Neurodegenerative and Cardiovascular Diseases. *ACS Medicinal Chemistry Letters*, *10*(9), 1251–1252. https://doi.org/10.1021/acsmedchemlett.9b00385

Kaushik, S., & Cuervo, A. M. (2018). The coming of age of chaperone-mediated autophagy. *Nature Reviews Molecular Cell Biology*, *19*(6), 365–381. https://doi.org/10.1038/s41580-018-0001-6

Kenten, J. H., & Roberts, S. F. (2001). *CONTROLLING PROTEIN LEVELS IN EUCARYOTIC ORGANISMS* (Patent No. US006306663B1).

Kim, Y. E., Hipp, M. S., Bracher, A., Hayer-Hartl, M., & Ulrich Hartl, F. (2013). Molecular Chaperone Functions in Protein Folding and Proteostasis. *Annual Review of Biochemistry*, *82*(1), 323–355. https://doi.org/10.1146/annurev-biochem-060208-092442

Kinoshita, E., & Kinoshita-Kikuta, E. (2011). Improved Phos-tag SDS-PAGE under neutral pH conditions for advanced protein phosphorylation profiling. *PROTEOMICS*, *11*(2), 319–323. https://doi.org/10.1002/pmic.201000472

Korb, E., & Finkbeiner, S. (2011). Arc in synaptic plasticity: From gene to behavior. *Trends in Neurosciences*, *34*(11), 591–598. https://doi.org/10.1016/j.tins.2011.08.007

Kostic, M., & Jones, L. H. (2020). Critical Assessment of Targeted Protein Degradation as a Research Tool and Pharmacological Modality. *Trends in Pharmacological Sciences*, *41*(5), 305–317. https://doi.org/10.1016/j.tips.2020.02.006

Lantero-Rodriguez, J., Camporesi, E., Montoliu-Gaya, L., Gobom, J., Piotrowska, D., Olsson, M., Burmann, I. M., Becker, B., Brinkmalm, A., Burmann, B. M., Perkinton, M., Ashton, N. J., Fox, N. C., Lashley, T., Zetterberg, H., Blennow, K., & Brinkmalm, G. (2024). Tau protein profiling in tauopathies: A human brain study. *Molecular Neurodegeneration*, *19*(1), 54. https://doi.org/10.1186/s13024-024-00741-9

Li, X., Zhao, X., Fang, Y., Jiang, X., Duong, T., Fan, C., Huang, C.-C., & Kain, S. R. (1998). Generation of Destabilized Green Fluorescent Protein as a Transcription Reporter. *Journal of Biological Chemistry*, *273*(52), 34970–34975. https://doi.org/10.1074/jbc.273.52.34970

Li, Z., Wang, C., Wang, Z., Zhu, C., Li, J., Sha, T., Ma, L., Gao, C., Yang, Y., Sun, Y., Wang, J., Sun, X., Lu, C., Difiglia, M., Mei, Y., Ding, C., Luo, S., Dang, Y., Ding, Y., … Lu, B. (2019). Allele-selective lowering of mutant HTT protein by HTT–LC3 linker compounds. *Nature*, *575*(7781), 203–209. https://doi.org/10.1038/s41586-019-1722-1

Li, Z., Zhu, C., Ding, Y., Fei, Y., & Lu, B. (2020). ATTEC: A potential new approach to target proteinopathies. *Autophagy*, *16*(1), 185–187. https://doi.org/10.1080/15548627.2019.1688556

Lisi, S., Malerba, F., Quaranta, P., Florio, R., Vitaloni, O., Monaca, E., Bruni Ercole, B., Bitonti, A. R., Del Perugia, O., Mignanelli, M., Perrera, P., Sabbatella, R., Raimondi, F., Piazza, C. R., Moles, A., Alfano, C., Pistello, M., & Cattaneo, A. (2024). Selection and characterization of human scFvs targeting the SARS-CoV-2 nucleocapsid protein isolated from antibody libraries of COVID-19 patients. *Scientific Reports*, *14*(1), 15864. https://doi.org/10.1038/s41598-024-66558-0

Luh, L. M., Scheib, U., Juenemann, K., Wortmann, L., Brands, M., & Cromm, P. M. (2020). Prey for the Proteasome: Targeted Protein Degradation—A Medicinal Chemist's Perspective. *Angewandte Chemie International Edition*, *59*(36), 15448–15466. https://doi.org/10.1002/anie.202004310

Mallery, D. L., McEwan, W. A., Bidgood, S. R., Towers, G. J., Johnson, C. M., & James, L. C. (2010). Antibodies mediate intracellular immunity through tripartite motif-containing 21 (TRIM21). *Proceedings of the National Academy of Sciences*, *107*(46), 19985–19990. https://doi.org/10.1073/pnas.1014074107

McCafferty, J., Griffiths, A. D., Winter, G., & Chiswell, D. J. (1990). Phage antibodies: Filamentous phage displaying antibody variable domains. *Nature*, *348*(6301), 552–554. https://doi.org/10.1038/348552a0

Melchionna, T., & Cattaneo, A. (2007). A Protein Silencing Switch by Ligand-induced Proteasome-targeting Intrabodies. *Journal of Molecular Biology*, *374*(3), 641–654. https://doi.org/10.1016/j.jmb.2007.09.053

Messaoudi, E., Kanhema, T., Soulé, J., Tiron, A., Dagyte, G., Da Silva, B., & Bramham, C. R. (2007). Sustained Arc/Arg3.1 Synthesis Controls Long-Term Potentiation Consolidation through Regulation of Local Actin Polymerization in the Dentate Gyrus *In Vivo*. *The Journal of Neuroscience*, *27*(39), 10445–10455. https://doi.org/10.1523/JNEUROSCI.2883-07.2007

Miao, Y., Gao, Q., Mao, M., Zhang, C., Yang, L., Yang, Y., & Han, D. (2021). Bispecific Aptamer Chimeras Enable Targeted Protein Degradation on Cell Membranes. *Angewandte Chemie International Edition*, *60*(20), 11267–11271. https://doi.org/10.1002/anie.202102170

Möckli, N., & Auerbach, D. (2004). Quantitative β-galactosidase assay suitable for high-throughput applications in the yeast two-hybrid system. *BioTechniques*, *36*(5), 872–876. https://doi.org/10.2144/04365PT03

Möglich, A., Ayers, R. A., & Moffat, K. (2009). Structure and Signaling Mechanism of Per-ARNT-Sim Domains. *Structure*, *17*(10), 1282–1294. https://doi.org/10.1016/j.str.2009.08.011

Murakami, Y., Matsufuji, S., & Kameji, T. (1992). *Ornithine decarboxylase is degraded by the 265 proteasome without ubiquitination*.

Muyldermans, S., Baral, T. N., Retamozzo, V. C., De Baetselier, P., De Genst, E., Kinne, J., Leonhardt, H., Magez, S., Nguyen, V. K., Revets, H., Rothbauer, U., Stijlemans, B., Tillib, S., Wernery, U., Wyns, L., Hassanzadeh-Ghassabeh, Gh., & Saerens, D. (2009). Camelid immunoglobulins and nanobody technology. *Veterinary Immunology and Immunopathology*, *128*(1–3), 178–183. https://doi.org/10.1016/j.vetimm.2008.10.299

Nabet, B., Roberts, J. M., Buckley, D. L., Paulk, J., Dastjerdi, S., Yang, A., Leggett, A. L., Erb, M. A., Lawlor, M. A., Souza, A., Scott, T. G., Vittori, S., Perry, J. A., Qi, J., Winter, G. E., Wong, K.-K., Gray, N. S., & Bradner, J. E. (2018). The dTAG system for immediate and target-specific protein degradation. *Nature Chemical Biology*, *14*(5), 431–441. https://doi.org/10.1038/s41589-018-0021-8

Nguyen, J. A., & Yates, R. M. (2021). Better Together: Current Insights Into Phagosome-Lysosome Fusion. *Frontiers in Immunology*, *12*, 636078. https://doi.org/10.3389/fimmu.2021.636078

O'-Donoghue, L., & Smolenski, A. (2024). *Analysis of protein phosphorylation using Phos-tag gels—ScienceDirect*. https://doi.org/10.1016/j.jprot.2022.104558

Oleinikovas, V., Gainza, P., Ryckmans, T., Fasching, B., & Thomä, N. H. (2024). From Thalidomide to Rational Molecular Glue Design for Targeted Protein Degradation. *Annual Review of Pharmacology and Toxicology*, *64*(1), 291–312. https://doi.org/10.1146/annurev-pharmtox-022123-104147

Paudel, R. R., Lu, D., Roy Chowdhury, S., Monroy, E. Y., & Wang, J. (2023). Targeted Protein Degradation via Lysosomes. *Biochemistry*, *62*(3), 564–579. https://doi.org/10.1021/acs.biochem.2c00310

Pegg, A. E. (2006). *Regulation of Ornithine Decarboxylase*. https://doi.org/10.1074/jbc.R500031200

Persic, L., Roberts, A., Wilton, J., Cattaneo, A., Bradbury, A., & Hoogenboom, H. R. (1997). An integrated vector system for the eukaryotic expression of antibodies or their fragments after selection from phage display libraries. *Gene*, *187*(1), 9–18. https://doi.org/10.1016/S0378-1119(96)00628-2

Piecyk, M., Fauvre, J., Duret, C., Chaveroux, C., & Ferraro-Peyret, C. (2024). SUrface SEnsing of Translation (SUnSET), a Method Based on Western Blot Assessing Protein Synthesis Rates in vitro. *BIO-PROTOCOL*, *14*(3). https://doi.org/10.21769/BioProtoc.4933

Plückthun, A., & Skerra, A. (1989). [34] Expression of functional antibody Fv and Fab fragments in Escherichia coli. In *Methods in Enzymology* (Vol. 178, pp. 497–515). Elsevier. https://doi.org/10.1016/0076-6879(89)78036-8

Raiborg, C., & Stenmark, H. (2009). The ESCRT machinery in endosomal sorting of ubiquitylated membrane proteins. *Nature*, *458*(7237), 445–452. https://doi.org/10.1038/nature07961

Renicke, C., Schuster, D., Usherenko, S., Essen, L.-O., & Taxis, C. (2013). A LOV2 Domain-Based Optogenetic Tool to Control Protein Degradation and Cellular Function. *Chemistry & Biology*, *20*(4), 619–626. https://doi.org/10.1016/j.chembiol.2013.03.005

Reymann, K. G., & Frey, J. U. (2007). The late maintenance of hippocampal LTP: Requirements, phases, 'synaptic tagging', 'late-associativity' and implications. *Neuropharmacology*, *52*(1), 24–40. https://doi.org/10.1016/j.neuropharm.2006.07.026

Ridgway, J. B. B., Presta, L. G., & Carter, P. (1996). 'Knobs-into-holes' engineering of antibody C_H3 domains for heavy chain heterodimerization. *Protein Engineering, Design and Selection*, *9*(7), 617–621. https://doi.org/10.1093/protein/9.7.617

Russo, A., Scardigli, R., La Regina, F., Murray, M. E., Romano, N., Dickson, D. W., Wolozin, B., Cattaneo, A., & Ceci, M. (2017). Increased cytoplasmic TDP-43 reduces global protein synthesis by interacting with RACK1 on polyribosomes. *Human Molecular Genetics*, *26*(8), 1407–1418. https://doi.org/10.1093/hmg/ddx035

Sakamoto, K. M., Kim, K. B., Kumagai, A., Mercurio, F., Crews, C. M., & Deshaies, R. J. (2001). Protacs: Chimeric molecules that target proteins to the Skp1–Cullin–F box complex for ubiquitination and degradation. *Proceedings of the National Academy of Sciences*, *98*(15), 8554–8559. https://doi.org/10.1073/pnas.141230798

Samarasinghe, K. T. G., & Crews, C. M. (2021). Targeted protein degradation: A promise for undruggable proteins. *Cell Chemical Biology*, *28*(7), 934–951. https://doi.org/10.1016/j.chembiol.2021.04.011

Schmidt, E. K., Clavarino, G., Ceppi, M., & Pierre, P. (2009). SUnSET, a nonradioactive method to monitor protein synthesis. *Nature Methods*, *6*(4), 275–277. https://doi.org/10.1038/nmeth.1314

Sengupta, J., Nilsson, J., Gursky, R., Spahn, C. M. T., Nissen, P., & Frank, J. (2004). Identification of the versatile scaffold protein RACK1 on the eukaryotic ribosome by cryo-EM. *Nature Structural & Molecular Biology*, *11*(10), 957–962. https://doi.org/10.1038/nsmb822

Shih, H. H., Tu, C., Cao, W., Klein, A., Ramsey, R., Fennell, B. J., Lambert, M., Ní Shúilleabháin, D., Autin, B., Kouranova, E., Laxmanan, S., Braithwaite, S., Wu, L., Ait-Zahra, M., Milici, A. J., Dumin, J. A., LaVallie, E. R., Arai, M., Corcoran, C., … Finlay, W. J. J. (2012). An Ultra-specific Avian Antibody to Phosphorylated Tau Protein Reveals a Unique Mechanism for Phosphoepitope Recognition. *Journal of Biological Chemistry*, *287*(53), 44425–44434. https://doi.org/10.1074/jbc.M112.415935

Sibler, A., Courtête, J., Muller, C. D., Zeder-Lutz, G., & Weiss, E. (2005). Extended half-life upon binding of destabilized intrabodies allows specific detection of antigen in mammalian cells. *The FEBS Journal*, *272*(11), 2878–2891. https://doi.org/10.1111/j.1742-4658.2005.04709.x

Takahashi, D., Moriyama, J., Nakamura, T., Miki, E., Takahashi, E., Sato, A., Akaike, T., Itto-Nakama, K., & Arimoto, H. (2019). AUTACs: Cargo-Specific Degraders Using Selective Autophagy. *Molecular Cell*, *76*(5), 797-810.e10. https://doi.org/10.1016/j.molcel.2019.09.009

Tischer, D., & Weiner, O. D. (2014). Illuminating cell signalling with optogenetic tools. *Nature Reviews Molecular Cell Biology*, *15*(8), 551–558. https://doi.org/10.1038/nrm3837

Tonelli, F., Iannello, L., Gustincich, S., Di Garbo, A., Pandolfini, L., & Cremisi, F. (2025). Dual inhibition of MAPK/ERK and BMP signaling induces entorhinal-like identity in mouse ESC-derived pallial progenitors. *Stem Cell Reports*, 102387. https://doi.org/10.1016/j.stemcr.2024.12.002

Usherenko, S., Stibbe, H., Muscó, M., Essen, L.-O., Kostina, E. A., & Taxis, C. (2014). Photo-sensitive degron variants for tuning protein stability by light. *BMC Systems Biology*, *8*(1), 128. https://doi.org/10.1186/s12918-014-0128-9

Visintin, M., Meli, G. A., Cannistraci, I., & Cattaneo, A. (2004). Intracellular antibodies for proteomics. *Journal of Immunological Methods*, *290*(1–2), 135–153. https://doi.org/10.1016/j.jim.2004.04.014

Visintin, M., Quondam, M., & Cattaneo, A. (2004). The intracellular antibody capture technology: Towards the high-throughput selection of functional intracellular antibodies for target validation. *Methods*, *34*(2), 200–214. https://doi.org/10.1016/j.ymeth.2004.04.008

Visintin, M., Settanni, G., Maritan, A., Graziosi, S., Marks, J. D., & Cattaneo, A. (2002). The intracellular antibody capture technology (IACT): Towards a consensus sequence for intracellular antibodies. *J Mol Biol*, *317*(1), 73-83. https://doi.org/10.1006/jmbi.2002.5392

Visintin, M., Tse, E., Axelson, H., Rabbitts, T. H., & Cattaneo, A. (1999). Selection of antibodies for intracellular function using a two-hybrid *in vivo* system. *Proceedings of the National Academy of Sciences*, *96*(21), 11723–11728. https://doi.org/10.1073/pnas.96.21.11723

Wang, W., Zhou, Q., Jiang, T., Li, S., Ye, J., Zheng, J., Wang, X., Liu, Y., Deng, M., Ke, D., Wang, Q., Wang, Y., & Wang, J.-Z. (2021). A novel small-molecule PROTAC selectively promotes tau clearance to improve cognitive functions in Alzheimer-like models. *Theranostics*, *11*(11), 5279–5295. https://doi.org/10.7150/thno.55680

Wang, Y., & Mandelkow, E. (2016). Tau in physiology and pathology. *Nature Reviews Neuroscience*, *17*(1), 22–35. https://doi.org/10.1038/nrn.2015.1

Winter, G. E., Buckley, D. L., Paulk, J., Roberts, J. M., Souza, A., Dhe-Paganon, S., & Bradner, J. E. (2015). Phthalimide conjugation as a strategy for in vivo target protein degradation. *Science*, *348*(6241), 1376–1381. https://doi.org/10.1126/science.aab1433

Wu, H.-Y., Chen, S.-F., Hsieh, J.-Y., Chou, F., Wang, Y.-H., Lin, W.-T., Lee, P.-Y., Yu, Y.-J., Lin, L.-Y., Lin, T.-S., Lin, C.-L., Liu, G.-Y., Tzeng, S.-R., Hung, H.-C., & Chan, N.-L. (2015). *Structural basis of antizyme-mediated regulation of polyamine homeostasis*. https://doi.org/10.1073/pnas.1508187112

Xie, X., Yu, T., Li, X., Zhang, N., Foster, L. J., Peng, C., Huang, W., & He, G. (2023). Recent advances in targeting the "undruggable" proteins: From drug discovery to clinical trials. *Signal Transduction and Targeted Therapy*, *8*(1), 335. https://doi.org/10.1038/s41392-023-01589-z

Yang, C., & Wang, X. (2021). Lysosome biogenesis: Regulation and functions. *Journal of Cell Biology*, *220*(6), e202102001. https://doi.org/10.1083/jcb.202102001

Yoo, Y. D., Mun, S. R., Ji, C. H., Sung, K. W., Kang, K. Y., Heo, A. J., Lee, S. H., An, J. Y., Hwang, J., Xie, X.-Q., Ciechanover, A., Kim, B. Y., & Kwon, Y. T. (2018). N-terminal arginylation generates a bimodal degron that modulates autophagic proteolysis. *Proceedings of the National Academy of Sciences*, *115*(12). https://doi.org/10.1073/pnas.1719110115

Yu, D., Lee, H., Hong, J., Jung, H., Jo, Y., Oh, B.-H., Park, B. O., & Heo, W. D. (2019). Optogenetic activation of intracellular antibodies for direct modulation of endogenous proteins. *Nature Methods*, *16*(11), 1095–1100. https://doi.org/10.1038/s41592-019-0592-7

Zhang, H., Han, Y., Yang, Y., Lin, F., Li, K., Kong, L., Liu, H., Dang, Y., Lin, J., & Chen, P. (2021). *Covalently Engineered Nanobody Chimeras for Targeted Membrane Protein Degradation*. https://pubs.acs.org/doi/10.1021/jacs.1c08521

Zhang, W., Wu, J., Ward, M. D., Yang, S., Chuang, Y.-A., Xiao, M., Li, R., Leahy, D. J., & Worley, P. F. (2015). Structural Basis of Arc Binding to Synaptic Proteins: Implications for Cognitive Disease. *Neuron*, *86*(2), 490–500. https://doi.org/10.1016/j.neuron.2015.03.030

Zhao, B., Cowan, C. M., Coutts, J. A., Christy, D. D., Saraph, A., Hsueh, S. C. C., Plotkin, S. S., Mackenzie, I. R., Kaplan, J. M., & Cashman, N. R. (2023). Targeting RACK1 to alleviate TDP-43 and FUS proteinopathy-mediated suppression of protein translation and neurodegeneration. *Acta Neuropathologica Communications*, *11*(1), 200. https://doi.org/10.1186/s40478-023-01705-8

Zhao, L., Zhao, J., Zhong, K., Tong, A., & Jia, D. (2022). Targeted protein degradation: Mechanisms, strategies and application. *Signal Transduction and Targeted Therapy*, *7*(1), 113. https://doi.org/10.1038/s41392-022-00966-4

Zhong, G., Chang, X., Xie, W., & Zhou, X. (2024). Targeted protein degradation: Advances in drug discovery and clinical practice. *Signal Transduction and Targeted Therapy*, *9*(1), 308. https://doi.org/10.1038/s41392-024-02004-x

Zhou, P., Robert Bogacki, R. B., McReynolds, L., & Howley, P. M. (2000). *Harnessing the Ubiquitination Machinery to Target the Degradation of Specific Cellular Proteins*. https://doi.org/10.1016/S1097-2765(00)00074-5

Zinatizadeh, M. R., Schock, B., Chalbatani, G. M., Zarandi, P. K., Jalali, S. A., & Miri, S. R. (2021). The Nuclear Factor Kappa B (NF-kB) signaling in cancer development and immune diseases. *Genes & Diseases*, *8*(3), 287–297. https://doi.org/10.1016/j.gendis.2020.06.005

Acknowledgement

At the end of my PhD journey, I would like to express my gratitude to Professor Cattaneo for mentoring me throughout these years. The role of a supervisor evolves as the student grows, and navigating this transformation has been a meaningful challenge.

I'm thankful to the members of the Intrabody group, who helped shape my scientific thinking. I would like to thank Drs. Simonetta Lisi, and Ottavia Vitaloni for guiding me through the first part of my PhD and for allowing me to appreciate and to improve the strength, the patience and the resilience required to be a scientist.

A heartfelt thank you to Dr. Ajesh Jacob, he often speaks my silent language and, at the right moment, offers the kindest and most helpful words. Thanks also to Martina D'Assoro for sharing very last-minute experiments with me.

To my lab friends Letizia, Roberta, Eleonora, Arianna, Greta, Marianna, Fabrizio, Filippo thank you because I needed to learn how to share the most genuine part of myself, and with all of you, I always felt understood. I've had the chance to grow not only as a scientist but also as a person.

A special thank you to Simone, my outlier, who joined this journey during one of its most difficult chapters. Truly understanding another person's inner world takes effort, but we do like the efforts and walking that path with you has been a gift.

Finally, a big thank you to my family the ones who have celebrated every success with joy, more than I can do, and carried the weight of every failed experiment with me.

Your support has been my foundation.